Experiments with a Spectra Cumulus Parameterization Theory

Pedro Leite Silva Dias
Wayne H. Schubert

Department of Atmospheric Science
Colorado State University
Fort Collins, Colorado

Colorado State University

Department of Atmospheric Science

Paper No. 275

EXPERIMENTS WITH A SPECTRAL CUMULUS PARAMETERIZATION THEORY

Pedro Leite Silva Dias
Wayne H. Schubert

The research reported here has been supported by the Global Atmospheric Research Program, Climate Dynamics Research Section, National Science Foundation, Grants DES 74-11438 and ATM 76-09370

Department of Atmospheric Science
Colorado State University
Fort Collins, Colorado

July 1977

Atmospheric Science Paper No. 275

ABSTRACT

The thermodynamic equation and the water vapor equation, with the effects of cumulus convection parameterized according to the Arakawa-Schubert theory, are integrated during a short time interval and the resultant temperature and moisture tendencies are then studied. The quasi-equilibrium assumption is formulated as an optimization problem in which the objective is to minimize the changes in the cloud work function. The feedback loop consists of temperature and moisture changes due to large-scale vertical motion, radiative cooling and surface fluxes. The response of the model to different patterns of the above three types of forcing is compared to observations.

The model suggests a suppressive effect of deep convection on shallow convection, which is shown to be strongly coupled to boundary layer forcing through surface fluxes of heat and moisture. The distribution of clouds is shown to be sensitive to the choice of the radiative cooling profile when the dynamical forcing is small. In the static control a lateral detrainment coefficient is introduced as well as a cloud type dependent autoconversion coefficient in the parameterization of rain.

ACKNOWLEDGEMENTS

We have benefited from discussions with many colleagues including Dr. Alan Betts, Dr. William Gray, Dr. Warren Hall, Mr. James Hack and Ms. Maria Silva Dias.

This research was done while one of us (P.S.D.) was on leave from the *Departamento de Meteorologia* of the *Instituto Astronômico e Geofísico* of the *Universidade de São Paulo*, Brazil. The *Coordenadoria de Aperfeiçoamento de Pessoal de Nivel Superior--CAPES* provided the scholarship.

Many thanks are due Ms. Dorothy Chapman who helped in all phases of the preparation of the manuscript. The figures were drafted by Ms. Janella Owen.

This research was supported by the Global Atmospheric Research Program, Climate Dynamics Research Section, National Science Foundation, Grants DES 74-11438 and ATM 76-09370.

TABLE OF CONTENTS

TABLE OF CONTENTS Continued

LIST OF FIGURES

LIST OF FIGURES Continued

1. INTRODUCTION

Recently we have observed an advance in the physical understanding of the interaction processes between a cumulus ensemble and its large-scale environment. Diagnostic and prognostic studies have been made leading to an improvement in the theory of parameterization of cumulus convection. Several schemes have been suggested for parameterization. Early schemes included moist adiabatic adjustment (Manabe et al., 1965) and large-scale convergence in the boundary layer (Ooyama, 1964, 1969; Ogura, 1964); Charney and Eliassen (1964) and Kuo (1965) proposed parameterizations in which cumulus heating is specified by the net convergence of water vapor not only in the boundary layer but also in the troposphere. However, these schemes were based on many unvalidated assumptions and bypassed physical processes of the mutual interaction.

Diagnostic studies on the trade cumulus regime have been quite abundant and research programs (such as BOMEX and ATEX) have contributed to the knowledge of the effect of cumulus clouds on the sub-grid fluxes of heat and moisture (Augstein et al., 1973; Holland and Rasmusson, 1973; Betts, 1975; Williams and Gray, 1973). Several methods have been developed that use synoptic-scale meteorological observations and simple cloud models to diagnose the interaction between cumulus convection and the large-scale circulation (Gray, 1973; Yanai et al., 1973; Ogura and Cho, 1973; Nitta, 1975). The spectral cloud model was applied by Yanai et al. (1976) to the data set taken in the Marshall Islands area for a 100-day period in 1956; the effect of radiative cooling upon the cloud base mass spectrum was examined and the dependence of daily cloud mass spectra on the large-scale vertical motion and the evaporation

from the sea was studied. The recent GATE project has given a new impulse to research on the interaction between cumulus ensembles and the large-scale environment (Nitta, 1977).

Ooyama (1971) was the first to propose a cumulus parameterization theory taking into account the coexistence of clouds of different sizes on the assumption that cumulus clouds can be represented by independent buoyant elements. Although it is not a closed theory, a few experiments have been made (Ooyama, 1973, and Rosenthal, 1973). Arakawa and Schubert (1974) proposed a closed theory for the parameterization of a cumulus ensemble. The mutual interaction between clouds and the large-scale environment consists of feedback and control loops. The feedback loop describes how the detrainment and cumulus induced subsidence modify the large-scale temperature and moisture fields. The control loop describes how the properties of the cloud ensemble are controlled by the large-scale field. The Arakawa-Schubert theory predicts the mass spectrum of clouds and their effect thus allowing comparison with diagnostic studies which use the spectral cloud model.

The quasi-equilibrium assumption is the core of the Arakawa-Schubert cumulus parameterization theory. In this study the quasi-equilibrium assumption is formulated as an optimization problem as discussed by Hack and Schubert (1976). The purpose of this research is to study the response of the atmosphere, as predicted by the Arakawa-Schubert theory, in terms of the cumulus mass flux distribution, temperature and moisture changes when subjected to a known forcing, which consists of large-scale vertical motion, radiative cooling and surface fluxes. The large-scale vertical motion is a time-varying $\bar{\omega}$-field given by Reed and Recker (1971). The dependence on the

radiative cooling profile is also studied by means of typical profiles in cloud and cloud free regions, and the effect of varying the evaporation is studied assuming a time dependent functional relationship for the surface wind speed. The results are compared to Reed and Recker's and to Yanai's observations.

Lateral detrainment from cumulus clouds is introduced into the cloud model as well as a cloud type dependent auto-conversion coefficient in the parameterization of rain. The optimization approach of the quasi-equilibrium assumption introduces an undetermined set of coefficients in the model. The sensitivity of the Arakawa-Schubert theory to changes in these model parameters is also tested.

2. GOVERNING EQUATIONS (continuous form)

A great simplicity is attained in this model because the large-scale forcing is specified. The characteristic scales of individual convective clouds both in time and horizontal dimensions are much smaller than wave-like large-scale disturbances observed in the tropics. This fact suggests that the induced modification on the large-scale environment by the cumulus scale motions can be treated as sub-grid scale effects. The time changes of the environment are governed by the heat and moisture budget equations. The sub-grid effects are parameterized by the model presented by Arakawa and Schubert (1974). Surface fluxes of sensible heat, surface evaporation and tropospheric radiational cooling are also taken into account.

2.1 Area Averaged Equations and Separation of Scales

An important problem in dealing with the interaction between the cumulus convection and the large-scale flow is the derivation of the appropriate large-scale prognostic equations for heat and moisture (and momentum in more general models). These equations have to include sub-grid scale effects of cumulus convection on the unresolvable scales of motion. The assumption of parameterizability is that the properties of the sub-grid scale phenomena (cumulus convection) are related to the large-scale variables at any instant.

The area-averaged equations are obtained by the Reynold's averaging method in which the cumulus clouds are considered as eddies superimposed on the large-scale flow. The neglect of storage of heat and water vapor in the ensemble of clouds implies that the prediction

of the large-scale field is practically the same as the prediction of the cloud environment thermodynamic variables as was used by Arakawa (1969, 1972), Ooyama (1971), Yanai et al. (1973). Consequently it is suggested that the predictive equations for heat and moisture in the large-scale are composed of two types of terms: those which depend on large-scale terms such as large-scale advection and radiation (if no interaction between cloud cover and radiative cooling is allowed) and those which depend on the eddies such as cumulus convection and surface fluxes.

In sections 2.2 and 2.3 the large-scale equations and the sub-grid scale equations are presented.

2.2 Large-Scale Equations

2.2.1 The heat budget equation

From the budget of static energy s in the environment, we obtain

$$\frac{d\bar{s}}{dt} = \bar{Q}_{LS} + \bar{Q}_{C} \tag{2.1}$$

where the subscripts LS and C stand for the large-scale and convective effects respectively, on the time rate of change of the large-scale variables, which are denoted by the overbar; $s = c_p T + gz$ where c_p is the specific heat capacity of dry air at constant pressure, gz is the potential energy and $\bar{Q}_{LS}$ is the heating rate per unit mass due to large-scale diabatic processes. The actual form of (2.1) used in this model is

$$\left.\frac{\partial \bar{s}}{\partial t}\right|_{LS} = - \bar{\omega} \frac{\partial \bar{s}}{\partial p} + \bar{Q}_{LS} \, , \tag{2.2}$$

because of the horizontal homogeneity. The heating rate $\bar{Q}_{LS}$ includes the diabatic effects of radiation and water vapor condensation with the consequent release of latent heat when the air becomes saturated in a large-scale sense. The evaporational cooling of falling raindrops formed by the large-scale condensation of water vapor is also taken into account. This process of condensation and eventual evaporation of raindrops in a large-scale sense is known as large-scale precipitation as defined by Arakawa, Mintz et al. (1974). The computational procedures involved in the large-scale precipitation are explained in chapter 3. The $\bar{Q}_C$ term is discussed in section 2.3.1.

The $\bar{Q}_{LS}$ term in (2.2) also includes the radiational heating given by the difference between the incoming solar (short-wave) and the outgoing (long-wave) radiation, which is assumed to be a known function of time and independent of the thermodynamic variables and cloudiness. Different radiative cooling rates were tested to determine the sensitivity of the model to this parameter.

2.2.2 The water budget equation

The continuity equation for the water vapor is

$$\frac{d\bar{q}}{dt} = -\bar{C} + \bar{E} \tag{2.3}$$

where $\bar{C}$ and $\bar{E}$ are a sink and a source term per unit mass due to phase change and $\bar{q}$ is the mixing ratio. As in the case of the heat budget equation there is no horizontal advection term in the water vapor equation, i.e. (2.3) can be written as

$$\left.\frac{\partial \bar{q}}{\partial t}\right|_{LS} = - \bar{\omega} \frac{\partial \bar{q}}{\partial p} + \bar{C}_{LS} - \bar{E}_{LS} \cdot \qquad (2.4)$$

The large-scale condensation term $\bar{C}_{LS}$ and the large-scale evaporation term $\bar{E}_{LS}$ are treated in chapter 3. Equation (2.4) states that, neglecting sub-grid scale phenomena, the local variation of the mixing ratio is only due to vertical advection and eventual condensation and evaporation in a large-scale sense (for instance a continuous upward vertical motion might generate supersaturation, consequent condensation and re-evaporation of falling raindrops in a sub-saturated environment). The cumulus effect on (2.3) is treated in section 2.3.1.

2.3 Sub-grid scale equations

The Arakawa-Schubert cumulus parameterization theory describes the interaction between a cumulus cloud ensemble and the large-scale environment. This mutual interaction is shown in Fig. 2.1 (after Schubert, 1974). The time changes of the environment are determined by the dry static energy and moisture budget equations with a spectral parameterization with respect to cloud types of the eddy fluxes associated with cumulus convection. The interaction between the eddy fluxes plus source/sink terms and the large-scale properties is shown in Fig. 2.1. The eddy fluxes depend on the cloud base mass flux which is assumed to be related to the time change of the large-scale variables thus closing the theory. The determination of the cloud base mass flux is the job of the dynamic control (Fig. 2.1). In order to define the eddy fluxes Arakawa and Schubert developed a spectral cloud model which determines the cloud properties on which the eddy fluxes are based; this is called the static control.

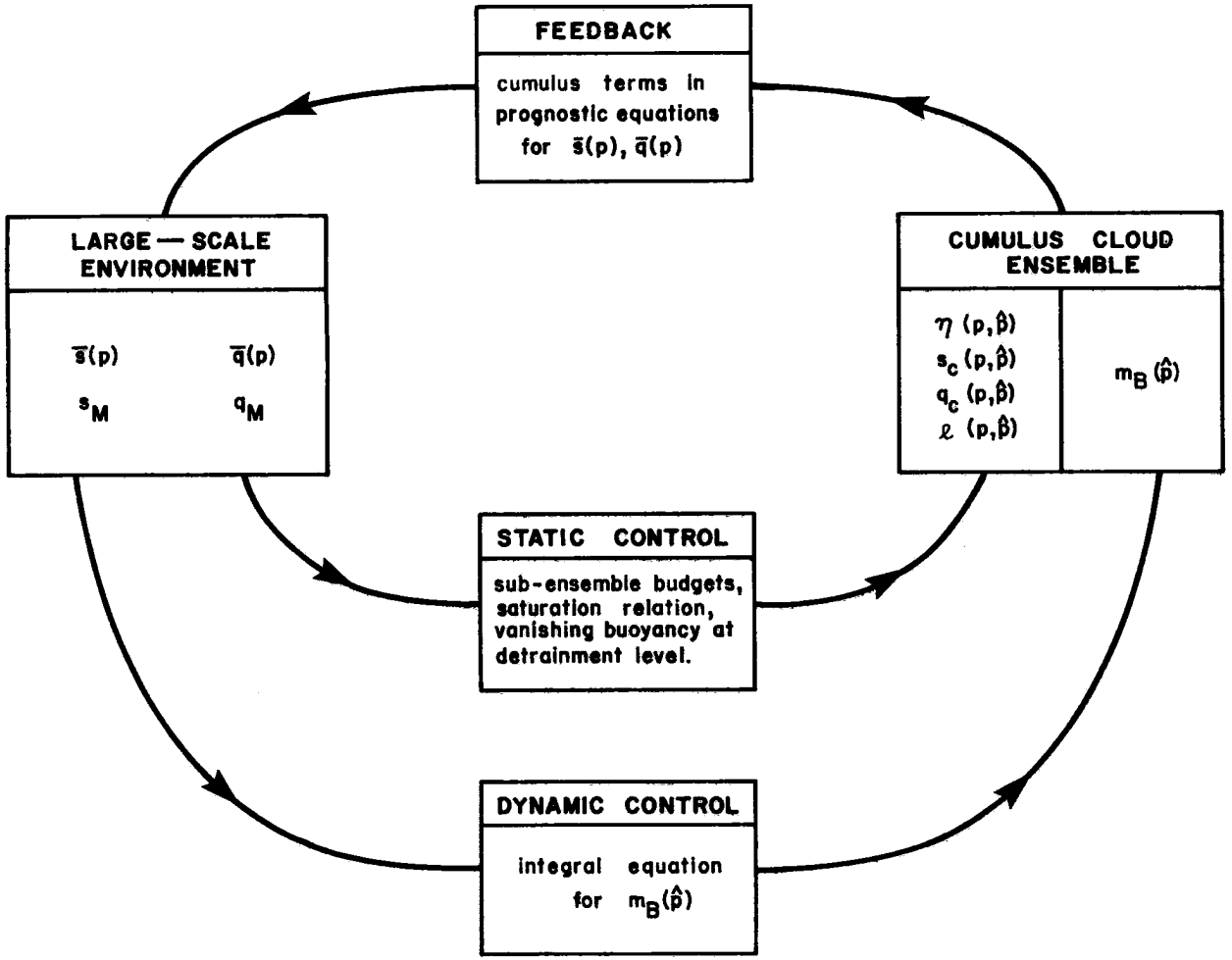

Fig. 2.1 Schematic representation of the mutual interaction of a cumulus cloud ensemble with the large-scale environment.

The spectral parameter in Arakawa and Schubert (1974) is the fractional rate of entrainment which is assumed to fully characterize a cloud type including its detrainment level. However, it turns out to be more appropriate to have the detrainment level as the spectral parameter as far as discrete modeling is concerned (see section 2.3.3). Thus clouds are spectrally divided according to their detrainment level $\hat{p}$ in what follows. The cloud variables are consequently determined by the fractional rate of entrainment associated with cloud type $\hat{p}$ which is assumed to be a constant with pressure for each cloud type.

A fractional rate of detrainment is also included in the cloud model to take account of the dying phase of the cumulus life cycle. However, the introduction of detrainment variable (λ^-) introduces an empiricism in the choice of this parameter. The parameter λ^- is assumed to be constant with p for the time-averaged mass flux of cloud type $\hat{p}$.

In this section we discuss the parameterization of cumulus convection in terms of the feedback, static control and dynamic control loops.

2.3.1 Feedback

The large-scale environment is divided into the subcloud mixed layer (from the surface pressure p_S up to the top of the mixed layer p_B) and a cumulus convective layer (from p_B up to the top of the model p_T). Following Yanai et al. (1973) we can write budget equations for heat and moisture in a cloud layer using the dry-static energy (s) and the mixing ratio (q). After averaging these equations over a certain scale, neglecting eddy horizontal transports and large-scale processes (which

were already taken into account by the larger scale processes in section 2.2) we obtain

$$\left.\frac{\partial \bar{s}}{\partial t}\right|_C = - g \frac{\partial}{\partial p} (\overline{\omega' s_\ell'}) + LR \tag{2.5}$$

$$\left.\frac{\partial \bar{q}}{\partial t}\right|_C = - g \frac{\partial}{\partial p} [\overline{\omega'(q'+\ell')}] - R \tag{2.6}$$

where s_ℓ is the liquid water static energy

$$s_\ell = s - L\ell \tag{2.7}$$

(ℓ is the liquid water mixing ratio). The variable s_ℓ is the static energy analog of the liquid water potential temperature discussed by Betts (1975). The primes denote deviations from the horizontal averages ($\bar{}$), the subscript C refers to the cumulus effect and R is the sub-grid scale liquid water sink term (associated with cumulus precipitation). The eddy transports on the right hand sides of (2.5) and (2.6) will be interpreted as convective transports. Following Schubert (1974), let us define the sub-grid scale fluxes of dry static energy, water vapor and liquid water in the cumulus convective layer as

$$\overline{\omega' s'} = F_s(p) = \int_{p_T}^{p} \eta(p,\hat{p})[s_c(p,\hat{p}) - \bar{s}(p)]m_B(\hat{p})d\hat{p}$$

$$\text{for } p \leq p_B \ , \tag{2.8a}$$

$$\overline{\omega' q'} = F_q(p) = \int_{p_T}^{p} \eta(p,\hat{p})[q_c(p,\hat{p}) - \bar{q}(p)]m_B(\hat{p})d\hat{p}$$

$$\text{for } p \leq p_B \ , \tag{2.8b}$$

$$\overline{\omega'\ell'} = F_\ell(p) = \int_{p_B}^{p} \eta(p,\hat{p})\ell(p,\hat{p})m_B(\hat{p})d\hat{p}$$

$$\text{for } p \leq p_B \ . \qquad (2.8c)$$

Below p_B the convective scale fluxes of s and q are linear in p with the values $(F_s)_S$ and $(F_q)_S$ at the surface and the values $(F_s)_B$ and $(F_q)_B$ at p_B. The convective scale flux of ℓ is zero in the mixed layer below p_B.

In the cumulus convective layer the eddy fluxes are accomplished by the cloud ensembles. Each cloud ensemble is characterized by its cloud depth defined as $p_B - \hat{p}$ where $\hat{p}$ is the detrainment level. Thus clouds are spectrally classified according to their detrainment level rather than according to the fractional rate of entrainment λ^+ as defined by Arakawa and Schubert. The main advantage in having $\hat{p}$ as a spectral parameter is that it is more suitable for adaptation to discrete models in the vertical (chapter 3). The variables $s_c(p,\hat{p})$, $q_c(p,\hat{p})$ and $\ell(p,\hat{p})$ are, respectively, the cloud dry static energy, cloud water vapor mixing ratio and cloud liquid water content at level p inside sub-ensemble $\hat{p}$, i.e., the sub-ensemble constituted of clouds which detrain at level $\hat{p}$; $m_B(\hat{p})d\hat{p}$ is the cloud base mass flux associated with the sub-ensemble $\hat{p}$; $\eta(p,\hat{p})$ is the normalized mass flux with respect to the cloud base mass flux, i.e., $\eta(p_B,\hat{p}) = 1$ for all cloud types. Thus $\eta(p,\hat{p})m_B(\hat{p})d\hat{p}$ is the vertical mass flux at level p due to sub-ensemble $\hat{p}$.

The sub-ensemble eddy fluxes defined by the integrands in (2.8) are such that the total upward flux of a certain property x (s or q) is given by the difference between the upward flux of that variable

inside the sub-ensemble $\hat{p}$

$$\eta(p,\hat{p})x_c(p,\hat{p})m_B(\hat{p})d\hat{p} \ , \tag{2.9}$$

and the downward flux in the environment caused by the induced subsidence of sub-ensemble $\hat{p}$

$$\eta(p,\hat{p})\bar{x}(p,\hat{p})m_B(\hat{p})d\hat{p} \ . \tag{2.10}$$

Thus the total upward flux at level p due to sub-ensemble $\hat{p}$ is

$$\eta(p,\hat{p})[x_c(p,\hat{p}) - \bar{x}(p)]m_B(\hat{p})d\hat{p} \ . \tag{2.11}$$

In order to obtain the total ensemble flux at a certain level p we need to integrate the sub-ensemble flux at level p over all sub-ensembles which detrain above p or, equivalently, the domain of integration for (2.11) is

$$p_T \leq \hat{p} \leq p \ , \tag{2.12}$$

if cumulus convection does not penetrate level p_T.

A combination of the three basic fluxes defined by (2.8) allows us to write the governing equations for the large-scale environment (equations (2.5) and (2.6)) for the region above the mixed layer as

$$\left.\frac{\partial \bar{s}}{\partial t}\right|_C = g\frac{\partial}{\partial p}F_{s-L\ell} + LR \ , \tag{2.13}$$

$$\left.\frac{\partial \bar{q}}{\partial t}\right|_C = g\frac{\partial}{\partial p}F_{q+\ell} - R \ , \tag{2.14}$$

where

$$F_{s-L\ell}(p) = F_s(p) - LF_\ell(p) \ , \tag{2.15}$$

$$F_{q+\ell}(p) = F_q(p) + F_\ell(p) \ . \tag{2.16}$$

In addition to the flux divergence terms the heat and moisture budgets above the mixed layer contain the convective scale liquid water sink term R (rain term), defined by

$$R(p) = g\int_{p_T}^{p_B} n(p,\hat{p})r(p,\hat{p})m_B(\hat{p})d\hat{p} \ , \tag{2.17}$$

where $gn(p,\hat{p})r(p,\hat{p})m_B(\hat{p})d\hat{p}$ is the sub-ensemble sink of liquid water (dimensions of sec^{-1}). R(p) is the total ensemble sink of liquid water. Integrating R(p) over the whole depth of the model we obtain the total precipitation (P) that falls from the column bounded by p_S and p_T

$$P = \int_{p_T}^{p_S} R(p)\,\frac{dp}{g} \ . \tag{2.18}$$

In the general case we should allow the effect of cumulus convection and surface fluxes on the variation of the pressure at the top of the mixed layer p_B as shown in Schubert (1974). However in this model we assume a mixed layer of fixed depth. The inclusion of an explicit boundary layer with the proper parameterization would involve complications in the definition of the vertical coordinate. However, we do allow an interaction between the mixed layer and the cumulus convective layer through the budget equations for dry static energy and moisture in the mixed layer (s_M and q_M respectively). These equations are

$$\left.\frac{\partial s_M}{\partial t}\right|_C = \frac{g}{p_S - p_B}\left[(F_s)_S - (F_s)_B\right] , \tag{2.19}$$

$$\left.\frac{\partial q_M}{\partial t}\right|_C = \frac{g}{p_S - p_B}\left[(F_q)_S - (F_q)_B\right] , \tag{2.20}$$

where

$$(F_s)_B = \Delta s M_C(p_B) , \tag{2.21}$$

$$(F_q)_B = \Delta q M_C(p_B) . \tag{2.22}$$

In (2.21) and (2.22) the symbol delta represents the jump of a quantity across the transition level p_B, e.g. $\Delta s = \bar{s}(p_{B_-}) - s_M$ and $\Delta q = q(p_{B_-}) - q_M$. $M_C(p_B)$ is total mass flux at p_B associated with all sub-ensembles, i.e.

$$M_C(p_B) = \int_{p_T}^{p_B} m_B(\hat{p})d\hat{p} . \tag{2.23}$$

In this formulation of the governing equations of the mixed layer the eddy fluxes of s and q are continuous across the top of the mixed layer although those variables are discontinuous.

Equations (2.13), (2.14), (2.19) and (2.20) have some interesting integral properties as far as the cumulus effect on the large-scale is concerned. Integrating (2.13) with respect to p from the top of the model to p_B and combining the result with (2.19) we obtain

$$\frac{\partial}{\partial t}\int_{p_T}^{p_S} \bar{s}\,\frac{dp}{g} = (F_s)_S + L\int_{p_T}^{p_S} R(p)\,\frac{dp}{g} , \tag{2.24}$$

assuming that $F_{s\text{-}L\ell}(p_T) = 0$. The left hand side of (2.24) is the time change of the total dry-static energy per unit area in a column extending from the surface to the top of the model p_T assuming p_S constant. Equation (2.24) shows that cumulus convection increases the total dry-static energy in the column only if there is a surface heat flux or precipitation from the column.

Similarly, integrating (2.14) and combining the result with (2.20) we obtain

$$\frac{\partial}{\partial t}\int_{p_T}^{p_S} \bar{q}\,\frac{dp}{g} = (F_q)_S - \int_{p_T}^{p_S} R(p)\,\frac{dp}{g}\,. \tag{2.25}$$

The quantity on the LHS of (2.25) is the time change of the total mass of water vapor per unit area in the column $p_S - p_T$. Equation (2.25) shows that the total mass of water can only be changed by evaporation from the surface and by cumulus convection when there is precipitation from the column. Combining (2.24) and (2.25) gives

$$\frac{\partial}{\partial t}\int_{p_T}^{p_S} \bar{h}\,\frac{dp}{g} = (F_h)_S \tag{2.26}$$

which shows that the total moist static energy per unit area in the column is unaffected by cumulus convection. However (2.26) does not constrain $\bar{h}$ to remain unaltered because it is an integral property; cumulus convection transports moist static energy from the lower levels to the higher levels.

2.3.2 Static control

The cloud variables $\eta(p,\hat{p})$, $h_c(p,\hat{p})$, $q_c(p,\hat{p})$ and $\ell(p,\hat{p})$ are determined in the static control through a cloud model based on a constant fractional rate of entrainment $\lambda^+(\hat{p})$ for each sub-ensemble $\hat{p}$.

Let us consider now the budgets of mass, moist static energy and water substance for the sub-ensemble $\hat{p}$. The mass budget gives

$$\frac{\partial \eta(p,\hat{p})}{\partial p} = -\lambda(\hat{p})\eta(p,\hat{p}) \ , \tag{2.27}$$

where

$$\lambda(\hat{p}) = \lambda^+(\hat{p}) - \lambda^-(\hat{p}) \ . \tag{2.28}$$

Equation (2.27) states that $\eta(p,\hat{p})$ varies in the vertical depending on the entrainment rate $\lambda^+(\hat{p})$ and on the detrainment rate $\lambda^-(\hat{p})$ of the sub-ensemble $\hat{p}$. Similarly the moist static energy gives

$$\frac{\partial}{\partial p}\left[\eta(p,\hat{p})h_c(p,\hat{p})\right] = -\left[\lambda^+(\hat{p})\bar{h}(p) - \lambda^-(\hat{p})h_c(p)\right]\eta(p,\hat{p}) \ , \tag{2.29}$$

while the water substance budget gives

$$\frac{\partial}{\partial p}\left\{\eta(p,\hat{p})\left[q_c(p,\hat{p}) + \ell(p,\hat{p})\right]\right\} = -\left\{\lambda^+(p)\bar{q}(p) - \lambda^-(\hat{p})\left[q_c(p,\hat{p}) + \ell(p,\hat{p})\right]\right\}\eta(p,\hat{p}) + \eta(p,\hat{p})r(p,\hat{p}) \ , \tag{2.30}$$

where $r(p,\hat{p})$ in the precipitation produced by sub-ensemble $\hat{p}$ at level p. Equation (2.30) is valid above the condensation level p_C which will be assumed to coincide with p_B. If the air inside the cloud is saturated and if the effect on $q^* = q^*(T,p)$ of a pressure difference between the cloud and its environment is neglected we obtain an equation for

$q_c(p,\hat{p})$ as a function of large-scale variables and $h_c(p,\hat{p})$, i.e.

$$q_c(p,\hat{p}) = \bar{q}^*(p) + \frac{\gamma(p)}{1+\gamma(p)} \frac{1}{L} [h_c(p,\hat{p}) - \bar{h}^*(p)] \ , \tag{2.31}$$

where

$$\gamma = \frac{L}{c_p} \left[\frac{\partial q^*}{\partial \bar{T}}\right]_p \tag{2.32a}$$

and

$$\bar{h}^* = c_p \bar{T} + gz + Lq^* \tag{2.32b}$$

as shown by Arakawa (1969).

It is convenient to illustrate some properties of the variation of $h_c(p,\hat{p})$ with height by combining (2.27) and (2.29) and expanding the derivatives. The result is

$$\frac{\partial}{\partial p} h_c(p,\hat{p}) = \lambda^+(\hat{p})[h_c(p,\hat{p}) - \bar{h}(p)] \ , \tag{2.33}$$

a statement that $h_c(p,\hat{p})$ depends on the entrainment rate $\lambda^+(\hat{p})$ and on the difference between the moist static energy inside the sub-ensemble and that in the environment. Similarly,

$$\frac{\partial}{\partial p} [q_c(p,\hat{p})+\ell(p,\hat{p})] = \lambda^+(\hat{p})[q_c(p,\hat{p})+\ell(p,\hat{p}) - \bar{q}(p)] + r(p,\hat{p}) \ . \tag{2.34}$$

As in Arakawa and Schubert (1974) the entrainment rate $\lambda^+(\hat{p})$ is determined by the vanishing buoyancy condition which defines the maximum height of each cloud type. Therefore

$$s_{v_c}(\hat{p},\hat{p}) = \bar{s}_v(\hat{p}) \ , \tag{2.35}$$

where the effect of virtual temperature correction has been taken into account (subscript v). More details of the determination of $\lambda^+(\hat{p})$ are given in appendix A.

If $r(p,\hat{p})$ is regarded as a known function of $\ell(p,\hat{p})$, (2.27), (2.29), (2.30), (2.31) and (2.35) constitute a set of five equations in the six unknowns $\eta(p,\hat{p})$, $h_c(p,\hat{p})$, $q_c(p,\hat{p})$, $\ell(p,\hat{p})$, $\lambda^+(\hat{p})$ and $\lambda^-(\hat{p})$. In order to close the system we need another equation; at this point an empiricism is introduced by assuming that

$$\lambda^-(\hat{p}) = f[\lambda^+(\hat{p})] \ , \tag{2.36}$$

where the function f is assumed to be known. Since one of our objectives is to test the sensitivity of the model to the introduction of a continuous detrainment in the vertical for cloud type $\hat{p}$ various forms of f were tested (section 4.2) and the result is discussed in section 4.4.

The system (2.27), (2.29), (2.30), (2.31), (2.35) and (2.36) is now closed. Equations (2.27), (2.29) and (2.30) are differential equations which are solved from p_B upward provided that a boundary condition at p_B is specified. Assuming that all types of clouds share the same lower boundary condition,

$$h_c(p_B,\hat{p}) = h_M \quad , \quad q_c(p_B,\hat{p}) = q_M \quad , \quad \eta(p_B,\hat{p}) = 1 \quad ,$$

$$\text{and} \qquad \ell(p_B,\hat{p}) = 0 \ . \tag{2.37}$$

The static control loop, as shown in figure 2.1, is complete.

Let us consider now some consequences of the inclusion of a lateral detrainment for each sub-ensemble $\hat{p}$. The large-scale modification of dry static energy $\bar{s}$ produced by cumulus convection is

$$\left.\frac{\partial \bar{s}}{\partial t}\right|_C = g \frac{\partial}{\partial p} \int_{p_T}^{p} \eta(p,\hat{p})[s_c(p,\hat{p}) - L\ell(p,\hat{p}) - s(p)]m_B(\hat{p})d\hat{p}$$

$$+ Lg \int_{p_T}^{p} \eta(p,\hat{p})r(p,\hat{p})m_B(\hat{p})d\hat{p} \ , \qquad (2.38)$$

which can also be written as

$$\left.\frac{\partial \bar{s}}{\partial t}\right|_C = g \int_{p_T}^{p} \lambda^{-}(\hat{p})[s_c(p,\hat{p}) - L\ell(p,\hat{p}) - s(p)]\eta(p,\hat{p})m_B(\hat{p})d\hat{p}$$

$$+ g\eta(p,p)\,[\hat{s}(p) - L\ell(p,p) - s(p)]m_B(p)$$

$$- gM_c(p)\,\frac{\partial \bar{s}}{\partial p}\,(p) \ , \qquad (2.39)$$

where

$$\hat{s}(p) = s(p) - \frac{L\varepsilon(p)}{1+\gamma(p)\varepsilon(p)\delta}\,[\delta\bar{q}^{*}(p) - q(p)] \ ,$$

$$\text{and} \qquad \varepsilon(\hat{p}) = \frac{c_p \bar{T}(\hat{p})}{L} \ , \qquad \delta = 0.608 \ . \qquad (2.40)$$

In (2.39) the first terms can be interpreted as the effect on the environment of the detrainment of cloud dry static energy at level p due to all clouds which penetrate level p. The second term in (2.39) corresponds to the increase or decrease of $\bar{s}(p)$ (depending on the sign $\hat{s}(p) - L\ell(p,p) - \bar{s}(p)$) due to the detrainment at cloud top of sub-ensemble p. Finally, the third term can be interpreted as the parameterization of the convective change in terms of the additional

subsidence of the environment forced by the convection associated with all clouds which lose buoyancy above p. Equation (2.39) is the detrainment form of (2.13).

Similarly the detrainment form of the budget equation for moisture can be written as

$$\left.\frac{\partial \bar{q}}{\partial t}\right|_C = g\int_{p_T}^{p} \lambda^-(\hat{p})[q_c(p,\hat{p}) + \ell(p,\hat{p}) - \bar{q}(p)]n(p,\hat{p})m_B(\hat{p})d\hat{p}$$

$$+ gn(p,p)[\hat{q}(p) + \ell(p,p) - q(p)]m_B(p)$$

$$- gM_C(p)\frac{\partial \bar{q}}{\partial p}(p) , \qquad (2.41)$$

where

$$\hat{q}(p) = \bar{q}^*(p) - \frac{\gamma(p)\varepsilon(p)}{1+\gamma(p)\varepsilon(p)\delta}[\bar{q}^*(p) - \bar{q}(p)] . \qquad (2.42)$$

The first term on the RHS of (2.41) corresponds to the continuous detrainment of total water with height; the second term is the detrainment at cloud top and the third term reflects the compensating subsidence.

2.3.3. Dynamic control

The problem of parameterizing cumulus convection is now reduced to finding the mass flux distribution function $m_B(\hat{p})$. Once $m_B(\hat{p})$ is known the large-scale fields can be predicted from (2.13) and (2.14). In order to close the problem Arakawa and Schubert considered the rate of generation of kinetic energy due to work done by buoyancy forces

associated with all clouds of the same type. The work done per unit $m_B(\hat{p})$ is

$$A(\hat{p}) = \frac{R}{c_p} \int_{\hat{p}}^{p_B} \eta(p,\hat{p})[s_{v_c}(p,\hat{p}) - \bar{s}_v(p)] \frac{dp}{p} , \qquad (2.43)$$

where the index v stands for the virtual temperature effect on buoyancy. $A(\hat{p})$ is call "cloud work function" and it is an integral measure of the buoyancy force associated with cloud type $\hat{p}$, with the weighting function $\eta(p,\hat{p})$. Consequently, $A(\hat{p})$ is a measure of the efficiency of the kinetic energy generation by a certain cloud type.

The generation of kinetic energy depends not only on the condition $A(\hat{p}) > 0$, but also on $m_B(\hat{p})$, for kinetic energy generation is zero if there is no mass flux. However, if $A(\hat{p}) > 0$ we may expect the development of cumulus clouds provided that there is a triggering mechanism and, if we expect m_B to reach a significant size, $A(\hat{p})$ has to remain positive for a sufficient time. This indicates that the time rate of change of $A(\hat{p})$ may be an important parameter in cumulus parameterization.

The variables in the integrand of (2.43), as well as the upper limit of integration (in the most general case where p_B is allowed to vary), are prognostic variables or are diagnostically related to prognostic variables. Consequently, we can calculate the change of $A(\hat{p})$ in time from the prognostic equations for s_M, q_M, $\bar{s}(p)$, $\bar{q}(p)$ and p_B (eventually).

The spectral parameter in the Arakawa-Schubert cumulus parameterization theory, as originally formulated, is the fractional entrainment rate λ^+. Therefore the objective was to follow the process of

evolution of the cloud work function of a sub-ensemble λ^+ in time. It is important to note, at this point, that since we have spectrally classified clouds according to their detrainment level, we have to include the variation of $A(\hat{p})$ with time through the temporal change of the entrainment rate λ^+. Therefore we need one more predictive equation for λ^+ which is obtained by taking the time derivative of the vanishing buoyancy condition (2.35). The result is

$$\frac{\partial \lambda^+(\hat{p})}{\partial t} = \frac{\frac{\partial h_M}{\partial t} - \frac{\partial \hat{h}^*(\hat{p})}{\partial t} - \lambda^+(\hat{p}) \int_{\hat{p}}^{p_B} n(p,\hat{p})[\hat{h}^*(\hat{p}) - \bar{h}(p')]dp'}{[1+\lambda^+(\hat{p})] \cdot \int_{\hat{p}}^{p_B} n(p',\hat{p})[\hat{h}^*(\hat{p}) - \bar{h}(p')]dp'} \tag{2.44}$$

The above expression for the time change of $\lambda^+(\hat{p})$ is valid provided that $\lambda^+(\hat{p})$ is well defined in the sense of Appendix A.

Thus the change of the cloud work function in time can be expressed as

$$\frac{\partial A(\hat{p})}{\partial t} = \left(\frac{\partial A(\hat{p})}{\partial t}\right)_{\lambda^+} + \left(\frac{\partial A(\hat{p})}{\partial \lambda^+}\right)_t \frac{\partial \lambda^+}{\partial t} \quad . \tag{2.45}$$

In Arakawa and Schubert (1974) the second term on the RHS of (2.45) was ignored because the objective was to observe the time rate of change of A of cloud type λ^+.

Let us discuss now the use of $\hat{p}$ as the spectral parameter instead of λ^+. In a vertically discrete model a cloud type is characterized by its detrainment level $\hat{p}$. Thus we can not follow cloud type λ^+ in time because it would involve having a variable vertical grid spacing. In order to check the consistency of the equations in discrete form in predicting the time change of A and the reliability in the computer

coding it is necessary to interpolate the cloud work function in the λ^+-space. It turns out that this procedure is inaccurate and if the spectral parameter is the detrainment level $\hat{p}$, one source of error is eliminated [no interpolation is required in following $A(\hat{p})$]. Apart from this computational reason we have some arbitrariness in the cloud model; if the parameterization of the eddy fluxes associated with cumulus convection in the feedback loop is accepted, we might construct a different cloud model, in the static control, such that the cloud variables are not specified through the fractional rate of entrainment.

An inspection of the equations which govern the time rate of change of $\bar{s}(p)$, $\bar{q}(p)$, s_M and q_M show that they involve terms of two types: cloud terms which depend on the mass flux distribution through the eddy fluxes associated with cumulus convection (equations 2.13 and 2.14 in the feedback loop) and large-scale terms, represented by the heat and water budget equations in sections 2.2.1 and 2.2.2 respectively. The large-scale terms thus include large-scale advection (horizontal advection is absent in the present model), surface eddy fluxes and radiational heating. In a more general model an interaction between the cloud population and the radiative cooling profile should be included.

Consequently the time change of $A(\hat{p})$ can be expressed as being the sum of a large-scale change (in which surface eddy fluxes are included) and the cloud induced change,

$$\frac{\partial A(\hat{p})}{\partial t} = \left.\frac{\partial A(\hat{p})}{\partial t}\right|_C + \left.\frac{\partial A(\hat{p})}{\partial t}\right|_{LS}, \qquad (2.46)$$

where the subscripts C and LS denote the cloud terms and the large-scale terms respectively. The first term on the RHS of (2.46) is of the form expressed by (2.45).

The cloud terms linearly depend on $m_B(\hat{p})$ or are integral forms of $m_B(\hat{p})$. Because the whole spectrum of clouds participates in determining $\left.\frac{\partial A(\hat{p})}{\partial t}\right|_C$, we may write the cloud terms in the form

$$\left.\frac{\partial A(\hat{p})}{\partial t}\right|_C = \int_{p_T}^{p_B} K(p,\hat{p}) m_B(\hat{p}) d\hat{p} \ , \tag{2.47}$$

where $K(p,\hat{p})$ is the kernel. Then $K(p,\hat{p})m_B(\hat{p})d\hat{p}$ is the rate of increase of the cloud work function of sub-ensemble p through the modifications induced by cloud type $\hat{p}$.

Arakawa and Schubert's parameterization theory, as originally formulated, is closed by specifying a precise balance for each cloud sub-ensemble expressed by

$$\frac{\partial A(\hat{p})}{\partial t} = \left.\frac{\partial A(\hat{p})}{\partial t}\right|_C + \left.\frac{\partial A(\hat{p})}{\partial t}\right|_{LS} = 0 \ , \tag{2.48}$$

which is called the quasi-equilibrium assumption. Quasi-equilibrium occurs when the time scale of the large-scale forcing is much longer than the time taken by the cumulus ensemble to reach equilibrium in the absence of large-scale forcing. The quasi-equilibrium assumption expressed by (2.48) holds for each sub-ensemble $\hat{p}$ rather than λ^+ as in Arakawa-Schubert (1974). However (2.48) is still valid according to Arakawa (personal communication).

The constraint imposed by (2.48) takes the form of a Fredholm integral equation of the first kind with the further mathematical difficulty related to the non-negativity of the solution $m_B(\hat{p})$ as discussed by Arakawa and Schubert (1974). In order to overcome these difficulties another interpretation of the quasi-equilibrium assumption has been suggested (Hack and Schubert, 1976). The idea consists of minimizing the change of $A(\hat{p})$ in time thus transforming the quasi-equilibrium assumption into an optimization problem. The optimization problem takes the following mathematical form:

if S represents the subset of the $\hat{p}$ domain for

which $\left.\frac{\partial A(\hat{p})}{\partial t}\right|_{LS} > 0$,

$$\text{minimize} \quad \int_S c(\hat{p}) \frac{\partial A(\hat{p})}{\partial t} d\hat{p} \ , \tag{2.49a}$$

$$\text{subject to} \quad \frac{\partial A(\hat{p})}{\partial t} = \int_S K(p,\hat{p}) m_B(\hat{p}) d\hat{p} + \left.\frac{\partial A(\hat{p})}{\partial t}\right|_{LS} \tag{2.49b}$$

$$\text{and} \quad m_B(\hat{p}) \geq 0 \tag{2.49c}$$

$$\frac{\partial A(\hat{p})}{\partial t} \geq 0 \tag{2.49d}$$

for all $\hat{p} \varepsilon S$.

In (2.49) both $m_B(\hat{p})$ and $\frac{\partial A(\hat{p})}{\partial t}$ are regarded as unknowns while $c(\hat{p})$, $K(p,\hat{p})$ and $\left.\frac{\partial A(\hat{p})}{\partial t}\right|_{LS}$ are known. The sensitivity of the model to $c(\hat{p})$ is discussed in section 4.2. The above formulation enforces quasi-equilibrium as closely as possible while still maintaining the

non-negativity of the cloud base mass flux whenever a cloud exists (a condition given by the static control).

In 2.49a, $c(\hat{p})$ is regarded as a positive quantity if the underadjustment case is considered, i.e. if (2.49d) holds; if (2.49d) is substituted by the condition

$$\frac{\partial A(\hat{p})}{\partial t} \leq 0 \tag{2.50}$$

then we have the overadjustment case in which $c(\hat{p})$ is negative in order to maintain a mathematically well posed minimization problem. Further discussions on the underadjustment and overadjustment cases are made in section 3.4.4.

An interesting situation that may arise is when $\left.\frac{\partial A}{\partial t}\right|_{LS}$ comes out to be negative for a certain $\hat{p}$. This is possible when the large-scale processes are acting towards decreasing $A(\hat{p})$ (e.g., a sinking motion) so that the atmosphere is in a stable situation for sub-ensemble $\hat{p}$. Therefore cloud type $\hat{p}$ does not play any role in the cooperative adjustment made by all sub-ensembles as expressed by (2.49). Mathematically the domain of integration in (2.49a) and (2.49b) is reduced to $S' = [p_B, p_T] - \{\hat{p}\}$.

The discrete form of the optimization problem expressed by (2.49) turns out to be a linear programming problem as shown in section 3.4.4.

Equation (2.49) constitutes the dynamic control loop shown in Fig. 2.1. The cumulus parameterization is now closed.

2.3.4 Surface flux parameterization

The surface fluxes are given by the traditional bulk aerodynamic formulation, i.e.

$$(F_s)_S = c_p \rho_S C_D |v_S| (T_{sea} - T_S) , \tag{2.50a}$$

and

$$(F_q)_S = \rho_S C_D |v_S| [q^*(T_{sea}, p_S) - q_S] . \tag{2.50b}$$

However v_S is not a predicted variable in our model and therefore it has to be specified. In (2.50) T_S and q_S are the surface air temperature and mixing ratio and T_{sea} is the sea surface temperature.

3. GOVERNING EQUATIONS (discrete form)

For realistic vertical profiles of the thermodynamic variables it seems to be impractical to obtain analytical solutions of the governing equations. In view of this fact we must use finite difference versions of the large-scale equations (2.13) and (2.14) as well as discrete versions of the feedback, static control and dynamic control loops. The vertical differencing scheme of the large-scale equations is identical to the UCLA GCM scheme proposed by Arakawa (1972) and Arakawa, Mintz et al. (1974). The vertical differencing scheme of the cumulus-scale equation is somewhat different than the UCLA GCM scheme due to the use of the flux form in the feedback loop and the inclusion of a continuous detrainment in the vertical for each cloud type.

3.1 Vertical differencing

The vertical structure of the model is shown in Fig. 3.1. The vertical coordinate presently used is a σ-coordinate where the upper boundary (p_T) is the 100 mb surface and the surface pressure (p_S) is held constant at 1000 mb. The atmosphere between the upper and lower boundaries is divided into 18 layers. The lowest layer is the sub-cloud layer and therefore the model allows a maximum number of 17 clouds.

The index k identifies each layer. The large-scale variables $\bar{q}$ and $\bar{T}$ are carried at the integer levels k (k = 1, 2, ...18) while $\pi\dot{\sigma}$ and the cloud variables (η, h_c, q_c and ℓ) are defined at the half levels k+½ (k = 0, 1, ...18). However, the cumulus scale equations

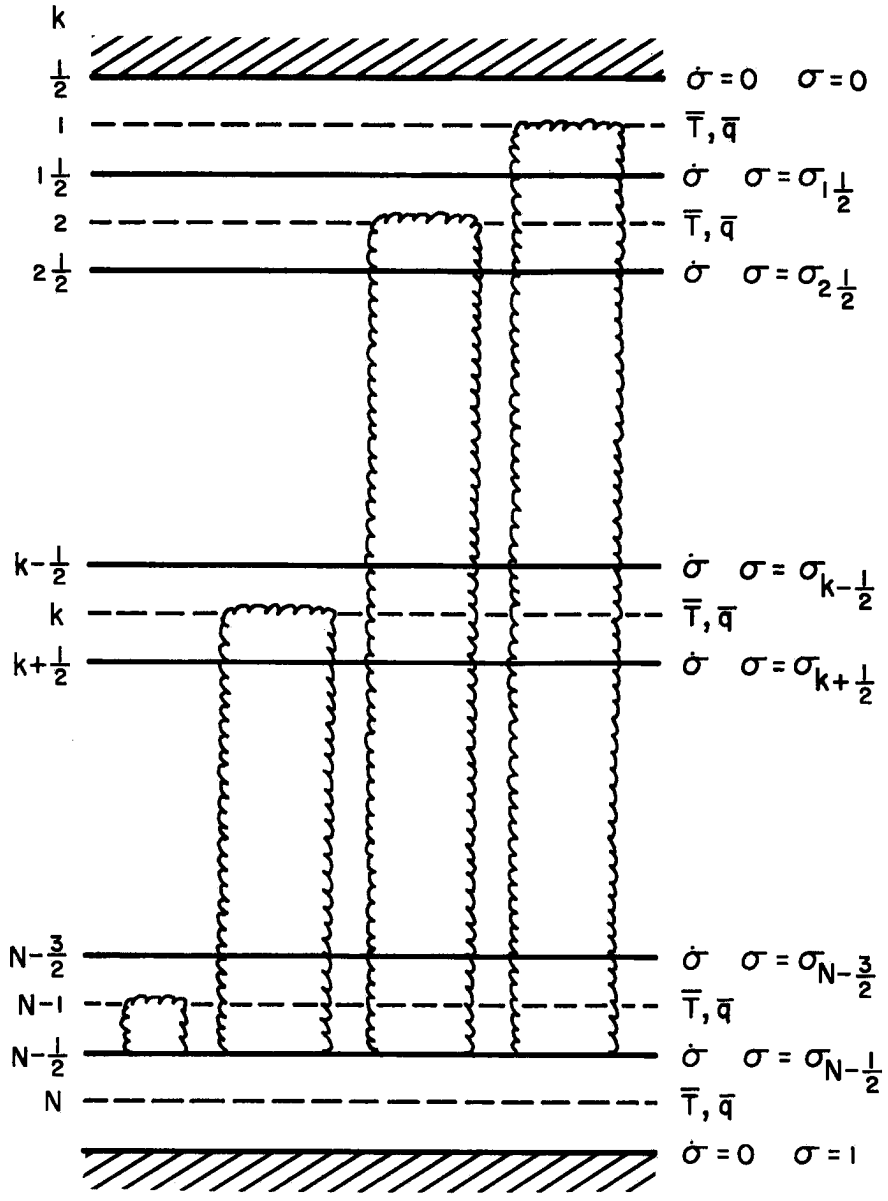

Fig. 3.1 Depiction of the vertical indexing. $\bar{T}$ and $\bar{q}$ are carried at integer levels; $\dot{\sigma}$ is computed at half levels. A cloud detraining at level k belongs to sub-ensemble k.

are written in terms of the pressure at each σ-level and the layer thickness is given by

$$\Delta p_k = \pi \Delta \sigma_k \ , \tag{3.1}$$

where

$$\pi = p_S - p_T \ , \tag{3.2}$$

and

$$\Delta \sigma_k = \sigma_{k+\frac{1}{2}} - \sigma_{k-\frac{1}{2}} \ . \tag{3.3}$$

3.2 Large-scale equations

The vertically discrete form of the large-scale part of the tendency of $\bar{s}$ can be written as

$$\left.\frac{\partial \bar{s}(k)}{\partial t}\right|_{LS} = \frac{1}{2\Delta\sigma_k}\left\{\dot{\sigma}_{k+\frac{1}{2}}[\bar{s}(k+\tfrac{1}{2}) - \bar{s}(k)] + \dot{\sigma}_{k-\frac{1}{2}}[\bar{s}(k) - \bar{s}(k-\tfrac{1}{2})]\right\} \ , \tag{3.4}$$

where

$$\bar{s}(k) = c_p \bar{T}(k) + gz(k) \ . \tag{3.5}$$

The interpolation of $\bar{s}$ at half levels in (3.4) is

$$\bar{s}(k+\tfrac{1}{2}) = \tfrac{1}{2}[\bar{s}(k) + \bar{s}(k+1)] \ . \tag{3.6}$$

The finite difference analogue of the large-scale part of the tendency of water vapor is

$$\left.\frac{\partial \bar{q}(k)}{\partial t}\right|_{LS} = \frac{1}{2\Delta\sigma_k}\left\{\dot{\sigma}_{k+\frac{1}{2}}[\bar{q}(k+\tfrac{1}{2}) - q(k)] + \dot{\sigma}_{k-\frac{1}{2}}[\bar{q}(k) - \bar{q}(k-\tfrac{1}{2})]\right\} \ . \tag{3.7}$$

According to Arakawa, Mintz et al. (1974) this form guarantees the conservation of total water vapor when there are no vapor sources and sinks. But the choice of $\bar{q}$ at half levels has to be done in a way which guarantees that $\bar{q}$ remains positive or zero and that does not tend to overestimate $\bar{q}$, eventually producing an excessive condensation in upper layers. The arithmetic average

$$\bar{q}(k+\tfrac{1}{2}) = \tfrac{1}{2}[\bar{q}(k) + \bar{q}(k+1)] \tag{3.8}$$

would produce a negative value of $\bar{q}(k)$ if $\bar{q}(k) = 0$, $\bar{q}(k+\frac{1}{2}) > 0$ and $\pi\dot{\sigma}_{k+\frac{1}{2}} > 0$, i.e. the sinking motion would remove a positive quantity of water vapor from an absolutely dry layer. There does not seem to exist a logical way to choose a particular scheme. Thus, we will use one (Hack and Schubert, 1976) which is believed to be reasonable. We repeat part of the derivation here for completeness and convenience of the reader.

Let us relate $\bar{q}(k+\frac{1}{2})$ to $\bar{q}(k)$ and $\bar{q}(k+1)$ through an interpolation of relative humidity such that

$$\frac{\bar{q}(k+\frac{1}{2})}{\bar{q}^*(k+\frac{1}{2})} = \frac{1}{2}\left[\frac{\bar{q}(k)}{\bar{q}^*(k)} + \frac{\bar{q}(k+1)}{\bar{q}^*(k+1)}\right] \tag{3.9}$$

where

$$\bar{q}^*(k) = \bar{q}^*[\bar{T}(k), p(k)] \tag{3.10}$$

and

$$\bar{q}^*(k+1) = \bar{q}^*[\bar{T}(k+1), p(k+1)] \ . \tag{3.11}$$

If we consider $\bar{q}^*(k+\frac{1}{2})$ as a known quantity based on the interpolation scheme for temperature (3.7), (3.10) may produce an interpolated value

larger than its integer level neighbors. Thus, we require that

$$\text{smaller neighbor} \leq \bar{q}(k+\tfrac{1}{2}) \leq \text{larger neighbor} \ . \tag{3.12}$$

Equation (3.10) can also be written as

$$\bar{q}(k+\tfrac{1}{2}) = \frac{\bar{q}^*(k+\frac{1}{2})}{2\bar{q}^*(k)}\,\bar{q}(k) + \frac{\bar{q}^*(k+\frac{1}{2})}{2\bar{q}^*(k+1)}\,\bar{q}(k+1) \ , \tag{3.13}$$

and if (3.12) is to be valid it is required that

$$\frac{\bar{q}^*(k+\frac{1}{2})}{2\bar{q}^*(k)} + \frac{\bar{q}^*(k+\frac{1}{2})}{2\bar{q}^*(k+1)} = 1 \ . \tag{3.14}$$

Thus $\bar{q}^*(k+\frac{1}{2})$ is the harmonic mean of $\bar{q}^*(k)$ and $\bar{q}^*(k+1)$

$$\bar{q}^*(k+\tfrac{1}{2}) = \frac{2\bar{q}^*(k)\bar{q}^*(k+1)}{\bar{q}^*(k) + \bar{q}^*(k+1)} \ . \tag{3.15}$$

Substituting (3.15) into (3.10) we obtain the interpolation formula for the mixing ratio at the half integer levels

$$\bar{q}(k+\tfrac{1}{2}) = \frac{\bar{q}^*(k+1)}{\bar{q}^*(k) + \bar{q}^*(k+1)}\,\bar{q}(k) + \frac{\bar{q}^*(k)}{\bar{q}^*(k) + \bar{q}^*(k+1)}\,\bar{q}(k+1) \ . \tag{3.16}$$

Since $\bar{q}^*(k+1)$ is typically greater than $\bar{q}^*(k)$, $\bar{q}_{k+\frac{1}{2}}$ tends to be closer to $\bar{q}(k)$ than to $\bar{q}(k+1)$. Thus a downward current is less likely to remove more water vapor than actually exists in a certain layer. At the same time this interpolation scheme does not tend to make $\bar{q}$ homogeneous in the vertical.

3.3 Large-scale precipitation

In the course of integration it is possible that the air becomes saturated and remains saturated in a large-scale sense. However, it has been our experience that, even under strong forcing by means of a large upward vertical motion, it is unlikely to observe saturation on the scale of the grid except when deep cumulus are present. The liquid water detrained at the top of deep clouds can easily saturate the environment and if there are no other mechanisms to remove it (sinking motion for example), the layer may become supersaturated.

The removal of the excess water whenever a layer is supersaturated is called large-scale precipitation. The mathematical procedure, which is described below, is identical to that developed by A. Arakawa and J. W. Kim for the UCLA GCM.

The water vapor equation can be written as

$$\frac{d\bar{q}}{dt} = - \bar{C} + \bar{E} \ , \tag{3.17}$$

and, neglecting all forms of heating other than that due to phase change, the first law of thermodynamics can be written as

$$\frac{d}{dt} (c_p \bar{T}) - \bar{\omega}\alpha = L(\bar{C} - \bar{E}) \ , \tag{3.18}$$

where $\bar{C}$ and $\bar{E}$ are respectively the rate of condensation and evaporation per unit mass of dry air. Under saturated conditions, $\bar{E}$ vanishes and $\bar{C}$ is related to the individual change of the saturation mixing ratio such that

$$\bar{C} = - \frac{d\bar{q}^*}{dt} \ . \tag{3.19}$$

The procedure in our model is to compute $\bar{q}$ and $\bar{T}$ from the discrete version of (3.17) and (3.18) for several time steps with $\bar{C}$ and $\bar{E}$ neglected (because, as noticed above, the supersaturation does not happen often and usually the degree of supersaturation is small), and then check for supersaturation. If supersaturation exists, large-scale condensation and release of latent heat is assumed to occur and the excess water is allowed to precipitate into the next lower layer where it is completely evaporated. This process may supersaturate that layer in which case the same process is repeated. When the bottom layer of the model is reached any excess is assumed to fall to the earth's surface as large-scale precipitation.

The excess water in the supersaturated case is $\bar{q}(k) - \bar{q}^*(k)$ and this condensation, denoted by $\bar{C}(k)\Delta t$, will reduce $\bar{q}(k)$ to $\bar{q}'(k)$ and increase $\bar{T}(k)$ to $\bar{T}'(k)$,

$$\bar{q}'(k) = \bar{q}(k) - \bar{C}(k)\Delta t \ , \tag{3.20}$$

$$\bar{T}'(k) = \bar{T}(k) + \frac{L}{c_p} \bar{C}(k)\Delta t \ , \tag{3.21}$$

where

$$\bar{q}'(k) = \bar{q}^*[\bar{T}'(k), p(k)] \ . \tag{3.22}$$

Equations (3.20), (3.21) and (3.23) form a closed system in the unknowns $\bar{q}'(k)$, $\bar{T}'(k)$ and $\bar{C}(k)\Delta t$. The procedure is to eliminate $\bar{q}'(k)$ and $\bar{C}(k)\Delta t$ to give

$$\bar{q}(k) - \bar{q}^*[\bar{T}'(k), p(k)] - \frac{c_p}{L} [\bar{T}'(k) - \bar{T}(k)] = 0 \ . \tag{3.23}$$

However, this is an implicit equation for $\bar{T}'(k)$ because of the complicated form of the function $\bar{q}^*(\bar{T},p)$ and consequently an iterative scheme has to be applied (Newton's method). The scheme is as follows:

a. Make an initial guess of $\bar{T}'(k)$, setting the iteration index, ν, to one.

b. Compute a new estimate of $\bar{T}'(k)$ from the previous estimate using

$$\frac{c_p}{L}\left[\bar{T}'(k)^{(\nu)} - \bar{T}'(k)^{(\nu-1)}\right] = \frac{\bar{q}(k) - \bar{q}^*\left[\bar{T}'(k)^{(\nu-1)},p(k)\right] - \frac{c_p}{L}\left[\bar{T}(k)^{(\nu-1)} - \bar{T}(k)\right]}{1+\gamma\left[\bar{T}'(k)^{(\nu-1)},p(k)\right]} \tag{3.24}$$

where

$$\gamma \equiv \frac{L}{c_p}\left(\frac{\partial \bar{q}^*}{\partial \bar{T}}\right)_p \quad . \tag{3.25}$$

c. Compute a new estimate of condensation from

$$\bar{C}(k)^{(\nu)}_{\Delta t} = \frac{c_p}{L}\left[\bar{T}'(k)^{(\nu)} - \bar{T}(k)\right] \quad . \tag{3.26}$$

d. Compute a new estimate of $\bar{q}(k)$ from

$$\bar{q}(k)^{(\nu)} = \bar{q}(k) - \bar{C}(k)^{(\nu)}_{\Delta t} \quad . \tag{3.27}$$

e. Test if

$$\left| \frac{\bar{q}^*\left[\bar{T}(k)^{(\nu)}, p(k)\right] - \bar{q}(k)^{(\nu)}}{\bar{q}^*\left[\bar{T}(k)^{(\nu)}, p(k)\right]} \right| < \text{some tolorable error.} \qquad (3.28)$$

If this is not true, set $\nu = \nu+1$ and return to (b).

f. Allow the condensate $\bar{C}(k)\Delta t$ to fall into the next lower layer and to evaporate entirely reducing $\bar{T}(k+1)$ by $\frac{L}{c_p} \bar{C}(k)\Delta t \left[\frac{\Delta\sigma(k)}{\Delta\sigma(k+1)}\right]$, and increasing $\bar{q}(k+1)$ by $\bar{C}(k)\Delta t \frac{\Delta\sigma(k)}{\Delta\sigma(k+1)}$. If the bottom layer of the model is reached the water is removed from the system as large-scale precipitation, its mass per unit horizontal area being

$$\frac{\pi}{g} [\bar{C}(k)\Delta t]\Delta\sigma_k . \qquad (3.29)$$

g. If the bottom layer of the model has not been reached return to (a) and repeat the procedure for the next level (k+1).

The tolerable error used in this model is 1×10^{-4} and it is usually reached in a few iterations whenever supersaturation is observed on the scale of the grid.

3.4 Cumulus-scale

As was emphasized in Chapter 2 the Arakawa-Schubert theory when applied in a discrete model in the vertical is conveniently adapted if

we classify clouds according to the level of vanishing buoyancy, rather than their fractional rate of entrainment.

Clouds are assumed to reach their level of vanishing buoyancy at an integer level 'j' and therefore are called cloud type 'j' (see Fig. 3.1); at this level cloud type 'j' experiences a total detrainment while cloud type 'i' ($0 < i < j$) is allowed to detrain at level 'j' at the rate of detrainment λ_i^-. Detrainment and entrainment occur at all layers centered at integer levels between cloud base and cloud top. Cloud base is assumed to be at the same level for all cloud types and is located at the top of the mixed layer ($k = N-\frac{1}{2}$).

Now we will describe the mutual interaction of a cumulus cloud ensemble with its large-scale environment in terms of the discrete version of the static control, feedback and dynamic control.

3.4.1 Static control

The sub-ensemble variables $\eta(p,\hat{p})$, $h_c(p,\hat{p})$, $q_c(p,\hat{p})$ and $\ell(p,\hat{p})$ are carried at the half levels and are denoted by $\eta(k,j)$, $h_c(k,j)$, $q_c(k,j)$ and $\ell(k,j)$. Given the thermodynamic vertical structure of the large-scale field we find the sub-ensemble variables according to the finite difference analogues of (2.27), (2.33) and (2.34) given below.

A discretization of the sub-ensemble normalized mass flux budget equation gives

$$\eta(k+\tfrac{1}{2},j) - \eta(k-\tfrac{1}{2},j) = -\lambda(j)\Delta p\,[\alpha\eta(k+\tfrac{1}{2},j) + \beta\eta(k-\tfrac{1}{2},j)]\ , \qquad (3.30)$$

where Δp is the pressure thickness of a layer centered at an integer level and bounded by the adjacent half levels. The consistency condition requires

$$\alpha + \beta = 1 \ . \tag{3.31}$$

The solution of (3.30) is

$$\eta(k-\tfrac{1}{2},j) = \frac{\eta(k+\tfrac{1}{2},j)[1 + \lambda(j)\Delta p\alpha]}{1 - \lambda(j)\Delta p\beta} \ . \tag{3.32}$$

We choose $\alpha = 1$ and $\beta = 0$ if $\lambda(j) > 0$ and $\alpha = 0$ and $\beta = 1$ if $\lambda(j) < 0$ because of the possibility of having a negative value for $\eta(k-\frac{1}{2})$ when $\lambda(j) < 0$, which is not realistic. With the boundary condition

$$\eta(N-\tfrac{1}{2},j) = 1 \ , \tag{3.33}$$

(3.32) gives us the normalized mass flux from cloud base up to level $k = j+\frac{1}{2}$. Since entrainment and detrainment can occur at each integer level above cloud base the discrete normalized mass flux can be interpreted as a step function with positive jumps at each integer level if the entrainment factor is larger than the detrainment factor and negative jumps otherwise. However at cloud top η shows a jump to zero corresponding to a total detrainment, i.e.,

$$\eta(j-\tfrac{1}{2},j) = 0 \ . \tag{3.34}$$

In terms of the boundary condition (3.33) the solution of (3.30) can also be written as

$$\eta(k-\tfrac{1}{2},j) = [1 + \lambda(j)\Delta p]^{N-k} \qquad \text{if} \quad \lambda(j) > 0 \ , \tag{3.35a}$$

$$\eta(k-\tfrac{1}{2},j) = [1 - \lambda(j)\Delta p]^{-(N-k)} \qquad \text{if} \quad \lambda(j) < 0 \ . \tag{3.35b}$$

The sub-ensemble moist static energy for $j-\frac{1}{2} \le k \le N-\frac{1}{2}$ is found in a similar way to $\eta(k-\frac{1}{2},j)$. After considering the computational

problems associated with the discrete form of (2.33) we arrived at the solution

$$h_c(k-\tfrac{1}{2},j) = \frac{h_c(k+\tfrac{1}{2},j) + \lambda^+(j)\Delta p\bar{h}(k)}{1 + \lambda^+(j)\Delta p\bar{h}(k)} \ . \qquad (3.36)$$

The above equation corresponds to a forward sequence in space where the space derivative is taken in the opposite direction of the order of integration, i.e. we start from the lower boundary condition

$$h_c(N-\tfrac{1}{2},j) = h_M = \bar{h}(N) \ , \qquad (3.37)$$

then computing $h_c(N-\tfrac{3}{2},j)$ and so on until cloud top is reached. At the level of vanishing buoyancy 'j', h_c is interpolated according to the formula

$$h_c(j,j) = \frac{h_c(j-\tfrac{1}{2},j) + h_c(j+\tfrac{1}{2},j)}{2} \qquad (3.38)$$

which is assumed to be a representative value of the moist static energy of cloud type j at the integer level 'j'.

An alternative expression for $h_c(k-\tfrac{1}{2},j)$ is

$$[1+\lambda^+(j)\Delta p]^{N-k} h_c(k-\tfrac{1}{2},j) = h_M + \sum_{i=k}^{N-1} [1+\lambda^+(j)\Delta p]^{N-i-1} \bar{h}(i) \qquad (3.39)$$

which directly relates h_c at any level with the large-scale variables h_M and $\bar{h}$. The LHS represents the flux of cloud moist static energy (h_c) at level $k-\tfrac{1}{2}$; the first term on the RHS is the flux from the mixed layer into the clouds and the second term represents the entrainment from the environmental $\bar{h}$ from cloud base up to level k. Since cloud type j does not overshoot level $j+\tfrac{1}{2}$ we set

$$h_c(j+\tfrac{1}{2},j) = 0 \tag{3.40}$$

after having calculated the interpolated value $h_c(j,j)$ (Equation 3.38) at cloud top.

According to Arakawa and Schubert (1974) q_c above cloud base is obtained by the saturation condition (2.31), its discrete analogue being

$$q_c(k-\tfrac{1}{2},j) = \bar{q}(k-\tfrac{1}{2}) + \frac{\gamma(k-\frac{1}{2})}{1+\gamma(k-\frac{1}{2})}\frac{1}{L}\left[h_c(k-\tfrac{1}{2},j) - \bar{h}^*(k)\right] , \tag{3.41}$$

where

$$\gamma(k-\tfrac{1}{2}) = \frac{L}{c_p}\left(\frac{\partial \bar{q}^*}{\partial T}\right)_{k-\frac{1}{2}} . \tag{3.42}$$

Once q_c is known the liquid water mixing ratio $(k-\tfrac{1}{2},j)$ can be determined by the discrete analogue of the total water sub-ensemble budget (e.g. (2.34)). The final expression for $\ell(k-\tfrac{1}{2},j)$ is

$$\ell(k-\tfrac{1}{2},j) = \frac{(q_c+\ell)(k+\tfrac{1}{2},j) - q_c(k-\tfrac{1}{2},j) - \lambda^+(j)\Delta p[q_c(k-\tfrac{1}{2},j) - \bar{q}(k-\tfrac{1}{2})]}{1 + \lambda^+(j)\Delta p + c_0\Delta p}$$

$$j \le k < N , \tag{3.43}$$

with the boundary condition

$$\ell(N-\tfrac{1}{2},j) = 0 . \tag{3.44}$$

In order to get (3.43) the rain term was parameterized by an autoconversion coefficient (Arakawa and Schubert, 1974), i.e. $r(k,j) = c_0\ell(k,j)$, which will be discussed in section 4.2.

In order to close the static control we have to determine the fractional entrainment rate λ^+ for each cloud type ($\lambda^+(j)$, $j = 0, 1, \ldots N-1$). This is done by a modified form of the vanishing buoyancy condition (Equation 2.35) (Arakawa, 1972) expressed in its discrete form as

$$\hat{h}^*(j) - h_c(j,j) = 0 \ , \tag{3.45}$$

where $\hat{h}^*$ is given by

$$\hat{h}^*(j) = \bar{h}(j) - \frac{L\varepsilon(j)\delta}{\beta(j)} [\bar{q}^*(j) - \bar{q}(j)] \ , \tag{3.46}$$

with

$$\varepsilon(j) = \frac{c_p \bar{T}(j)}{L} \quad \text{and} \quad \beta(j) = \frac{[1 + \gamma(j)\varepsilon(j)\delta]}{1 + \gamma(j)} \ . \tag{3.47}$$

If we substitute $h_c(j,j)$ by its value given by (3.38) and then express $h_c(j+\frac{1}{2},j)$ and $h_c(j-\frac{1}{2},j)$ in terms of the large scale variable $\bar{h}(i)$ ($i = j, j+1, \ldots N$) we would obtain a $(N-\ell+1)^{th}$ degree polynomial in $\lambda^+(j)$. Instead of following this approach we define a function $G(j)$ by

$$G(j) = \hat{h}^*(j) - h_c(j,j) \ , \tag{3.48}$$

so that $\lambda^+(j)$ is a root of (3.45) which can be determined by an iterative process. The variable secant method finds the solution in a reasonable number of iterations (four or five) although this process needs two initial guesses to determine an improved root. Concerning computer time it is our experience that it is better to use the variable secant method than Newton's method due to the complexity and

cumbersome calculations involved in the derivative of G(j) with respect to $\lambda^+(j)$ in the later method, although it takes fewer iterations to reach the refined solution. The iteration formula has the following form in the variable secant method,

$$\lambda^+_{(n+1)}(j) = \lambda^+_{(n)}(j) - \frac{G_{(n)}(j)\,[\lambda^+_{(n)}(j) - \lambda^+_{(n-1)}(j)]}{G_{(n)}(j) - G_{(n-1)}(j)}\ , \qquad (3.49)$$

where the subscript n is the iterative index. However not all solutions of (3.45) are physically acceptable. A negative $\lambda^+(j)$ has to be rejected because $\lambda^+(j)$ is the fractional rate of entrainment. Of course the existence of a positive $\lambda^+(j)$ is related to the condition

$$h_M - \hat{h}^*(j) > 0\ . \qquad (3.50)$$

As long as (3.50) is satisfied cloud type j has the possibility to exist given a certain large-scale thermodynamic field although this is not a sufficient condition as is discussed in Appendix A. Actually, we only check for the saturated case under the conditionally unstable case ($\frac{\partial \bar{h}^*}{\partial p} > 0$). Otherwise we check for convergence in the variable secant method; if it fails to converge the discrete analogue of (A.7) is observed.

Cloud top has been defined as the level at which the cloud first reaches equilibrium with the environment in terms of buoyancy, taking into account the effect of the virtual temperature correction. In order to be consistent with the non-overshooting cloud model presented by Arakawa and Schubert, we have to check the positive buoyancy condition of each level k below the detrainment level of cloud type j.

This condition is verified if

$$h_c(k,j) > \hat{h}^*(k) \qquad k = j+1,\ j+2,\ \ldots N-1 \tag{3.51}$$

excluding the positive buoyancy condition at level N-1 for cloud types j = 1, 2, ...N-2 because we assume that the parcel has enough energy at the top of the mixed layer to overcome a negative buoyancy force at level N-1.

A negative buoyant region may be found below the zero-buoyancy level whenever a strong inversion is present. As shown by Nitta (1975), this situation is typical of the trade cumulus region where most of the clouds detrain below the trade inversion which can happen in our model.

The sequence of computations that are performed in the static control are summarized below:

i) Determine the large-scale variables $\bar{h}(i)$ and $\bar{h}^*(i)$ (i = 1, 2, ...N-1) and the interpolated values of the large-scale variables $\bar{h}(i+\frac{1}{2})$ and $\bar{q}(i+\frac{1}{2})$ (i = 0, 1, ...N).

ii) Check the condition $h_M \geq \hat{h}^*(j)$ for the deepest cloud. If it is not satisfied go to the next lower integer level and return to step (ii).

iii) Check if $\bar{h}(j) \geq \hat{h}^*(j)$ and $\frac{\partial h}{\partial p} < 0$ are satisfied simultaneously. Otherwise go to the next lower integer level and return to step (ii).

iv) Given two initial guesses of $\lambda^+(j)$ calculate $h_c(j,j)$.

v) Calculate G(j); if G(j) < 1 J kg^{-1}, which is equivalent to a difference of about 10^{-3} K between the virtual temperature of the representative

cloud top and the environment, go to step (vi). Otherwise compute a new $\lambda^+(j)$ by the variable secant method and re-calculate G(j).

vi) Now that $\lambda^+(j)$ is known with sufficient accuracy determine q_c, ℓ, $\lambda^-(j) = f[\lambda^+(j)]$ and η. After computing these terms go to the next lower level and return to step (ii).

The set of five variables $\eta(k+\frac{1}{2},j)$, $h_c(k+\frac{1}{2},j)$, $q_c(k+\frac{1}{2},j)$, $\ell(k+\frac{1}{2},j)$ ($k = 0, 1, \ldots N-1$) and $\lambda^+(j)$ ($j = 1, 2, \ldots N-1$) constitute the discrete static control.

3.4.2 Feedback loop

The cumulus transport terms $F_{s-L\ell}$, $F_{q+\ell}$ and R in (2.13) and (2.14) constitute the cumulus effect on the feedback loop shown in Fig. 2.1. The objective of this section is to find a finite difference scheme which is consistent with the finite difference form of the equations in the static control and that yields a reasonable discrete analogue of the detrainment form of the large-scale budget equations for $\bar{s}$ and $\bar{q}$.

Let us consider the moisture budget equation when only cumulus effects are considered. This equation, in continuous form, is

$$\left.\frac{\partial \bar{q}}{\partial t}\right|_C = g \frac{\partial F_{q+\ell}}{\partial p} - R \,. \tag{3.52}$$

The finite difference form of the first term on the RHS of (3.52) is

$$g\frac{\partial F_{q+\ell}}{\partial p} \approx \frac{g}{\Delta p}\left\{\sum_{j=1}^{k}\eta(k+\tfrac{1}{2},j)[q_c(k+\tfrac{1}{2},j)+\ell(k+\tfrac{1}{2},j)-\bar{q}(k+\tfrac{1}{2})]M_B(j)\right.$$

$$\left.-\sum_{j=1}^{k-1}\eta(k-\tfrac{1}{2},j)[q_c(k-\tfrac{1}{2},j)+\ell(k-\tfrac{1}{2},j)-\bar{q}(k-\tfrac{1}{2})]M_B(j)\right\} . \qquad (3.53)$$

The subgrid scale flux of $q_c+\ell$ at a certain half level $k+\frac{1}{2}$ is dependent on all clouds which detrain above $k+\frac{1}{2}$, i.e. the summation, which is the discrete analogue of the integral in the definition of F_q (Equation 2.8), and ranges from cloud type 1 to k. $M_B(j)$ is the sub-ensemble cloud base mass flux of clouds detraining at level j. It is related to $M_B(\hat{p})$ by

$$M_B(j) = \int_{\hat{p}_j-\frac{\Delta p}{2}}^{\hat{p}_j+\frac{\Delta p}{2}} M_B(p)dp . \qquad (3.54)$$

The discrete form of R in (3.52) which yields a discrete analogue of (3.52) equivalent to the detrainment form of (3.52) (Equation 2.41) is

$$R(k) = \sum_{j=1}^{k-1} gn(k+\tfrac{1}{2},j)c_o(j)\ell(k-\tfrac{1}{2},j)M_B(j) . \qquad (3.55)$$

3.4.3 Dynamic control

The closure of the Arakawa-Schubert cumulus parameterization theory is, as we have seen (section 2.3.3), made by the quasi-equilibrium assumption and the optimal adjustment method (Equation 2.49) which are now going to be formulated in discrete form.

The discrete analogue of the cloud work function for cloud type 'j' is

$$A(j) = \sum_{k=j}^{N-1} \eta(k+\tfrac{1}{2},j)\Big\{[h_c(k+\tfrac{1}{2},j)]\beta(k) + L\varepsilon(k)\delta[\bar{q}^*(k) - \bar{q}(k)]\Big\}\frac{\hat{\Delta}p}{p_b(k)} + \eta(k-\tfrac{1}{2},j)\Big\{[h_c(k-\tfrac{1}{2},j) - \bar{h}^*(k)]\beta(k) + L\varepsilon(k)\delta[\bar{q}^*(k) - \bar{q}(k)]\Big\}\frac{\hat{\Delta}p}{p_u(k)} \quad , \tag{3.56}$$

where the effect of the virtual temperature correction is included. The discrete normalized mass flux η and the moist static energy 'h_c' of the cloud sub-ensembles are defined by (3.35) and (3.39), respectively, and considered at half levels; β and ε are given by (3.47) at integer levels; the large-scale variables $\bar{h}^*$, $\bar{q}^*$ and $\bar{q}$ are also defined at integer levels; the pressure interval of integration is

$$\hat{\Delta}p = \frac{\Delta p}{2} \tag{3.57}$$

while

$$p_b(k) = \frac{p_k + p_{k+\frac{1}{2}}}{2} \quad , \tag{3.58a}$$

$$p_u(k) = \frac{p_k + p_{k-\frac{1}{2}}}{2} \quad . \tag{3.58b}$$

In order to express the discrete change in time of A(j) we could consider the difference $A^{(n)}(j) - A^{(n-1)}(j)$, where the superscript refers to time step, and then rearrange the terms in such a way to isolate the predictive variables $\bar{h}$, $\bar{q}$ and λ^+. However, it turns out that this process yields a highly implicit relationship for M_B which is

computationally inadequate because it is time consuming in terms of computer time. Therefore we sacrifice exactness for efficiency in considering a first order approximation of the change of A(j).

The discrete cloud work function A(j) can be considered as a function of $\eta(k+\frac{1}{2},j)$, $h_c(k+\frac{1}{2},j)$ $(k = j, j+1, \ldots N-1)$, $\bar{h}^*(k)$, $\bar{q}^*(k)$ and $\bar{q}(k)$ $(k = j, j+1, \ldots N-1)$. Then an increment in A(j) will be related to an increment in η, h_c, $\bar{h}^*$, $\bar{q}^*$ and $\bar{q}$ by

$$A(j) \approx \sum_{k=j}^{N-1} \left[\frac{\partial A(j)}{\partial \eta(k+\frac{1}{2},j)} \Delta\eta(k+\tfrac{1}{2},j) + \frac{\partial A(j)}{\partial h_c(k+\frac{1}{2},j)} \Delta h_c(k+\tfrac{1}{2},j) \right.$$

$$+ \frac{\partial A(j)}{\partial \bar{h}^*(j)} \Delta\bar{h}^*(j) + \frac{\partial A(j)}{\partial \bar{q}^*(j)} \Delta\bar{q}(j)$$

$$\left. + \frac{\partial A(j)}{\partial \bar{q}(k)} \bar{q}(k) \right] \qquad (3.59)$$

provided that $\Delta\eta(k+\frac{1}{2},j)$, $\Delta h_c(k+\frac{1}{2},j)$, $\Delta\bar{h}^*(k)$, $\Delta\bar{q}^*(k)$ and $\Delta\bar{q}(k)$ are small.

Let's expand now each of the five terms under the summation sign in (3.59). The first term is

$$\frac{\partial A(j)}{\partial \eta(k+\frac{1}{2},j)} \Delta\eta(k+\tfrac{1}{2},j) = \left\{ [h_c(k+\tfrac{1}{2},j) - \bar{h}^*(k)]\beta(k) \right.$$

$$\left. + L\varepsilon(k)\delta[\bar{q}^*(k) - \bar{q}(k)] \right\} \frac{\hat{\Delta p}}{p_u(k)} (N-k)[1 + \lambda(j)\Delta p]^{N-k-1} \Delta p \frac{\partial \lambda(j)}{\partial \lambda^+(j)} \Delta\lambda^+(j) . \qquad (3.60)$$

In (3.60) we approximated $\Delta\eta$ by $\frac{\partial \eta}{\partial \lambda} \Delta\lambda$. The second term depends on $\Delta h_c(k+\frac{1}{2},j)$ which, according to (3.39), is a function of h_M, h(i) $(i = k, \ldots N-1)$ and $\lambda^+(j)$. Therefore

$$\Delta h_c(k+\tfrac{1}{2},j) \approx \frac{\Delta h_M}{[1+\lambda^+(j)\Delta p]^{N-k}} + \lambda^+(j)\,\frac{\sum_{i=N-1}^{k}[1+\lambda^+(j)\Delta p]^{N-i-1}\Delta p\Delta\bar{h}(i)}{[1+\lambda^+(j)\ p]^{N-k}}$$

$$+\Bigg[(-N+k)[1+\lambda^+(j)\Delta p]^{-N+k-1}\Delta p\, h_c(k+\tfrac{1}{2},j)[1+\lambda^+(j)\Delta p]^{N-k}$$

$$+[1+\lambda^+(j)\Delta p]^{-N+k}\Bigg\{\sum_{i=N-1}^{k}[1+\lambda^+(j)\Delta p]^{N-i-1}\Delta p\,\bar{h}(i)$$

$$+\lambda^+(j)\sum_{i=N-1}^{k}(N-i-1)[1+\lambda^+(j)\Delta p]^{N-i-2}\Delta p^2\bar{h}(i)\Bigg\}\Bigg]\Delta\lambda^+(j)$$

for $k \le N-1$. (3.61)

Let us define the following function:

$$a(i,j) = [1+\lambda^+(j)\Delta p]^{N-i} \qquad j \le i \le N\ ,\ j = 1, 2, \ldots N-1 \tag{3.62}$$

The second term under the summation sign in (3.59) can now be written as, after rearranging terms and applying the definition (3.62),

$$\frac{\partial A(j)}{\partial h_c(k+\frac{1}{2},j)}\,\Delta h_c(k+\tfrac{1}{2},j) = \frac{\beta(k)\eta(k+\frac{1}{2},j)\hat{\Delta p}}{p_u(k)}\Bigg(\frac{\Delta h_M}{a(k,j)}$$

$$+\frac{\lambda^+(j)\sum_{i=N-1}^{k}a(i+1,j)\Delta p\Delta\bar{h}(i)}{a(k,j)}$$

$$+\Bigg\{\frac{(-N+k)\Delta p\, h_c(k+\tfrac{1}{2},j)a(k,j)}{a(k-1,j)}$$

$$+\frac{\hat{\Delta p}}{a(k,j)}\Bigg[\sum_{i=N-1}^{k}a(i+1,j)\Delta p\bar{h}(i)$$

$$+\lambda^+(j)(N-i-1)a(i+2,j)\Delta p^2\bar{h}(i)\Bigg]\Bigg\}\Delta\lambda^+(j)\Bigg)\ . \tag{3.63}$$

In order to compute the third term in (3.59) we observe that

$$\Delta\bar{h}^*(k) = \Delta\bar{s}(k) + L\Delta\bar{q}^*(k) = [1+\gamma(k)]\Delta\bar{s}(k) \ , \tag{3.64}$$

(Arakawa and Schubert, 1974). Consequently

$$\frac{\partial A(j)}{\partial\bar{h}^*(k)}\,\Delta\bar{h}^*(k) = -\beta(k)\left[\frac{n(k+\frac{1}{2},j)}{p_b(k)} + \frac{n(k-\frac{1}{2},j)}{p_u(k)}\right]\hat{\Delta}p\,[1+\gamma(k)]\Delta\bar{s}(k) \ , \tag{3.65}$$

and analogously,

$$\frac{\partial A(j)}{\partial\bar{q}^*(k)}\,\Delta\bar{q}^*(k) = \beta(k)L\epsilon(k)\delta\left[\frac{n(k+\frac{1}{2},j)}{p_b(k)}+\frac{n(k-\frac{1}{2},j)}{p_u(k)}\right]\hat{\Delta}p\,\frac{\gamma(k)}{L}\,\Delta\bar{s}(k) \ . \tag{3.66}$$

Finally the last term in (3.59) can be written as

$$\frac{\partial A(j)}{\partial\bar{q}(k)}\,\Delta\bar{q}(k) = -\beta(k)L\epsilon(k)\delta\left[\frac{n(k+\frac{1}{2},j)}{p_b(k)} + \frac{n(k-\frac{1}{2},j)}{p_u(k)}\right]\hat{\Delta}p\,\Delta\bar{q}(k) \ . \tag{3.67}$$

The local variation of A(j) with time can now be written with the help of the predictive equations for $\bar{h}$, $\bar{s}$, $\bar{q}$ and h_M since $\frac{\partial\lambda^+}{\partial t}$ can be expressed as a function of $\frac{\partial\bar{h}}{\partial t}$, $\frac{\partial\bar{s}}{\partial t}$, $\frac{\partial\bar{q}}{\partial t}$ and $\frac{\partial h_M}{\partial t}$ (Appendix A). As in the continuous case, the cloud terms linearly depend on M_B and a discrete version of the kernel can be obtained (as shown by Hack, 1977).

3.4.4 Optimal adjustment method as a linear programming problem

The discrete form of (2.49) can be interpreted as a linear programming problem and is called the optimal adjustment method. The idea is to minimize the change of the cloud work function, made by both large-scale and convective-scale processes during the time interval over which those processes are acting (e.g. large-scale vertical motion,

radiational cooling and surface fluxes), through the stabilizing effects of cumulus convection. Before introducing the mathematical formulation of the optimal adjustment method it is convenient to analyze the problem of separation of scales suggested in the expression for the time rate of change of A(i) (large-scale and cumulus-scale), specifically, the large-scale forcing imposed by a large-scale vertical motion.

The general stability of the tropical atmosphere, including lower layers, suggests the need for a lifting mechanism to initiate parcel condensation up to the level of free convection. According to Lopez (1973), in order to generate cumulus over the oceans, the convergence under individual cumulus has to be of the magnitude of approximately $5 \times 10^{-3} s^{-1}$, i.e. much larger than the observed large-scale convergence. The objective of cumulus parameterization is to estimate the mass flux associated with the large-scale convergence underneath each cloud type ($m_B(\hat{p})$) and then compute the changes induced in the large-scale environment through cumulus convection (through a cloud model-static control and the feedback loop).

The large-scale vertical motion is interpreted as being the large-scale forcing imposed by a certain convergence-divergence field that acts over the averaging area. The vertical motion produced by such forcing at cloud base releases itself in weak spots, namely, cumulus clouds. The area average of the cloud base mass flux and the mass flux in the environment equals $\bar{\omega}(p_B)$ and the same argument is valid at any other level.

From the numerical modeling point of view, the idea is to allow the large-scale forcing to act during a certain time interval thus

modifying the cloud work function and then adjust its value through the cumulus induced changes (feedback loop). Therefore during a certain time interval, Δt_c, the model atmosphere does experience a large-scale motion (Fig. 3.2a); after having determined the adjustment that ought to be made for each sub-ensemble i, a cloud base mass flux is obtained as a consequence of the quasi-equilibrium assumption. During the adjustment period the cumulus are supposed to act over an atmosphere with $\bar{\omega}(k) = 0$ so that no mass flows through a hypothetical vertical wall around the large-scale averaging area (Fig. 3.2b).

The interaction between an ensemble of cumulus and the large-scale environment is thus assumed to take place in two phases: phase (a) corresponds to the large-scale forcing which may increase A(i), once the large-scale processes are "frozen"; phase (b) allows cumulus clouds to minimize the change A(i), reducing its value (typically the kernel is negative). The process described in phase (b) of the interaction between a cumulus ensemble and the large-scale environment is the so-called optimal adjustment method.

It should be observed that the final result in terms of mass transport, after phases (a) and (b), is that the large-scale vertical motion is a composition of the cloud mass flux (M_c) and the residual mass flux in the environment ($\tilde{\omega} = \bar{\omega} - M_c$).

Up to this point we have considered the large-scale forcing in A(i) imposed by a large-scale vertical motion $\bar{\omega}$. As we have seen, the second term on the RHS of (2.48) $\left[\frac{\partial A(i)}{\partial t}\Big|_{LS}\right]$ includes the effects of radiation and surface fluxes of heat and moisture (all of which usually tend to increase $A(\hat{p})$). In this case the destabilizing mechanism

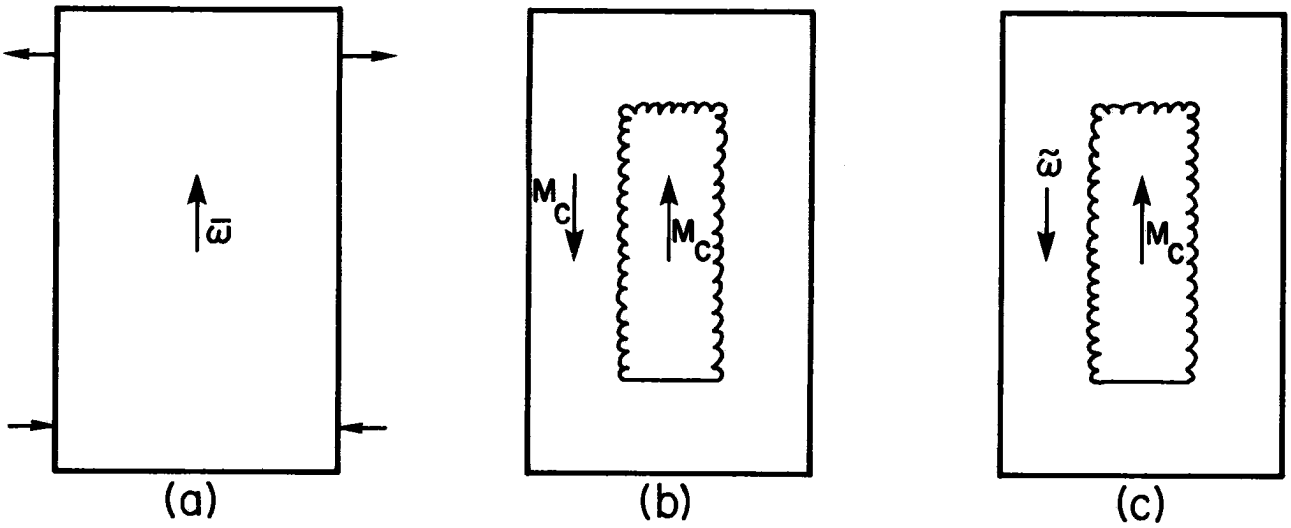

Fig. 3.2 Idealized view of the interaction between a cloud and its environment in terms of mass exchange. During a certain time interval Δt_c the model atmosphere experiences a large-scale vertical motion (a). The large-scale forcing is then temporarily neglected and the quasi-equilibrium assumption determines the cloud mass flux M_c (b). The result after phases (a) and (b) is an upward mass flux through the cloud (M_c) and an environmental movement $\tilde{\omega}$ (generally an environmental subsidence $\tilde{\omega} = \bar{\omega} - M_c > 0$).

represented by the large-scale vertical motion in phase (a) is replaced by the other forms of the large-scale forcing, radiation and surface fluxes. Phase (b) remains unaltered so that the net environmental vertical motion $\tilde{\omega}$ is controlled by radiation and the surface fluxes besides the large-scale $\bar{\omega}$ forcing.

As previously suggested, the quasi-equilibrium assumption can be interpreted as an optimization problem in which the objective is to minimize the time change of the cloud work function.

In order to understand the discrete form of the optimal adjustment method we start from the observational fact that the rate of change of A(i) is small compared to the large-scale forcing of A(i) $\left(\left.\frac{\partial A(i)}{\partial t}\right|_{LS}\right)$ and that having a positive A(i) does not imply the existence of cumulus cloud activity in the tropics in the absence of a triggering mechanism. The existence of a critical value of A(i), above which cumulus activity is assumed to develop, is then suggested.

Let us suppose now that we perform a hypothetical numerical experiment with an initial condition of stability in the sense that A(i) is smaller than the critical value $A_c(i)$ for every cloud type. If there is a destabilizing large-scale forcing, expressed by the second term of (2.48), cloud activity will not develop in order to oppose the destabilization process until A(i) reaches $A_c(i)$. From now on clouds will oppose the destabilization in such a way as to minimize the increase of A(i) forced by the large-scale processes represented by $\left.\frac{\partial A(i)}{\partial t}\right|_{LS}$ ($\bar{\omega}$, radiation, surface fluxes, etc.).

If we assume that the adjustment in A(i), made by cumulus activity, never brings A(i) to a value smaller than $A_c(i)$, we have an

underadjustment (because $A(i) \geq A_c(i)$ always). On the other hand we might assume that cumulus clouds are very efficient in reducing the cloud work function so that A(i) is brought below the critical value $A_c(i)$ corresponding to an overadjustment. The perfect equilibrium occurs if A(i) is brought exactly to $A_c(i)$.

Fig. 3.3a corresponds to the underadjustment case in which the large-scale forcing is assumed to have increased the cloud work function to $A(i)\big|_{LS}$ during the time span of the large-scale routine Δt_c. At this point the cumulus subroutine is called to bring A(i) as close as possible to $A_c(i)$ (preserving feasibility, i.e. $M_B(j) > 0$ for all j's) on the positive side,

$$A(i) \geq A_c(i) \ . \tag{3.68a}$$

The overadjustment case is represented in Fig. 3.3b and it is characterized by

$$A(i) \leq A_c(i) \ . \tag{3.68b}$$

A perfect adjustment corresponds to the equality sign in (3.68), and this is what we seek. Thus the objective is to minimize some convex function of $\delta A(i)$ in the general case, i.e.,

$$\min f[\delta A(i)] \tag{3.69}$$

where

$$\delta A(i) = A(i)\big|_{LS} + [\delta A(i)]_C - A_c(i) \tag{3.70}$$

subjected to

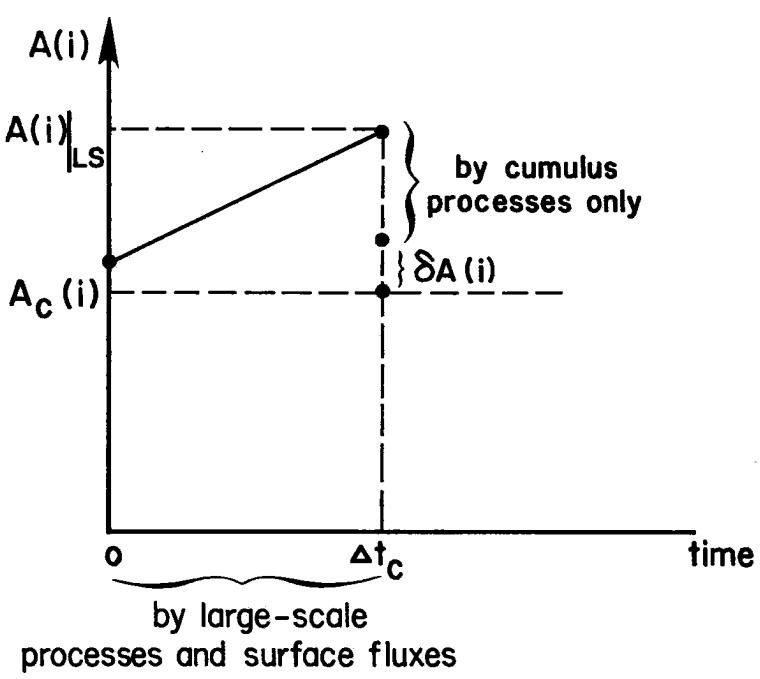

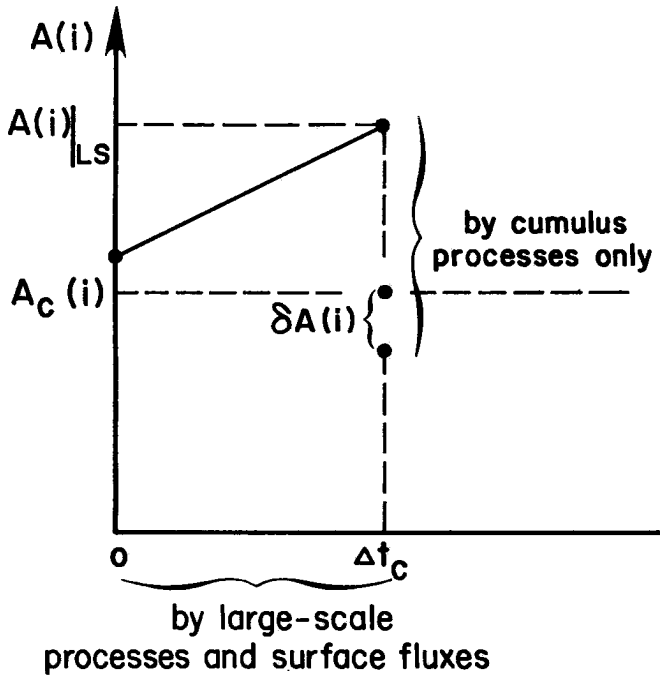

Fig. 3.3 (a) A(i) is increased during the time interval Δt_c by the forcing to $A(i)_{LS}$; then t cumulus subroutine is called bringing $A(i)_{LS}$ to $A_c(i) + \delta A(i)$ ($\delta A(i) \geq 0$) correspo to an underadjustment. (b) Same as case (a) except that it shows the overadjustme approach ($\delta A(i) \leq 0$).

$$[\delta A(i)]_C \geq A_c(i) - A(i)\Big|_{LS} = B(i) , \tag{3.71}$$

which is supposed to have taken place during the time interval Δt_c. Equation (3.71) corresponds to the underadjustment case, and if the overadjustment is considered the inequality sign has to be replaced by $\leq$. But $\frac{\partial A(i)}{\partial t}\Big|_C$ [1] is given by (2.47) and after multiplying both sides of (3.71) by -1 and noticing that under unstable situations the right hand side of (3.71) is negative we can easily transform the inequality to an equality through the introduction of slack variables $x(i)$ ($x(i) \geq 0$) which are a measure of how close the inequality is to the equality (i.e. to the perfect equilibrium in terms of $A_c(i)$). Thus, in the underadjustment case the minimization problem takes the form

$$\min \sum_{i=1}^{N-1} c(i)\, x(i) \tag{3.72a}$$

subject to

$$-\sum_{j=1}^{N-1} K(i,j) M_B(j) + x(i) = -B(i) , \tag{3.72b}$$

$$M_B(j) \geq 0 , \tag{3.72c}$$

$$x(i) \geq 0 , \tag{3.72d}$$

assuming that $f(\delta A(\hat{p}))$ is linear. In vector form we have

$$\min \; \mathbf{c}\,\mathbf{x} , \tag{3.73a}$$

---

[1] $\frac{\partial A(i)}{\partial t}\Big|_C dt = \delta A(i)\Big|_C$

subject to

$$- \mathbb{K}\,\mathbb{M}_B + \mathbb{x} = - \mathbb{B} \ , \tag{3.73b}$$

$$\mathbb{M}_B \geq 0 \ , \tag{3.73c}$$

$$\mathbb{x} \geq 0 \ , \tag{3.73d}$$

where $\mathbb{K}$ is the kernel matrix, $\mathbb{M}_B$ is the cloud base mass flux matrix and $\mathbb{x}$ is the slack variable which is a measure of the adjustment.

The problem represented by (3.73) is typical of linear programming and it can be easily solved by the simplex method. An initial basic feasible solution is provided by the slack variable x in order to start the simplex procedure when the underadjustment approach is being used. However if the overadjustment is considered such an initial basic feasible solution is not provided, making this approach disadvantageous from the point of view of computational time.

If there is a perfect equilibrium in the sense that A(i) is brought back to $A_c(i)$ for all possible i, it is clear that (3.73) has a minimum value of zero with $\mathbb{x} = 0$ and hence, except for degeneracy, the final solution will consist of all M_B being basic. The optimal basic feasible solution may, eventually, consist of both cloud base mass fluxes $M_B(i)$ and slack variables x(i) in which case (3.73) will have a minimum value different from zero except for degeneracy, which has not been found in the results presented here.

A discussion about the choice of the cost function $\mathbf{c}$ in (3.73) is made in section 4.2.

4. RESULTS

The objective of the experiments to be described now is to study the sensitivity of the Arakawa-Schubert cumulus parameterization theory, with the quasi-equilibrium assumption expressed as an optimization problem, to changes in the large-scale forcing $\left[\left(\frac{\partial A(\hat{p})}{\partial t}\right)_{LS}\right]$ and to specified parameters such as the detrainment rate $\lambda^{-}(\hat{p})$, the parameterization of rain and the weights on the adjustment function.

4.1 The Large-Scale Forcing

The large-scale forcing consists of a dynamical forcing represented by an imposed large-scale vertical motion $\bar{\omega}$, a radiative cooling profile and surface fluxes. The forcing acts upon the temperature and moisture fields given by Yanai's Marshall Islands observations at Eniwetok, which is located in the ITCZ (Yanai et al., 1973). Fig. 4.1 shows the vertical profile of the dry static energy $\bar{s}$, moist static energy $\bar{h}$ and saturation moist static energy $\bar{h}^*$ of the basic atmosphere over which the cumulus are supposed to act. Yanai's relative humidity field closely follows the typical profile of the Western Pacific cluster-environment areas (Gray et al., 1975). The temperature field used in this research is slightly more unstable in the lower troposphere than the typical cluster-environment region but similar to the mean tropical summer atmosphere of Jordan (1958).

The large-scale forcing is assumed to act during a certain time period generally destabilizing the atmosphere in the sense of increasing $A(\hat{p})$; then the cumulus subroutine is called which, in its turn,

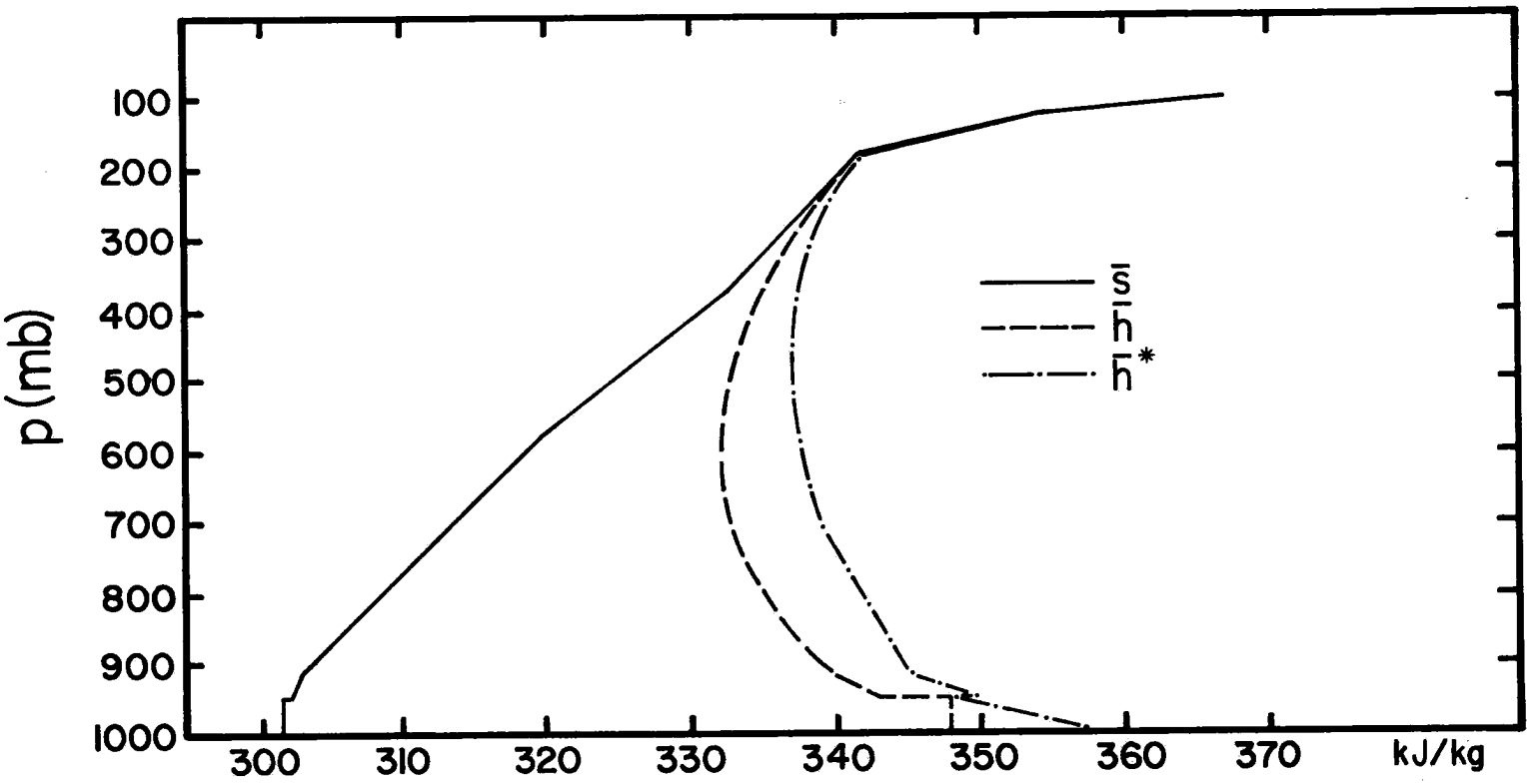

Fig. 4.1 Vertical profiles of the dry static energy $\bar{s}$, moist static energy $\bar{h}$ and saturation moist static energy h^*, based on Yanai's Marshall Islands observations (Yanai et al., 1973).

tries to minimize the change in $A(\hat{p})$ (for all $\hat{p}$) through the cumulus effects on the large-scale environment as shown in the feedback loop (Fig. 2.1). After one complete cycle through the large-scale forcing and subsequent stabilization by the cumulus subroutine (in terms of the cloud work function) the temperature and moisture fields are returned to the basic values, given by Yanai's data. Therefore we will be interested in studying the temperature and moisture tendencies ($\frac{\partial \bar{T}}{\partial t}$ and $\frac{\partial \bar{q}}{\partial t}$ respectively) after the complete cycle. Fig. 4.2 shows a schematic picture of the complete cycle represented by the large-scale forcing terms and the cumulus terms in the feedback loop equations. It is important to note that only the large-scale forcing changes in time since the modified temperature and moisture fields after the complete cycle are not allowed to feedback during the time span of the large-scale forcing.

In order to compare our results to observational studies we chose Reed and Recker's $\bar{\omega}$ field (Reed and Recker, 1971) assuming a five day period since 18 waves passed the stations during the three month period of their study giving an average interval between successive ridge portions of approximately five days. An analytical expression for $\bar{\omega}$ was obtained by considering the first 3 harmonic components of Reed and Recker's $\bar{\omega}$ field at each half-level. As shown in Fig. 4.3 the first 3 harmonics reproduce most of the original features such as the maximum upward velocity slightly to the west of the trough in the middle troposphere and the eastward tilt with height of the axis of maximum vertical motion. Upward motion predominates throughout the 5-day period and only

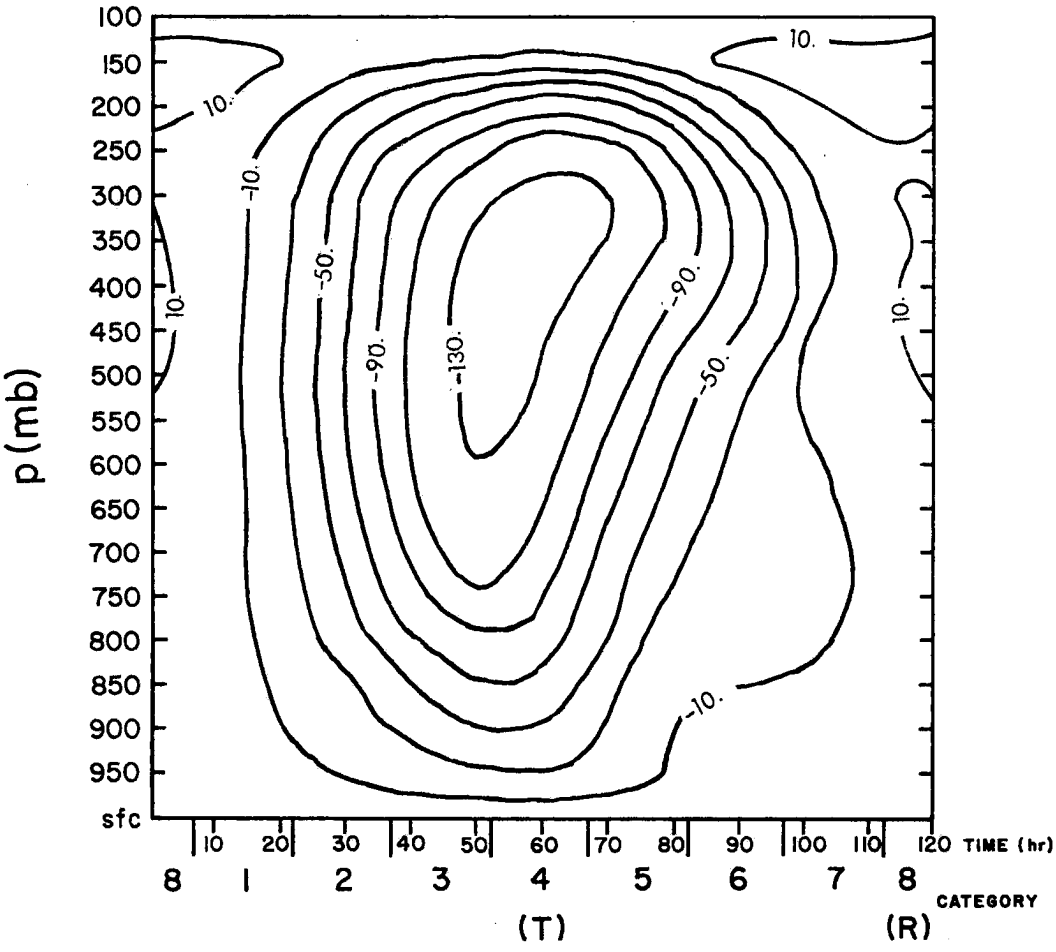

Fig. 4.3 Reed and Recker's $\bar{\omega}$-field after being harmonically analyzed (units in mb·day^{-1}).

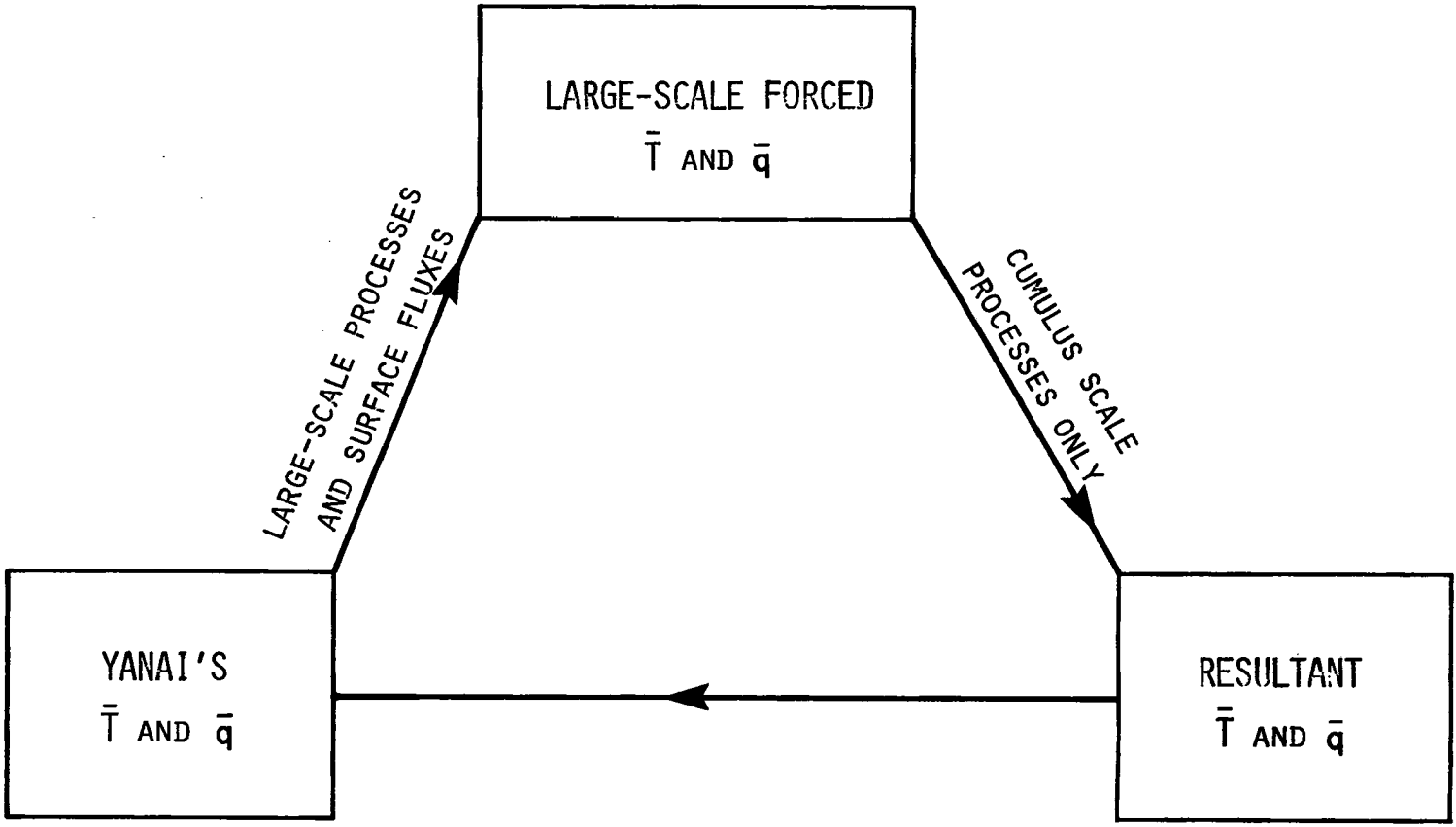

Fig. 4.2 This diagram shows a single computational cycle in the time integration of the model. Yanai's temperature and moisture fields are modified by a time dependent large-scale forcing and then the parameterized cumulus convection pushes the atmosphere toward a resultant $\bar{T}$ and $\bar{q}$ fields. Finally, we return to the initial values of $\bar{T}$ and $\bar{q}$ and go through the whole cycle with a new large-scale forcing.

in the vicinity of the ridge a small subsidence occurs. The maximum vertical motion is of the order of 140 mb/day at the 350 mb level.

It has been observed that large radiational differences exist between cloud and cloud-free regions which are probably a significant source of available potential energy for tropical weather systems (Albrecht and Cox, 1975; Jacobson and Gray, 1976). Therefore a time-height dependent radiative cooling profile was imposed as part of the radiative cooling profile as well as an average cooling profile to verify the effect of this type of large-scale forcing in modifying cumulus activity. The cloud and cloud-free radiative cooling profiles used in this model were obtained from Frank (1976) and are shown in Fig. 4.4 as well as the average profile. The cloud region was centered on the trough (time = 60 hr) where we would expect a dense cirrus shield while the cloud-free radiative cooling profile acts in the ridge region (time = 0 hr) where no cirrus shield is expected to exist. A sinusoidal radiative cooling profile was fitted to the trough and ridge data in order to obtain an analytical expression for the radiative large-scale forcing.

Imposing a cloud/cloud-free radiational difference in this model is expected to show its controlling effect on cumulus activity from the point of view of the resultant destabilization differences in terms of the cloud work function $A(\hat{p})$.

The third large-scale forcing considered in this study is related to the surface fluxes of heat and moisture. The variable in this case is assumed to be the surface wind speed in the bulk aerodynamic formula since the surface temperature is assumed to be constant. In order to

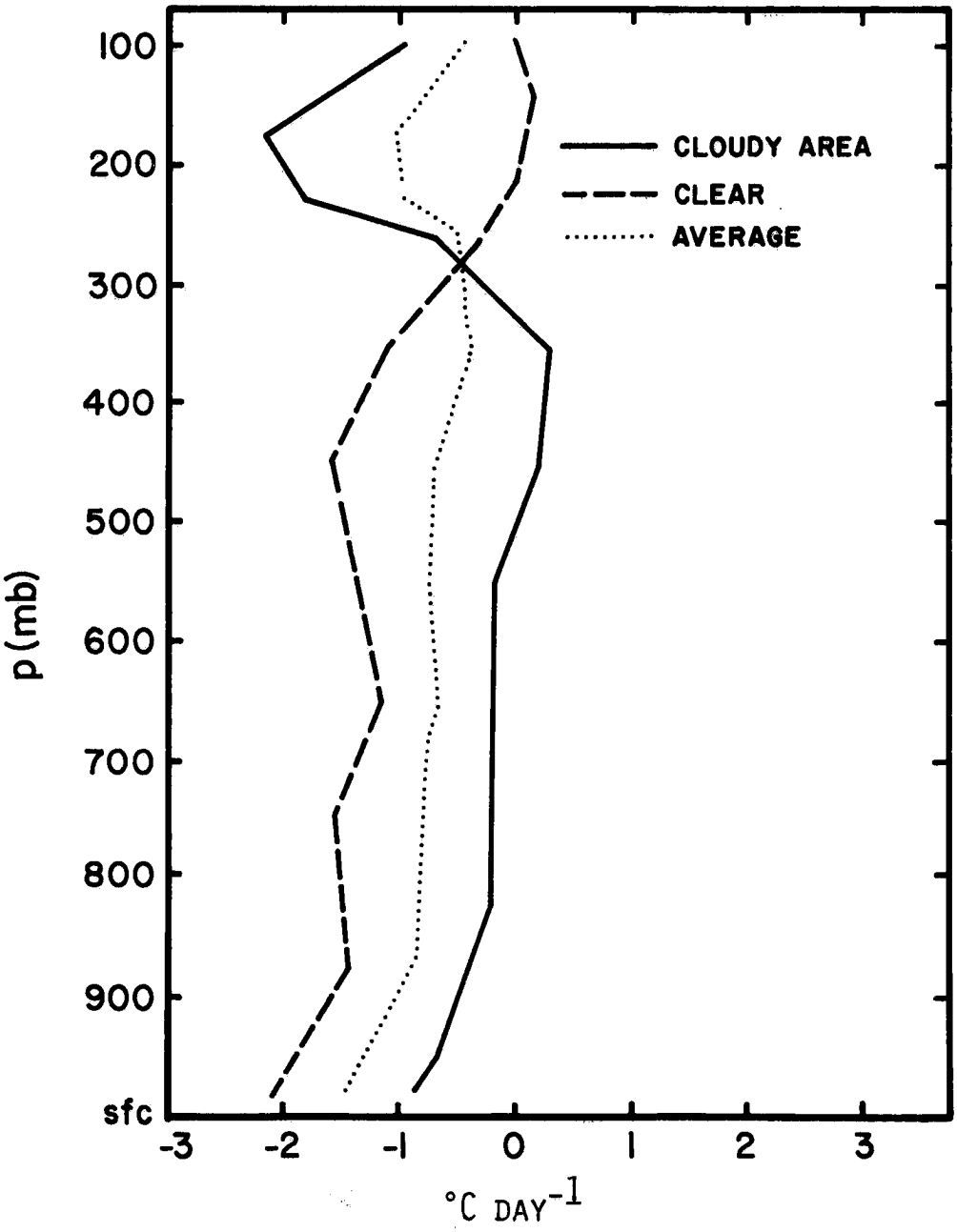

Fig. 4.4 Net radiational warming of tropical atmosphere with 100% dense cirrus cover (continuous line), clear conditions (dashed line) and an average situation (dotted line). After Frank (1976).

compute an analytical expression for the surface wind speed $V_S(t)$ we may consider the variation of evaporation as a function of wave position. Again, Reed and Recker's evaporation data were used to estimate $V_S(t)$ and subsequently an harmonic analysis was performed to obtain the analytical expression.

Fig. 4.5 shows the variation of the calculated surface wind speed and the associated average evaporation as a function of time. The evaporation averages 0.3 cm/day with the largest values occurring slightly to the east of the trough ($\approx$0.39 cm/day) and the smallest values occurring in the neighborhood of the ridge ($\approx$0.25 cm/day). Of course there is some uncertainty in the estimated evaporation in Reed and Recker's paper but the objective of this study is to analyze the controlling effect of surface fluxes on cumulus activity as predicted by the Arakawa-Schubert parameterization theory. The average Bowen ratio throughout the wave was calculated to be 0.075.

4.2 Internal Parameters

The nature of the simulated large-scale environment depends on the choice of the following model parameters:

-- the parameterization of the rain produced at a certain level k by sub-ensemble j [r(k,j)]

-- the detrainment coefficient $\lambda^-(j)$

-- the weighting function which defines the adjustment to be made in the dynamic control c(j)

Actually, one should include the definition of the critical value of the cloud work function in the optimal adjustment method (section 3)

a sub-ensemble are at random phases in their life cycle and, therefore, the summation of the precipitation over all members of the sub-ensemble is proportional to the precipitation of a single cloud averaged over its entire lifetime. If we are concerned with just one cloud the constant of proportionality is 1. Using the same values of cloud-base mass flux as those used by Lopez the cloud model, shown in the static control, suggested that the constant value of c_0 ($0.002\ m^{-1}$) may be underestimating the precipitation associated with deep clouds while shallow clouds are overestimated in terms of precipitation.

The sensitivity of the model to assuming a different conversion coefficient was tested using the constant c_0 profile (curve a in Fig. 4.6). Fig. 4.7 shows the precipitation efficiency, defined as the ratio of the precipitated water to the condensed water in the updraft as a function of cloud type for the constant c_0 and the variable c_0 assuming a unit cloud base mass flux for all cloud types. As mentioned before, the variable c_0 case produces more efficient deep clouds while shallow clouds are less efficient as compared to the constant c_0 case as suggested by Lopez (1973).

Some effort has been made recently to improve the cumulus cloud model of a one-dimensional, constant entrainment updraft, with detrainment occurring only at cloud top. Lateral mixing was shown to be important by Fraedrich (1973, 1974, 1976) and Betts (1975) and the contribution of cloud life cycle on the large-scale thermodynamic fields was emphasized by Cho (1977) who also considered the contribution by downdrafts. Fraedrich (1976) found that lateral detrainment is the dominant mixing mechanism for the shallow cloud population.

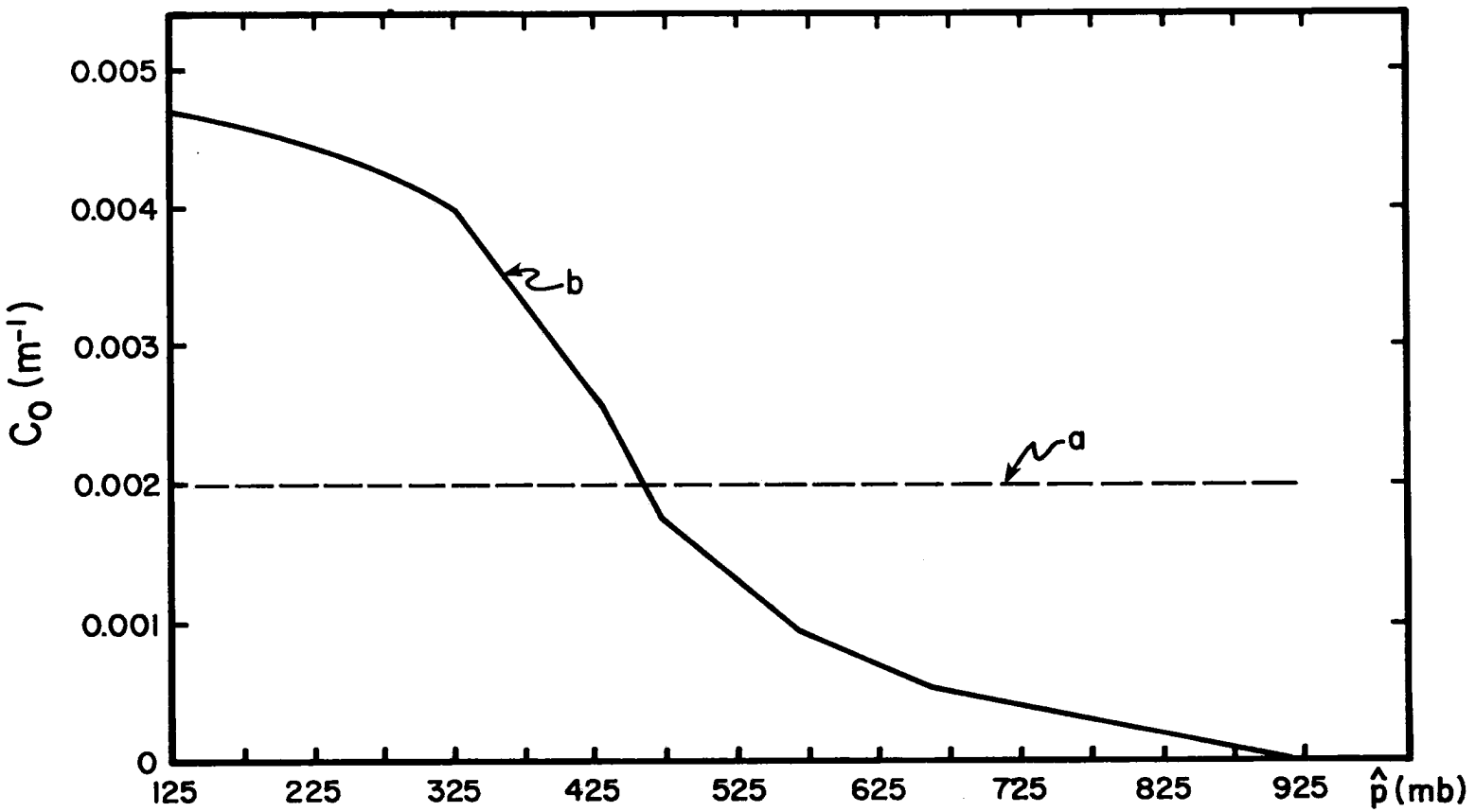

Fig. 4.6 The autoconversion coefficient c_0. Constant case (a) and cloud dependent case (b).

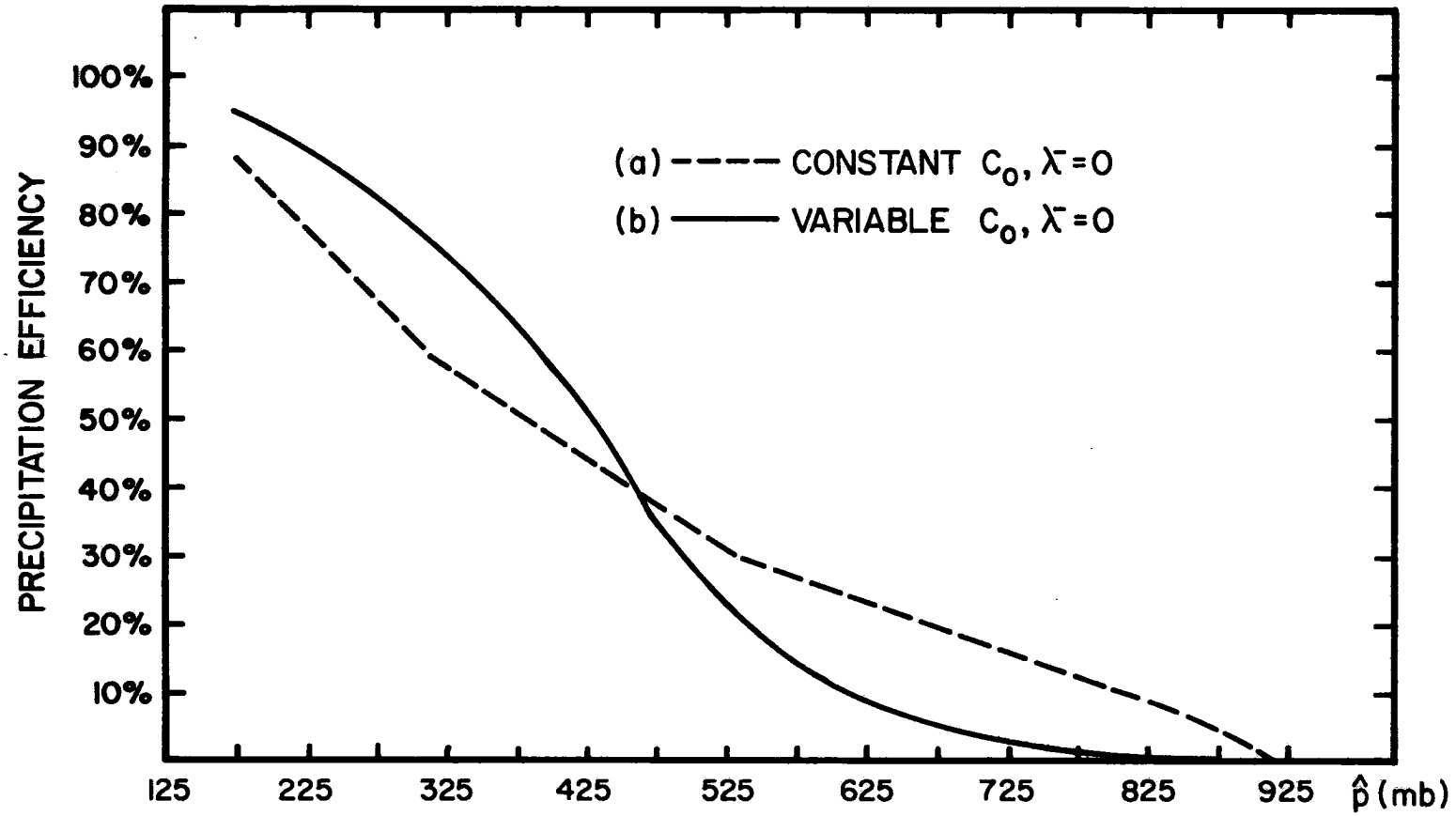

Fig. 4.7 Precipitation efficiency as a function of cloud type. Constant c_0 case (a) and cloud type dependent case (b).

Therefore a lateral detrainment rate $\lambda^-(j)$ was incorporated in the cloud model used in this study to partially take into account the life cycle of cloud sub-ensemble j and tests were performed to check the sensitivity of the model to this parameter.

Frank (1976) formulated the detrainment rate as a function of the entrainment rate and cloud top height; it was assumed that deep clouds have detrainment rate of $\lambda^- = 0.25\lambda^+$, middle level clouds $\lambda^- = 0.50\lambda^+$ and shallow clouds $\lambda^- = \lambda^+$. More recently Johnson (1977) assumed a more sophisticated relationship between the detrainment rate and the entrainment rate which allows for detrainment being larger than entrainment for middle and shallow clouds ($\lambda^- > \lambda^+$) while deep clouds were considered to show a slowly increasing updraft mass flux (corresponding to $\lambda^+ > \lambda^-$). In the results presented here, the detrainment rate $\lambda^-(j)$ is assumed to be given by a linear function of cloud type times the entrainment rate $\lambda^+(j)$, i.e.

$$\lambda^-(j) = f(j)\lambda^+(j) \tag{4.1}$$

where

$$f(j) = a + bj \tag{4.2}$$

Different combinations of the coefficients a and b were tested but it was always assumed that λ^- is smaller for deep clouds and larger for shallow clouds as suggested by the diagnostic studies. Fig. 4.8 shows a typical profile of $\lambda^+(j)$, $\lambda^-(j)$ and $\lambda(j) = \lambda^+(j) - \lambda^-(j)$ for Yanai's data when

$$f(j) = 0.903 - 0.053j \ . \tag{4.3}$$

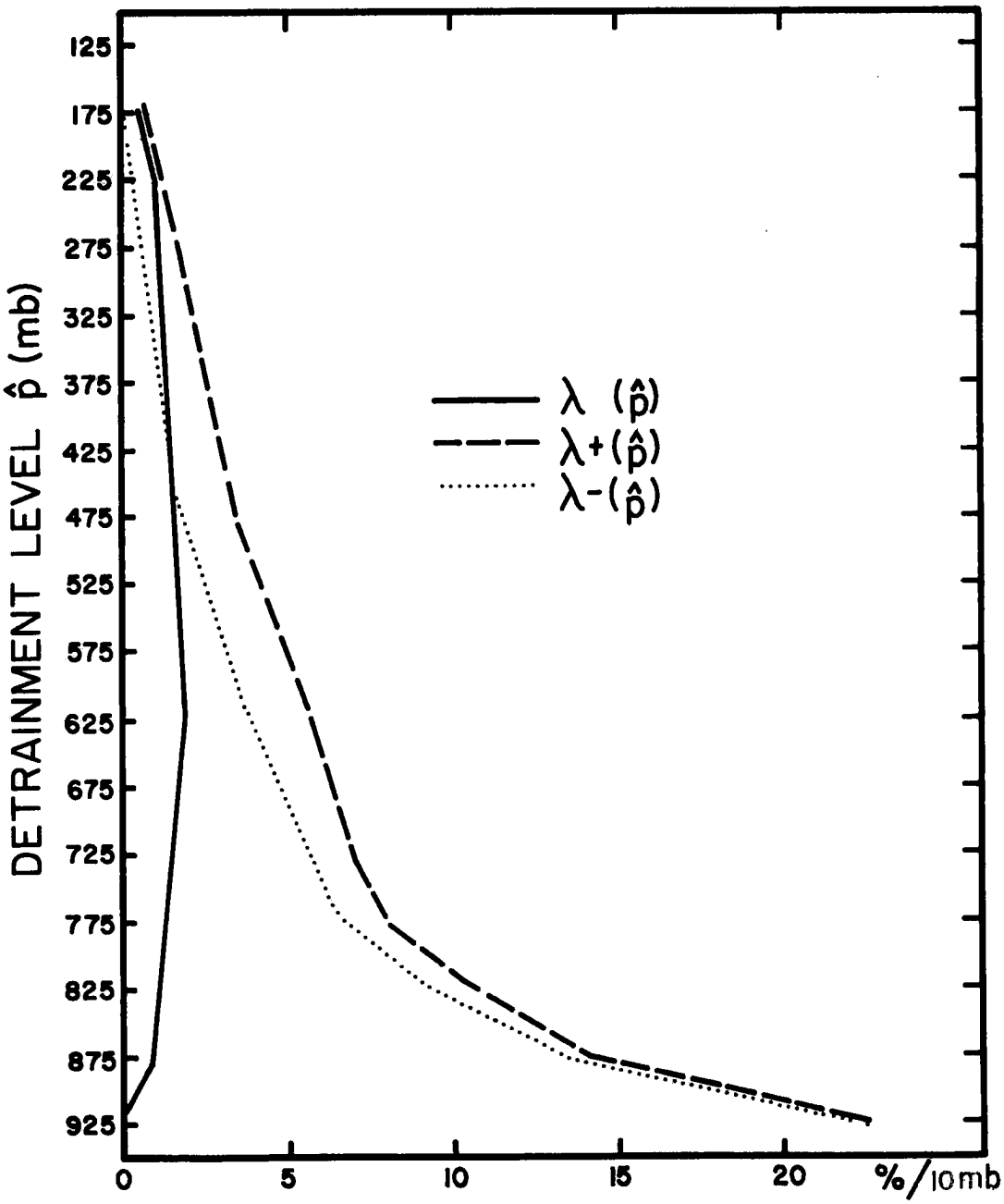

Fig. 4.8 Entrainment rate as a function of cloud type (dashed curve), detrainment rate computed according to (4.3) (dotted curve) and the fractional rate of increase of cloud mass flux with pressure (continuous curve), based on Yanai's data.

This figure shows that large entrainment rate is associated with shallower clouds because they lose buoyancy more easily than deeper clouds (more mixing with the environment). The detrainment with height associated with each cloud type is such that shallow clouds have an almost constant normalized mass flux $\eta(k,j)$ because $\lambda(j) \approx 0$ while deeper clouds show an increase of mass flux with height ($\lambda(j) > 0$).

As shown in section 3.4.5 the underadjustment approach yields a trivial initial basic feasible solution to start the simplex method, given by $\chi_B = IB$, in which case all cloud base mass fluxes $M_B(i)$ vanish, thus making no improvement in the sense of decreasing A(i) (for all i) by cumulus convection. If the weights in the objective function of the linear programming problem expressed by (3.44) are all equal to the unity, the cost of the above solution would be physically interpreted as an integral measure of the adjustment to be made by all possible cloud types. Let us consider now how this situation can be improved by bringing a cloud into the basis thus removing a slack variable.[1]

In considering whether or not the current solution is optimal, one considers a certain cloud type not in the basis and it has to be determined if it would be advantageous to bring it into the basis in the sense of reducing the measure of the underadjustment as expressed by the objective function (3.72a) (or equivalently, making A(i) as close as possible to $A_c(i)$ for all cloud types preserving feasibility). This decision, in the simplex method, is done by considering the so-called

[1]Actually, during the process of working toward the optimal solution in the simplex method, it is possible that a slack variable be replaced by another slack.

relative cost vector which is now going to be interpreted in the context of the optimal adjustment method. If cloud type 'j' is not in the basis we can construct an imaginary cloud which is equivalent to it, from the point of view of the reductive effect of cumulus clouds on the cloud work function, as a function of the elements that constitute the present basis (real clouds and slack variables). Considering now the efficiency in making the adjustment of the real cloud j and the imaginary cloud, one is concerned with the fact of whether bringing that real cloud into the basis is or is not going to remove one slack variable from the basis thus reducing the objective function. The relative cost is a measure of this efficiency and it is also a function of the weights in the objective function (Luenberger, 1973).

In the dynamic control, up to this point, the only arbitrary parameters are the weighting coefficients c(i). Thus it is suggested by the above reasoning that the effect of varying c(i) should be checked against its role in deciding which cloud type is to enter the basis. When the number of real clouds in the basis, as determined in the dynamic control, is small compared to the maximum number of possible clouds (given by the static control) it turns out that making c(i) larger for shallow clouds and smaller for deeper clouds tends to produce a spectrum of clouds displaced to the shallow type of convection. This experiment was performed assuming a certain ratio between c(1) and c(17) (the weights associated with the slack variable of the deepest and the shallowest cloud type respectively) and linearly interpolating the coefficients for the intermediate clouds. The ratio was varied from 1 to 10^5 and all the change in the spectrum occurred

between 1 and 10^2 while from 10^3 to 10^5 the solution usually remained unaltered but showed signs of being unstable in the sense that very small changes in the large-scale environment produced a large change in the spectrum of clouds. The author is currently performing a rigorous sensitivity analysis on the linear programming problem expressed by (3.73) to determine whether or not there is a physically optimum choice of the above parameters.

In situations of a large number of clouds being given by the dynamic control no change was observed in the solution upon varying the weighting function α. We have decided to use $c(i) = B(i)^{-1}$ (i.e. inversely proportional to the desired adjustment) which closely follows the ratio 10^2, as defined above, since it has produced better results from the physical point of view. The shallow type of convection is present under all types of synoptic situations in the tropics (Yanai et al., 1976) thus justifying the above choice of c(i).

4.3 Description of the Experiments

Based on the large-scale temperature and moisture fields described in section 4.1 (see Fig. 4.1) the Arakawa-Schubert cumulus parameterization theory was applied to the time dependent dynamical forcing $\bar{\omega}$ shown in Fig. 4.3 and the results checked against the controlling effects of surface fluxes, radiative cooling and some model parameters (λ^- and c_0). The experiments shown in this study were classified according to Table 1.

The capital letters A, B and C correspond to the experiment in which the model parameters λ^- and c_0 were varied, i.e. A has $\lambda^- = 0$ mb^{-1}

Table 1. Table of Experiments.

Experiment	Surface Fluxes (Wind Speed)	Radiational Cooling	Detrainment λ^- (mb^{-1})	Autoconversion Coefficient c_o (m^{-1})
A1	V_S = const (4 m/s)	Constant in time (average profile in Fig. 4.4)	$\lambda^- = 0$ for all types of clouds	c_o = const (0.002 m^{-1}) for all cloud types (Fig. 4.6)
A2	$V_S = V_S(t)$ (as shown in Fig. 4.5)	Constant in time (average profile in Fig. 4.4)	$\lambda^- = 0$ for all types of clouds	c_o = const (0.002 m^{-1}) for all cloud types (Fig. 4.6)
A3	$V_S = V_S(t)$ (as shown in Fig. 4.5)	Time dependent radiative cooling profile (Fig. 4.4)	$\lambda^- = 0$ for all types of clouds	c_o = const (0.002 m^{-1}) for all cloud types (Fig. 4.6)
B3	$V_S = V_S(t)$ (as shown in Fig. 4.5)	Time dependent radiative cooling profile (Fig. 4.4)	$\lambda^- = 0$ for all types of clouds	Cloud type dependent c_o (Fig. 4.6)
C3	$V_S = V_S(t)$ (as shown in Fig. 4.5)	Time dependent radiative cooling profile (Fig. 4.4)	Cloud type dependent λ^- (Fig. 4.8)	Cloud type dependent c_o (Fig. 4.6)

for all cloud types and c_0 = constant (0.002 m^{-1}) for all cloud types, B differs from A by the inclusion of a cloud type dependent c_0 as shown in Fig. 4.6 and C differs from B by a cloud type dependent lateral detrainment coefficient λ^- (see Fig. 4.8). The number that follows the capital letter identifies the type of forcing represented by surface fluxes forcing through the surface wind speed and the type of radiational forcing (Figs. 4.5 and 4.4 respectively). Thus, number 1 is associated with a constant surface wind speed (V_0 = 4 m/s) and a constant in time radiative cooling profile (the average profile in Fig. 4.5), number 2 differs from the previous case only by the inclusion of a time dependent surface wind speed (Fig. 4.5) while number 3 adds another degree of freedom by allowing a time dependent radiative cooling profile as discussed in section 4.2.

Therefore in series A one can study the effect of changing the forcing under constant model parameters (cases A1, A2 and A3). In series B only case B3 is shown in this study thus representing the effect of including a cloud type dependent coefficient c_0 in the rain parameterization under the forcing represented by a time dependent surface wind speed and radiative cooling profile. The lateral detrainment λ^- is discussed in case C3.

4.4 Results of the Experiments

A plot of the time series of the mass flux distribution function, as a function of cloud type $\hat{p}$ (in units of kg m^{-2} hr^{-1}), corresponding to case A1 is shown in Fig. 4.9a; the associated temperature tendency field (in units of °C hr^{-1}) and the moisture tendency field (in

$g\,kg^{-1}\,hr^{-1}$) are shown in Figs. 4.9b and 4.9c respectively. On the abscissa of Fig. 4.9 (time) the periods corresponding to each of the eight wave categories as given by Reed and Recker (1971) are indicated. The correlation coefficients r(j,k) between the time-series of $M_B(j)$ and $\bar{M}(k)$ (the large-scale mass flux defined by $\bar{M}(k) = -\bar{\omega}(k)$) for all cloud types (j = 2, 3, ...17) and all levels (k = 3, 4, ...18) were computed in order to depict the dependency of the cloud base mass flux $M_B(\hat{p})$ upon the model parameters (c_0 and $\bar{\lambda}$) and the forcing. Hence the 16 x 16 correlation coefficient matrix measures the linear dependence between $M_B(j)$ and $\bar{M}(k)$; a large positive value of r(j,k) means that high values of the large-scale mass flux at level k tend to be associated with high values of cloud base mass flux of cloud type j.

In analyzing the correlation coefficient matrix we have to realize that the Arakawa-Schubert parameterization theory predicts a highly interactive behavior among all cloud types through the kernel (2.47). The most dominant effect in the kernel is the decrease of $A(\hat{p})$ through the adiabatic warming of the environment due to the subsidence induced by cloud type $\hat{p}'$ where $\hat{p}' < \hat{p}$. Shallow clouds increase the cloud work function of deeper clouds through the cooling and moistening of the environment due to the detrainment of cloud air. Therefore we may expect that enhanced deep convection suppresses shallower convection producing a negative correlation between M_B of shallow clouds and $\bar{M}$ at all levels since deep convection is positively correlated to $\bar{M}$ (Yanai et al., 1976). The correlation coefficient matrix for experiment A1 is shown in Fig. 4.9d.

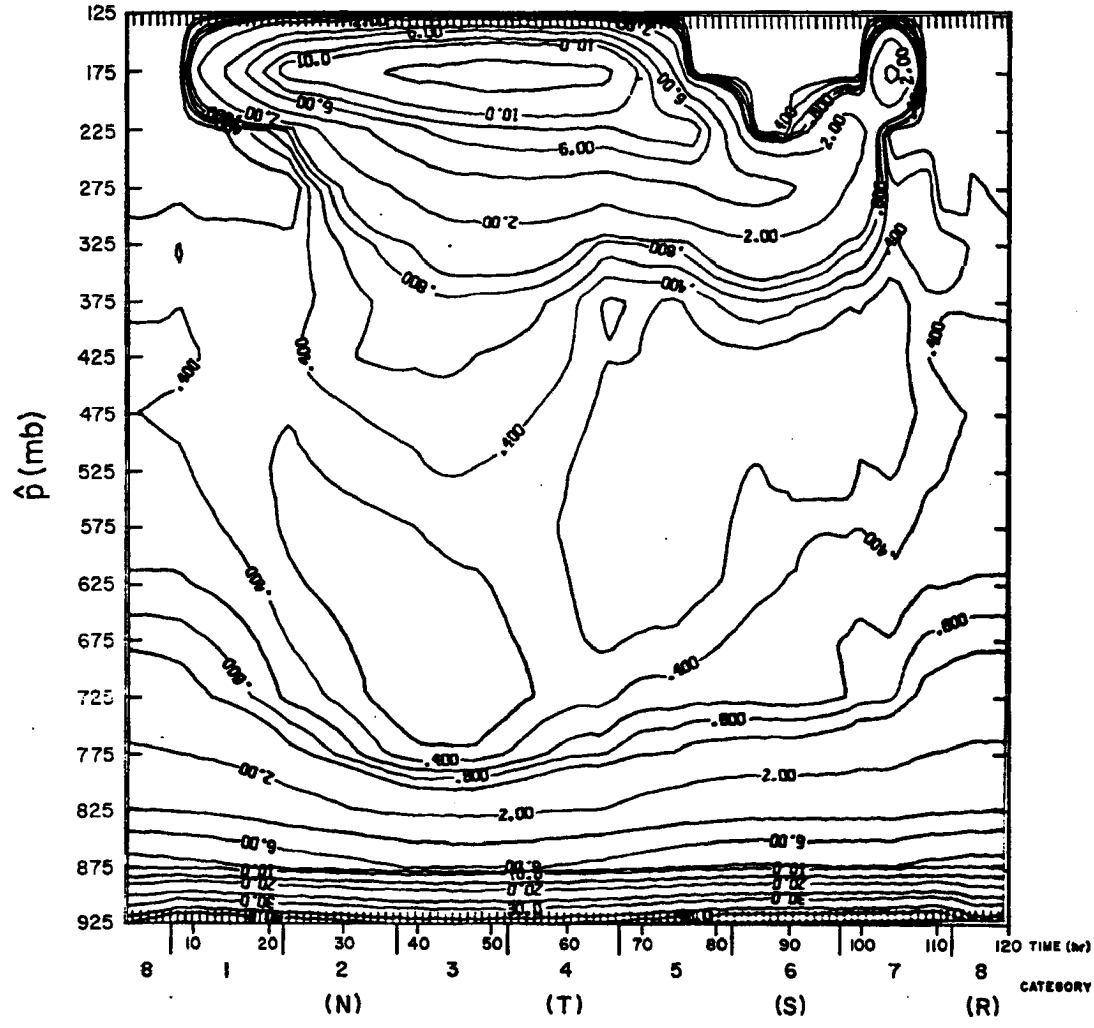

Fig. 4.9a Cloud base mass flux (in $kg\,m^{-2}\,hr^{-1}$) as a function of cloud type $\hat{p}$ (ordinate) and time (abscissa) or wave category (as defined by Reed and Recker, 1971) for case A1. In experiment A1 $V_S = 4\ ms^{-1}$, $\lambda^- = 0$, c_0 = constant and the radiative cooling profile is constant in time.

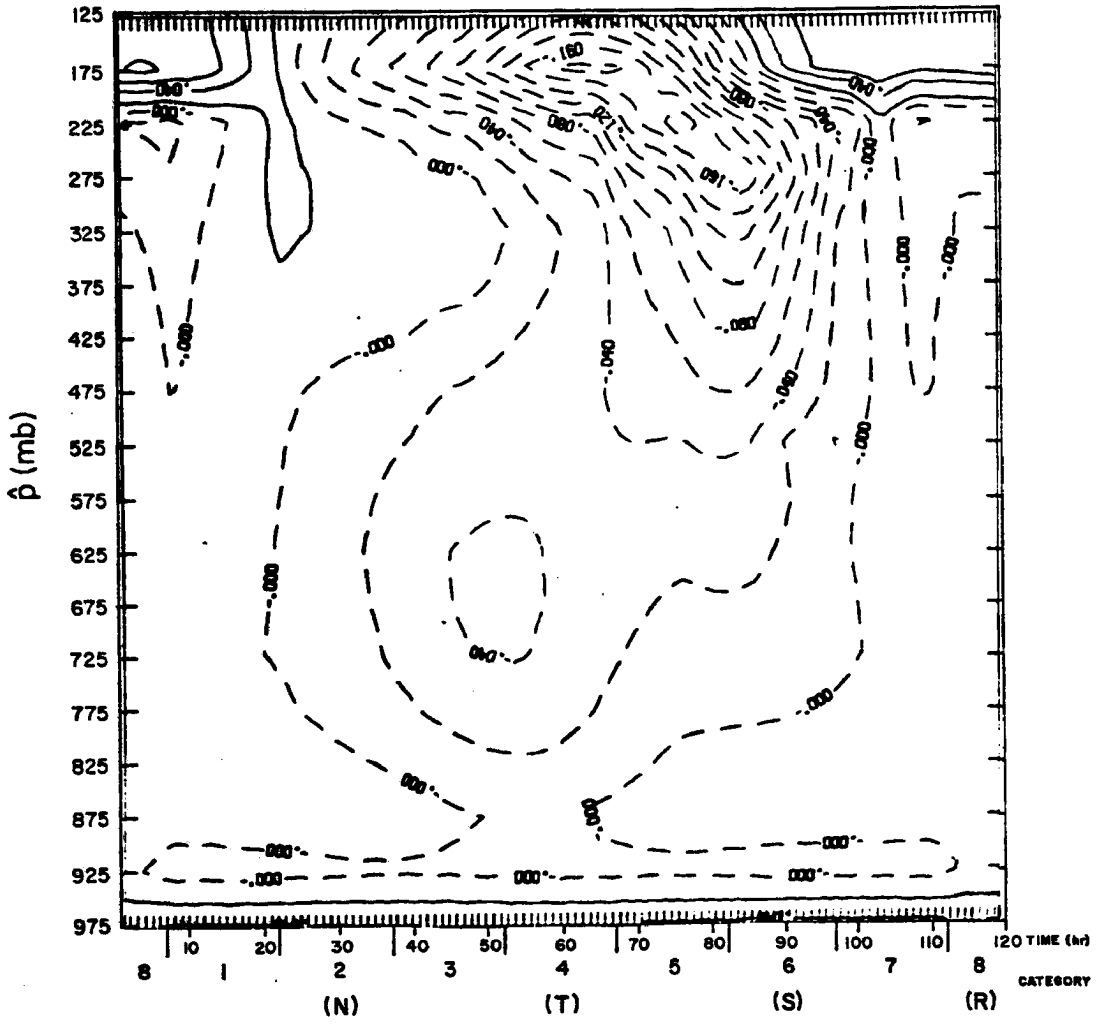

Fig. 4.9b Temperature tendency (°C hr^{-1}) in experiment A1.

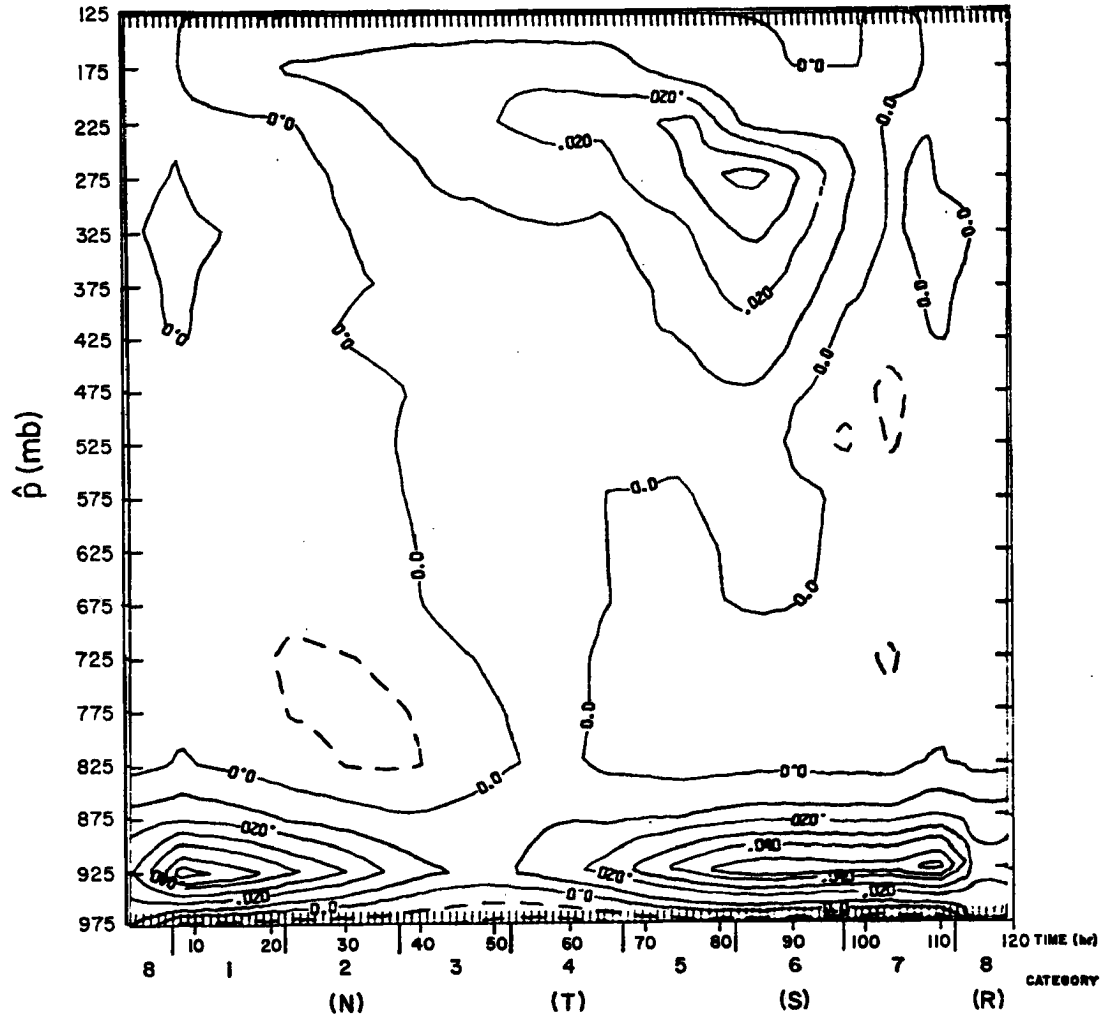

Fig. 4.9c Moisture tendency ($g\,kg^{-1}\,hr^{-1}$) in experiment A1.

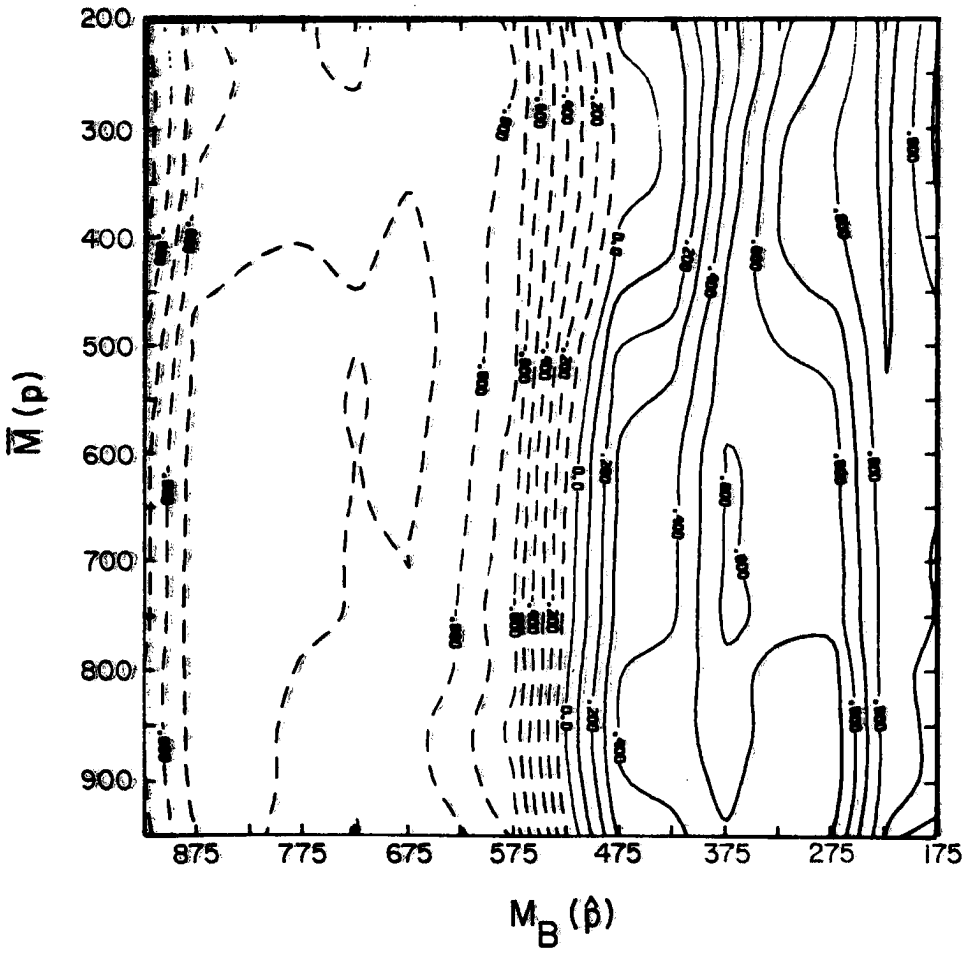

Fig. 4.9d Correlation coefficient between the time series of the large-scale vertical motion $\bar{M}(p)$ at all levels and the cloud base mass flux $M_B(\hat{p})$ in experiment A1.

A bimodal structure in the mass flux distribution function is clearly visible mainly in categories 3 and 4 (Fig. 4.9a) near the trough axis, where the most intense upward large-scale vertical motion occurs (Fig. 4.3). This fact has been observed by many authors for an average tropical summer condition (Yanai et al., 1973; Ogura and Cho, 1973; etc.) and by Cho and Ogura (1974) in a diagnostic study using the cloud spectral method applied to Reed and Recker's easterly wave composite. The deepest type of cloud found in experiment A1 is cloud type 2 ($\hat{p}$ = 175 mb) which shows a maximum of 18.6 $kg\,m^{-2}\,hr^{-1}$ at 51 hr, a secondary small maximum of 4.6 $kg\,m^{-2}\,hr^{-1}$ at 103 hr and a minimum (i.e. absence) in the ridge category. Convection reaching 275 mb to 525 mb shows a wave-like distribution with two maxima: one at category 3 and another at category 6. The later peak seems to be related to the absence of the deepest type of cloud which suppresses the shallower types of convection as can be seen in the distribution of cloud base mass flux of shallow convection. Shallow and middle level convection are enhanced around the ridge category. The shallowest cloud type has its mass flux weakly modulated by the deep type of convection. The maximum number of cloud types occurs in categories 3 and 4, being equal to the number of cloud types allowed by the static control (i.e. 16), thus providing a perfect equilibrium in terms of the cloud work function as discussed in section 2.3.4 ($\frac{\partial A(\hat{p})}{\partial t} = 0$).

The correlation coefficient matrix (Fig. 4.9d) shows two marked regions: clouds which detrain above 500 mb are positively correlated to $\bar{M}$ at all levels while shallower clouds are negatively correlated to $\bar{M}$. An interesting feature is the fact that $M_B(2)$ is better correlated

to $\bar{M}$ at lower levels while all other deeper clouds are better correlated to $\bar{M}$ slightly below their detrainment level. Middle level clouds are weakly correlated with $\bar{M}$ but shallow clouds are negatively correlated with $\bar{M}$ at all levels showing minimum values slightly above the detrainment level. More discussions about the connection between M_B and $\bar{M}$, as shown by the correlation coefficient matrix, will be made after showing the results of the other experiments.

The temperature tendency distribution (Fig. 4.9b) shows a slight warming of the boundary layer ($\approx$0.04°C/hr) throughout the period. In the ridge category and its neighbors a warming is observed throughout the middle troposphere; on upper layers a slight cooling is observed due to the radiative cooling profile which does not compensate for the sinking warming (since the cloud effect on these layers is very small). The largest cooling tendency is observed to the east of the trough at level p = 175 mb (maximum of -0.20°C hr^{-1}). Fig. 4.10 shows the cumulus effect on the temperature change (°C hr^{-1}) typical of each wave cagetory.

The convergence of s-Lℓ gives a warming effect in the boundary layer in all wave categories proportional to the total cloud base mass flux as shown in Fig. 4.9a. Above cloud base the flux divergence cools the atmosphere except in category 8 where a slight warming is observed right above cloud base; in the upper layers a warming is observed except in category 8. The largest numbers occur in category 4 ($\approx$0.03°C hr^{-1} at 675 mb). The warming produced by the rain term in Equation (2.13) (Fig. 4.10) is about 8 to 10 times larger than the flux divergence term around the trough ($\approx$0.35°C hr^{-1} at approximately 425 mb).

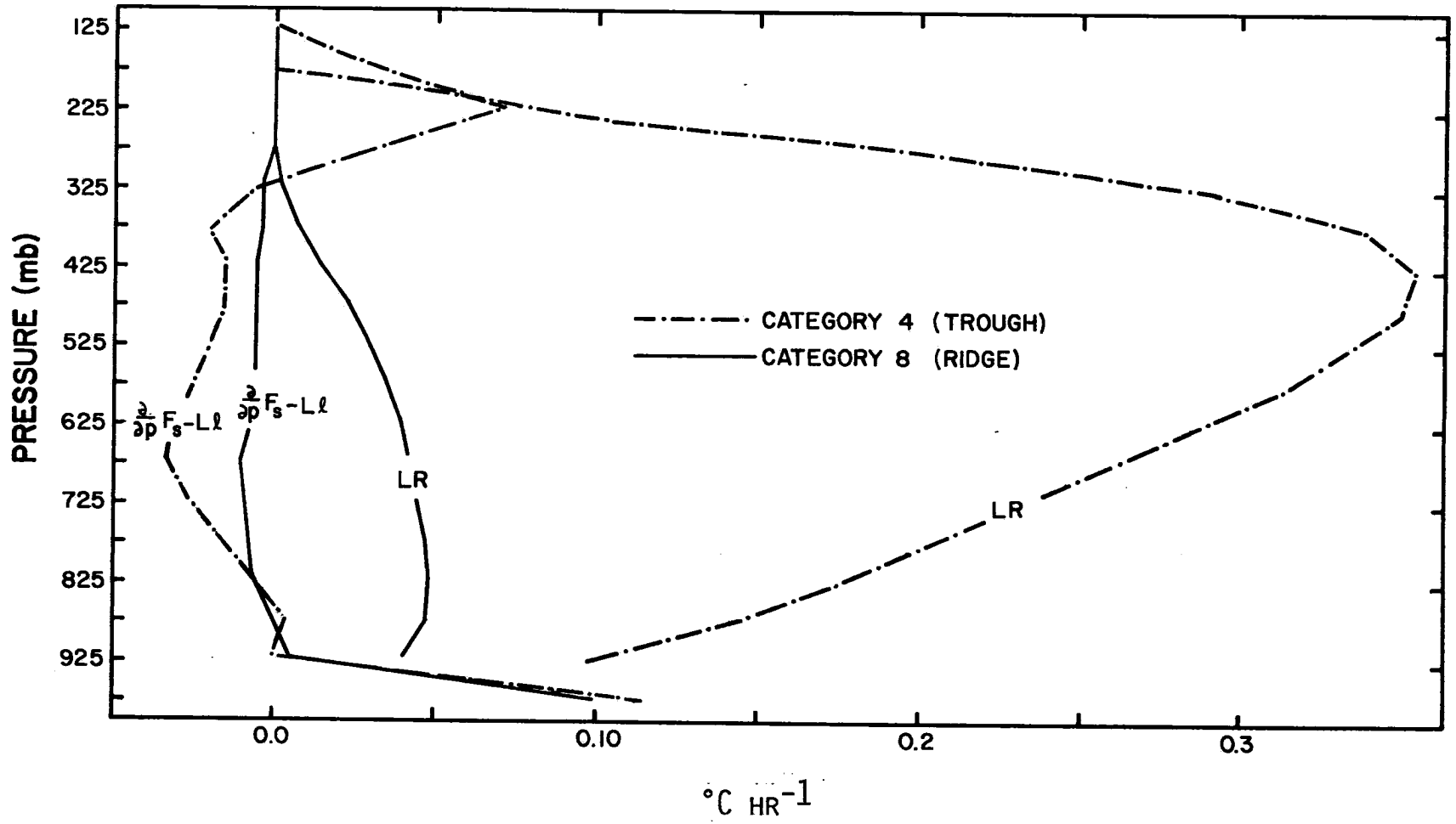

Fig. 4.10 Cumulus effect on the dry static energy balance at categories 8 (continuous line) and 4 (dashed line) for case A1.

In the ridge the profile of the rain term is similar to the trough one but smaller.

Fig. 4.9c shows the moisture tendency field. Large positive tendencies are found in lower levels (≈925 mb) where the moistening effect of the detrainment of liquid water at cloud top is prominent. In the region of maximum deep cloud activity the drying effect of the cumulus induced subsidence is larger thus decreasing the magnitude of the moistening effect; in this same region cumulus convection has a drying effect on the boundary layer probably because of the lack of parameterization of the effects of the falling rain through the boundary layer.

Considering both cumulus and large-scale processes, we observe a general drying effect in and around the ridge category and a moistening effect near the trough which is spread over all wave categories in the lower troposphere. This moistening shows a narrow branch in the middle troposphere and a canopy in the upper troposphere with maximum values (≈ 0.04 g kg^{-1} hr^{-1}) to the east of the trough.

The moistening effect of cumulus convection is shown in Fig. 4.11. This figure shows that the depletion of moisture by the rain term in (2.14) is not the predominant effect as it is in the heat balance. The total water flux divergence has a drying effect in the lower troposphere in category 4. In category 8 (ridge) a moistening in the boundary layer is observed as opposed to a drying in all other wave categories.

Case A2 shows the controlling effect of surface fluxes on the shallow cloud population. In the ridge category, where the surface wind speed is smaller, the cloud base mass flux associated with shallow

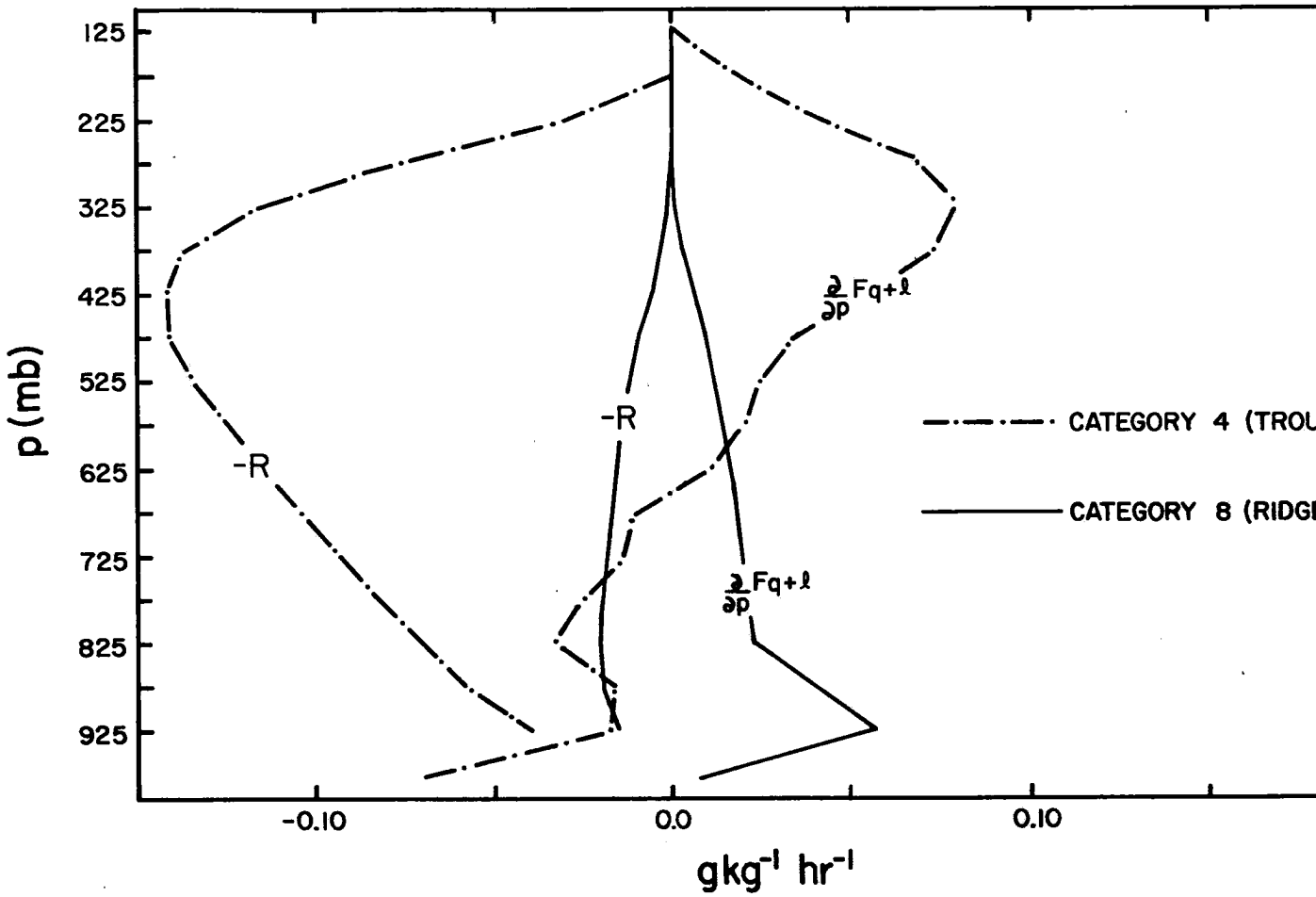

Fig. 4.11 Same as Figure 4.10 except for water vapor balance.

clouds has experienced most of the change (Fig. 4.12a), decreasing in intensity while middle and deep convection is less affected by the variation in the intensity of the surface fluxes. The correlation coefficient matrix between $\bar{M}$ and M_B (Fig. 4.12d) shows that the shallow type of convection is positively correlated to $\bar{M}$ at all levels, the highest values being found when the vertical motion at higher levels is considered; the maximum evaporation occurs to the west of the trough (Fig. 4.5) as well as the maximum vertical motion (Fig. 4.3) and the cloud base mass flux of shallow clouds shows a hump to the west of the trough. Deeper clouds do not show as much change as shallower clouds. Thus it is shown that the Arakawa-Schubert parameterization predicts a high degree of dependency between the surface fluxes and the modulation of the shallow type of convection.

The negative region in the correlation coefficient matrix of case A2 (Fig. 4.12d) extends to about the same height in terms of $\hat{p}$ ($\approx$525 mb), being similar to the A1 case except that the values are slightly larger suggesting that the controlling effect of surface fluxes in modifying the cloud population extends through the lowest 8-9 cloud types. From the physical point of view, the extra heat and moisture, available in the boundary layer by the increase of the surface wind speed, has to be removed and the partitioning among all cloud types tends to favor the shallower ones.

The region of cooling tendency in the middle and upper troposphere as observed in case A2 (Fig. 4.12b) is broader but its magnitude is slightly smaller mainly in the middle troposphere due to the warming effect of the predominant rain terms in (2.13) which is slightly larger

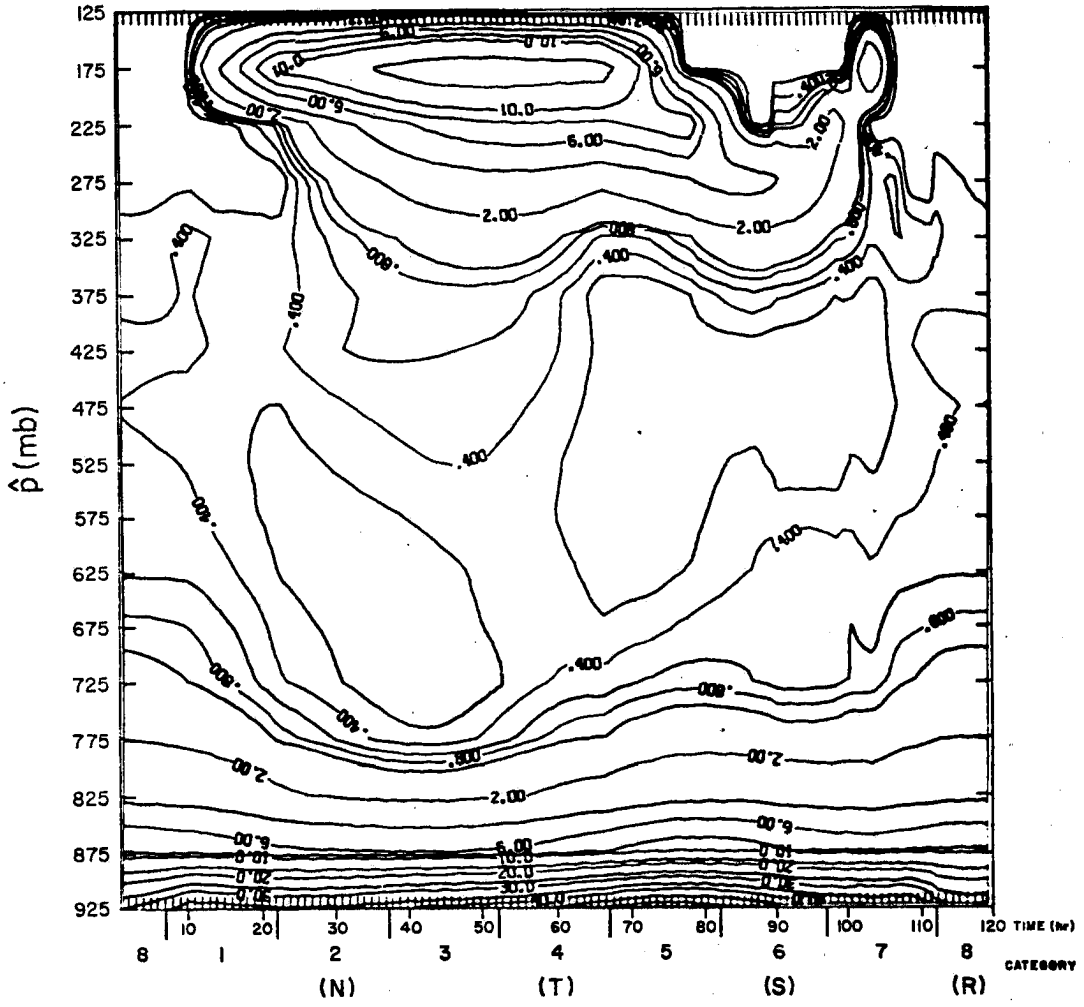

Fig. 4.12a This figure shows the results of experiment A2 in which $V_S = V_S(t)$, $\lambda^- = 0$, c_0 = constant and the radiative cooling profile is a constant. Cloud base mass flux in $kg\,m^{-2}\,hr^{-1}$.

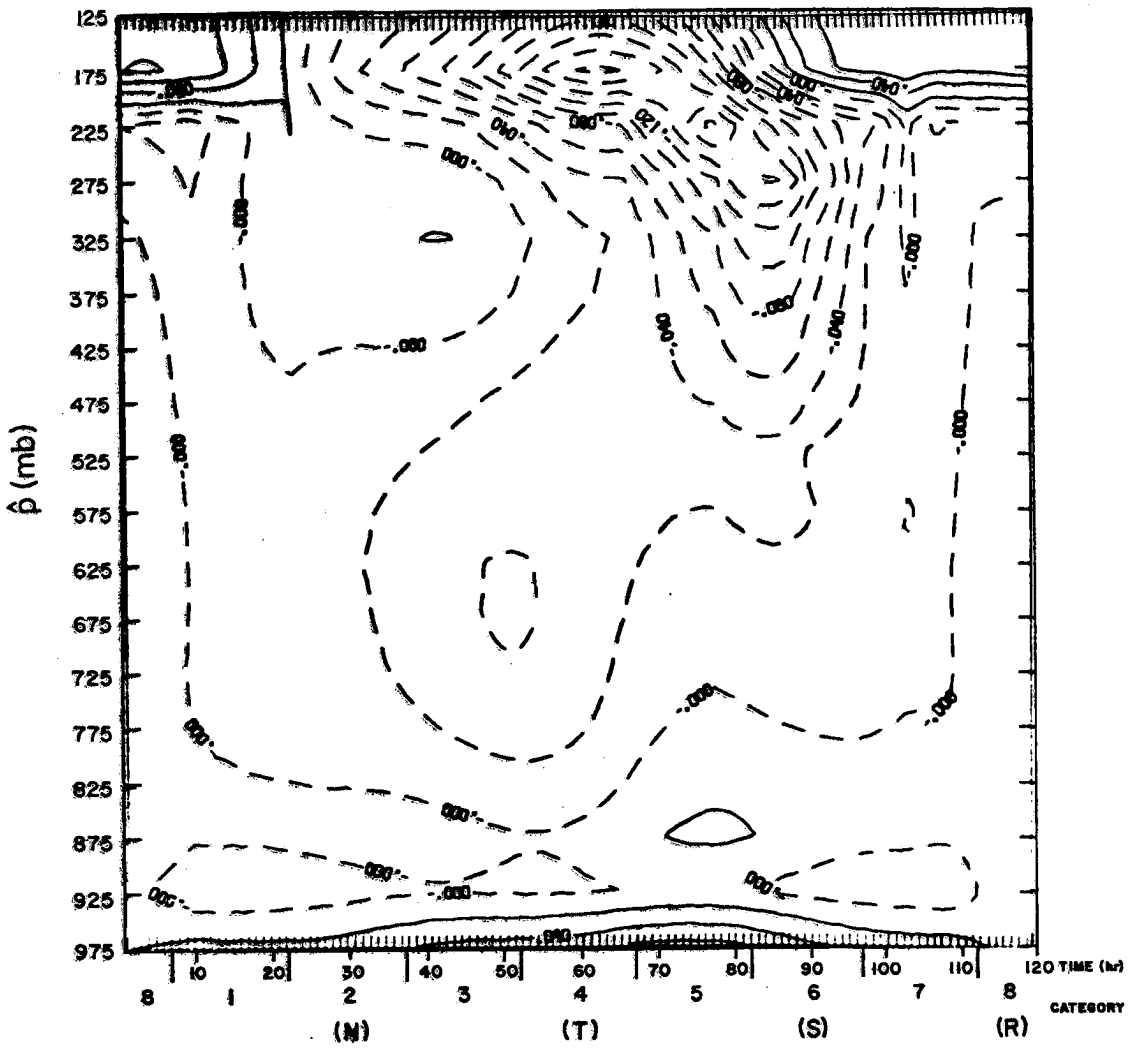

Fig. 4.12b Temperature tendency (°C hr^{-1}) in experiment A2.

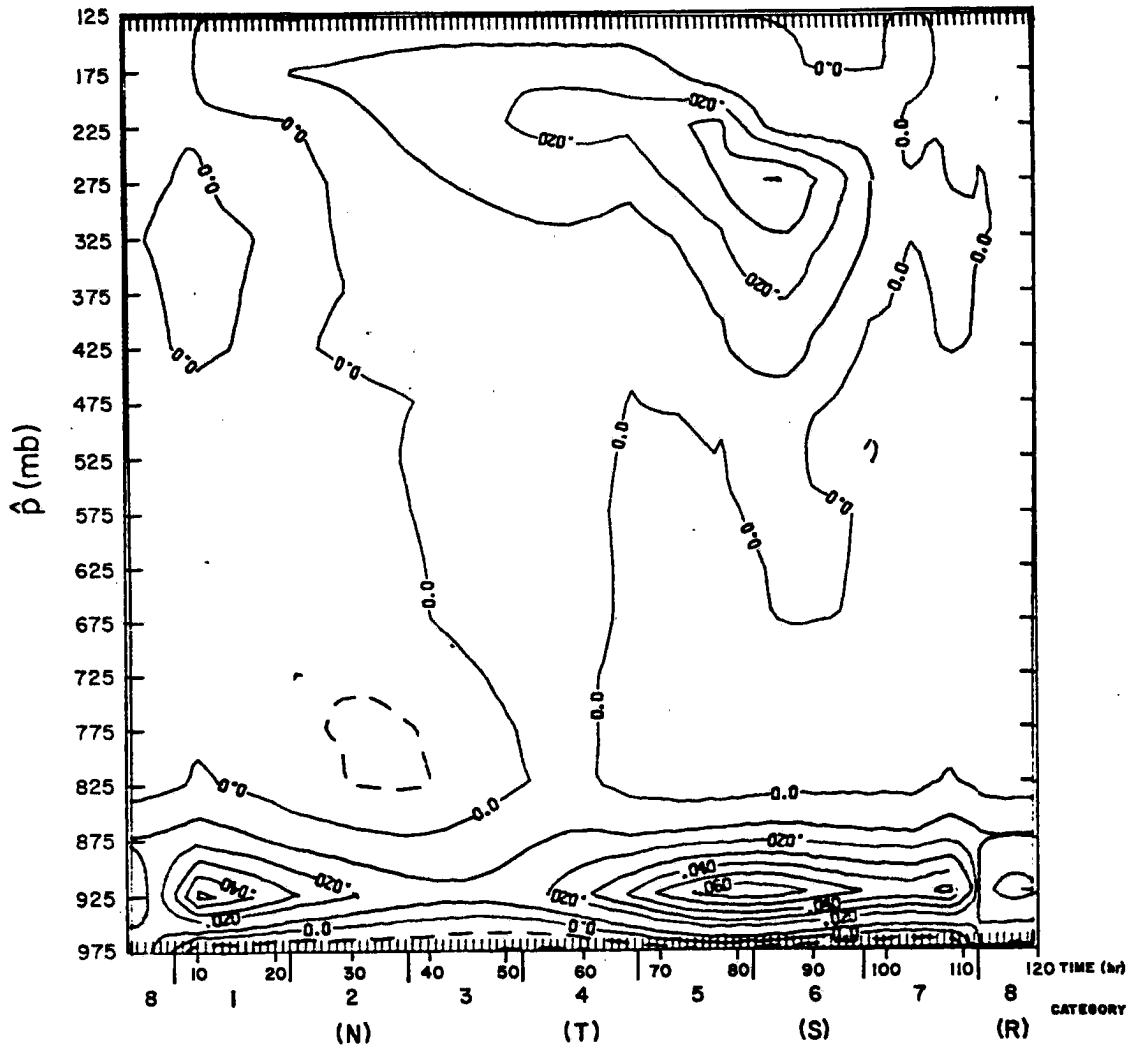

Fig. 4.12c Moisture tendency (g kg^{-1} hr^{-1}) in experiment A2.

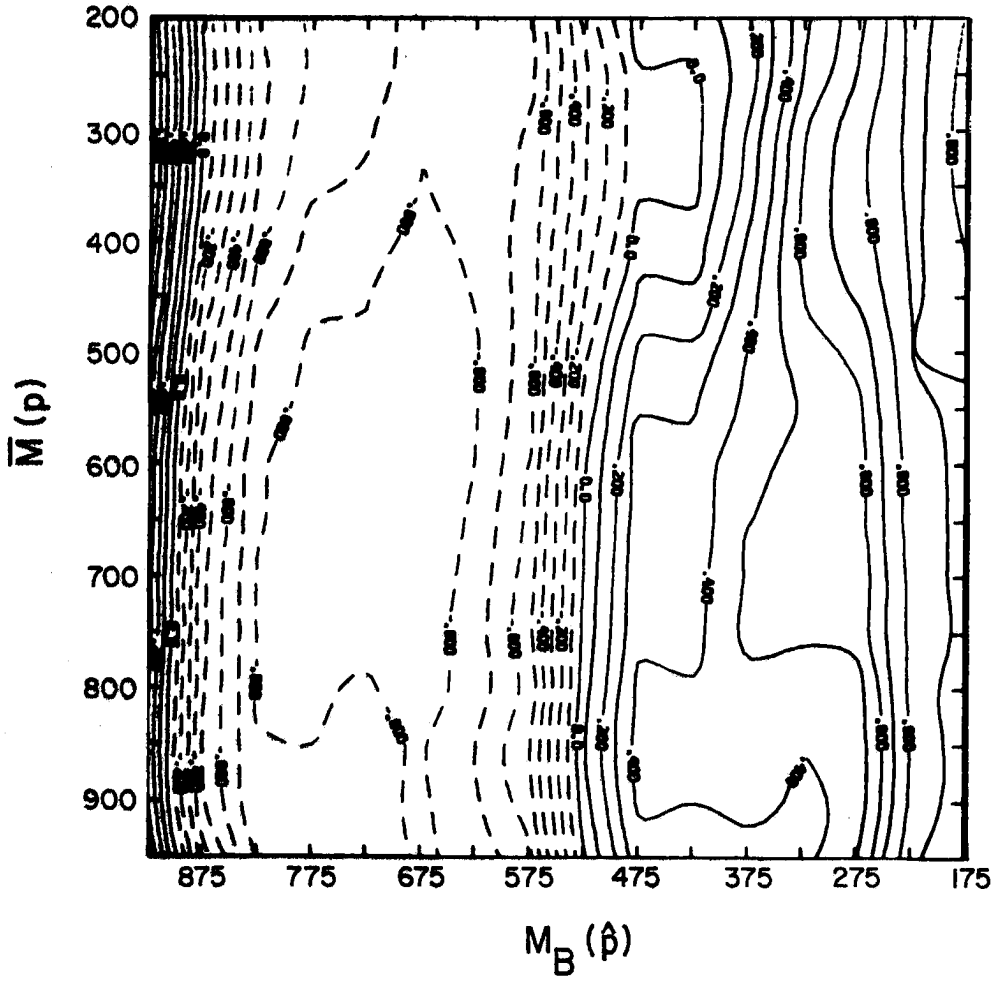

Fig. 4.12d Correlation coefficient between $\bar{M}(p)$ and $M_B(\hat{p})$ in experiment A2.

than in case A1, in the regions where the surface fluxes are enhanced. Similarly, the explanation for the broader cooling is related to a slight decrease of the warming effect produced by the rain term in the ridge region. In the boundary layer the warming around the trough is enhanced by approximately 60% while in the ridge it is decreased by approximately 50%. This result is tied to the fact the cumulus convection tends to warm the boundary layer (see (2.19) and Fig. 4.12b). The main feature in the moisture tendency field (Fig. 4.12c) is the larger moistening where the shallow cloud activity is enhanced (to the east of the trough), associated with the larger detrainment of liquid water at cloud top. Correspondingly, a slight drying is observed in the ridge category as a result of the suppressed shallow convection.

The introduction of a radiative cooling profile dependent on the expected cloud cover, which gives a net larger loss of energy in the ridge than in the trough as compared to the average profile (shown in Fig. 4.4), is the objective of case A3. The cloud base mass flux associated with shallow convection does not change as much as the deep type; cloud type 2 is now present in the ridge category (Fig. 4.13a) while the magnitude of M_B for deeper clouds in the trough category is decreased. The correlation coefficient matrix of case A3 (Fig. 4.13d) shows the effect of the variable radiative cooling profile when compared to the one obtained in case A2 (Fig. 4.12d). The correlation coefficients for the deep type of convection (cloud types 2, 3, and 4) is still positive but smaller, thus showing that a cirrus shield has a negative effect on increasing the cloud mass flux from the point of view of destabilizing the atmosphere. However, as discussed by

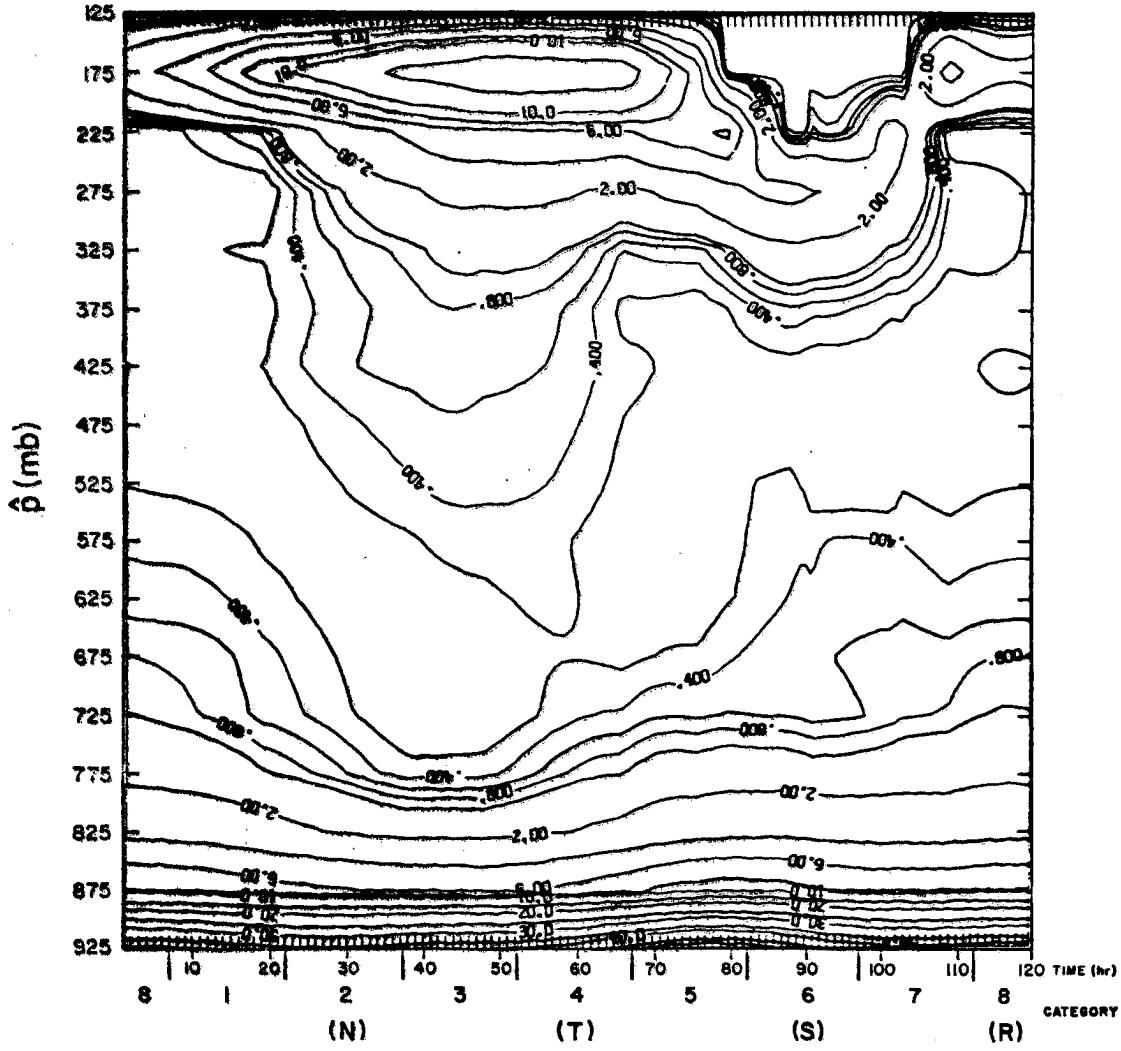

Fig. 4.13a This figure shows the results of experiment A3 in which $V_S = V_S(t)$, $\lambda^- = 0$, c_0 = constant and the radiative cooling profile is a function of time. Cloud base mass flux in $kg\,m^{-2}\,hr^{-1}$.

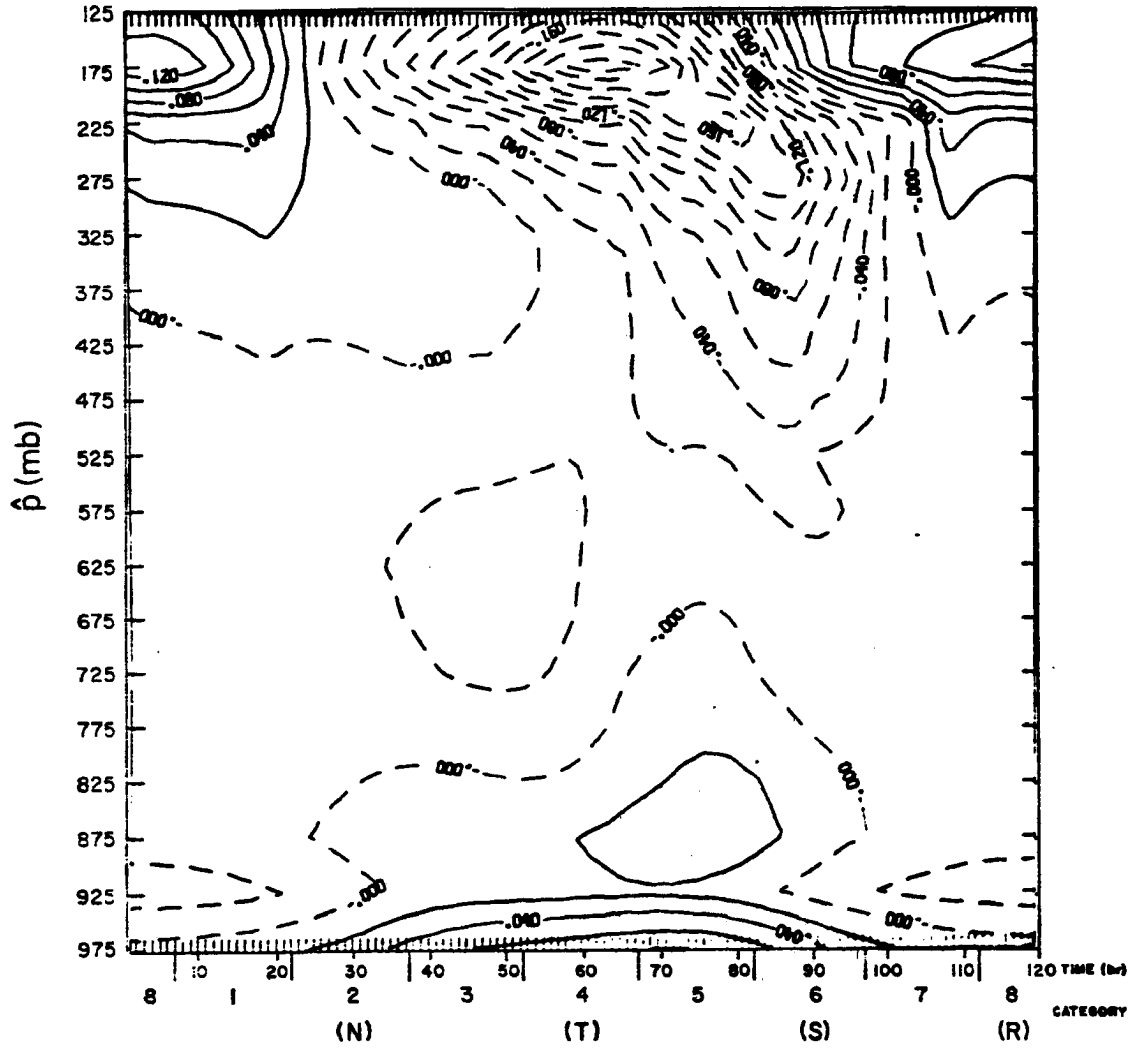

Fig. 4.13b Temperature tendency (°C hr^{-1}) in experiment A3.

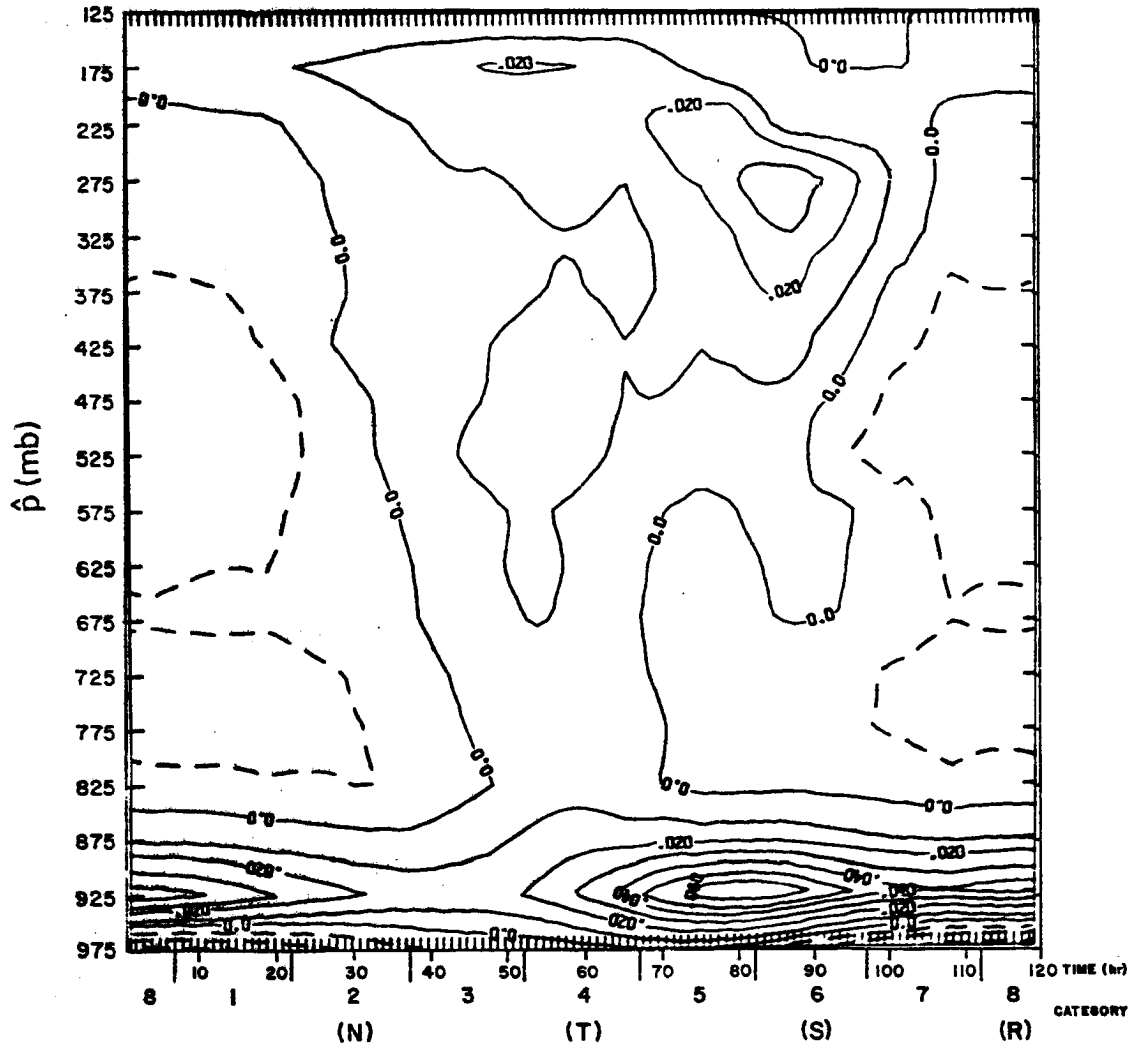

Fig. 4.13c Moisture tendency ($g\,kg^{-1}\,hr^{-1}$) in experiment A3.

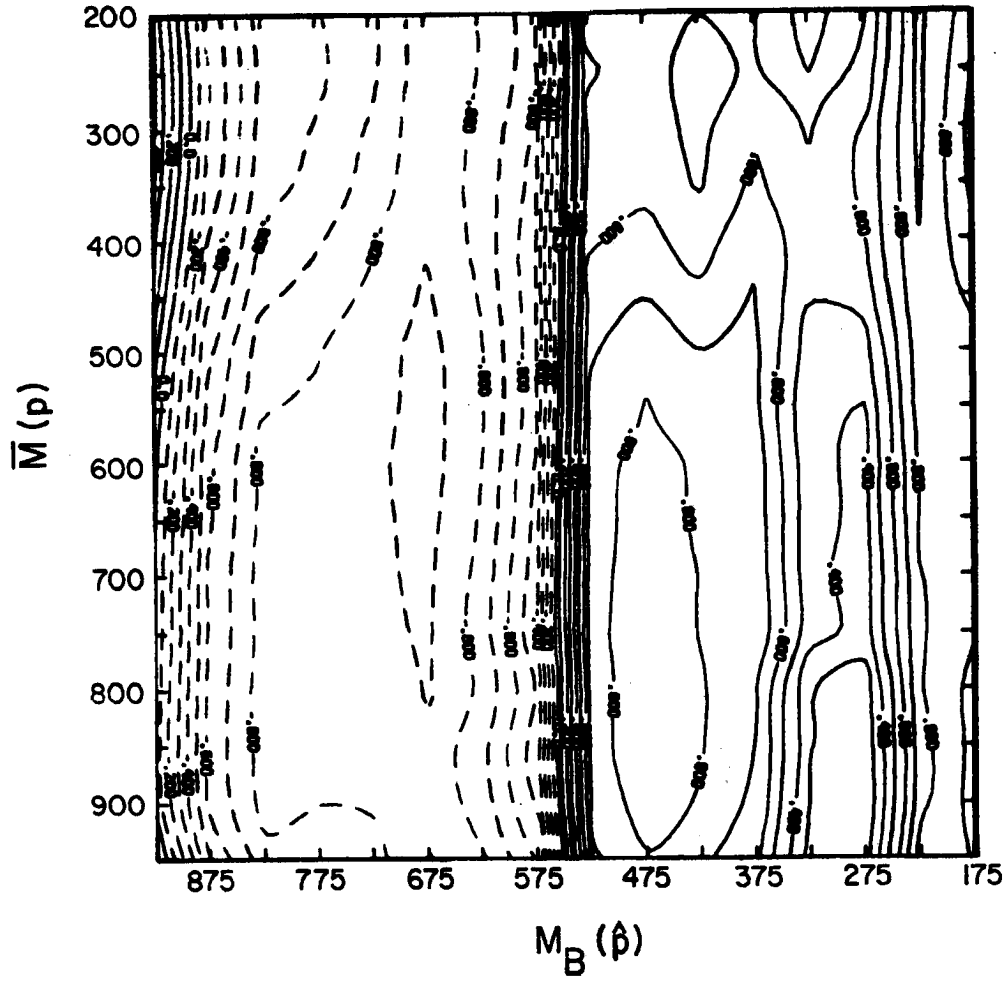

Fig. 4.13d Correlation coefficient between $\bar{M}(p)$ and $M_B(\hat{p})$ in experiment A3.

Jacobson and Gray (1976) it is possible that the extra convergence due to the differential heating does increase the dynamical forcing but this has to be shown in a model which allows an interaction between the dynamics and the thermodynamics.

The negative temperature tendency now includes the ridge region between levels p = 425 mb and p = 925 mb with warming above (Fig. 4.13b). Around the trough category a distinct warming region below and cooling region above is observed. The warming in the boundary layer is smaller ($\approx$0.001°C hr^{-1}) in the ridge and larger in the trough ($\approx$0.08°C hr^{-1}) than in case A2. The moisture tendency field is shown in Fig. 4.13c; a larger middle and lower tropospheric drying in the ridge category, due to the increased drying effect of the compensating subsidence induced by deep convection, is observed.

Let us now consider the effect of changing the autoconversion coefficient c_0 in the rain parameterization. Experiment B3 (Fig. 4.14) differs from A3 only by the inclusion of a cloud type dependent c_0 which makes deeper clouds more efficient and shallow clouds less efficient in producing rain as shown in Fig. 4.7. In terms of the reductive effect on the cloud work function it is clear that a deep cloud does not affect A of a shallow cloud if the lateral detrainment is zero. However, a shallow cloud has its detrainment of liquid water at cloud top enhanced if it is less efficient in producing rain, thus favoring the buoyancy of deeper clouds through the evaporative cooling and making shallow clouds less efficient in reducing A of deeper clouds; the opposite effect is observed when considering the influence of a cloud with a larger autoconversion coefficient on a deeper cloud.

The effect of varying the precipitation efficiency of clouds in the distribution of $M_B(j)$ is, however, hardly discernible as shown in Fig. 4.14a and in the correlation coefficient matrix (Fig. 4.14d). Although small, the effect on $M_B(j)$ is such that deep clouds are increased and shallow clouds are decreased. This agrees with the discussion in the previous paragraph since deeper clouds, being more efficient in reducing the cloud work function of all other clouds, would be preferred by the dynamical control; this effect is more sensitive in the ridge as shown by Fig. 4.14a. Although the change in the mass flux distribution is small, the effect of changing the precipitation efficiency affects the temperature and moisture tendencies (Figs. 4.14b and 4.14c respectively). No sign changes are observed but the magnitude of the cooling at upper levels is reduced mainly in categories 4 and 5 while the warming above cloud base is decreased. In general the destabilization effect produced by cumulus convection, as observed in the temperature tendency of case A3 (Fig. 4.13b), has been reduced in case B3 and although by a small amount it may have a significant effect upon an integration of the model in which the modified temperature and moisture changes are allowed to feedback. In terms of moisture tendency changes, the anticipated effect, i.e. a smaller moistening at upper layers around the trough category was observed; the slight increase in deep convection, which has a drying effect in lower levels, tied to the slight decrease of shallow convection, which has a moistening effect, contribute to the smaller moistening tendencies in the lower troposphere.

The lateral detrainment modifies the effect of a deep cloud on a shallow one because it changes the environment not only by the

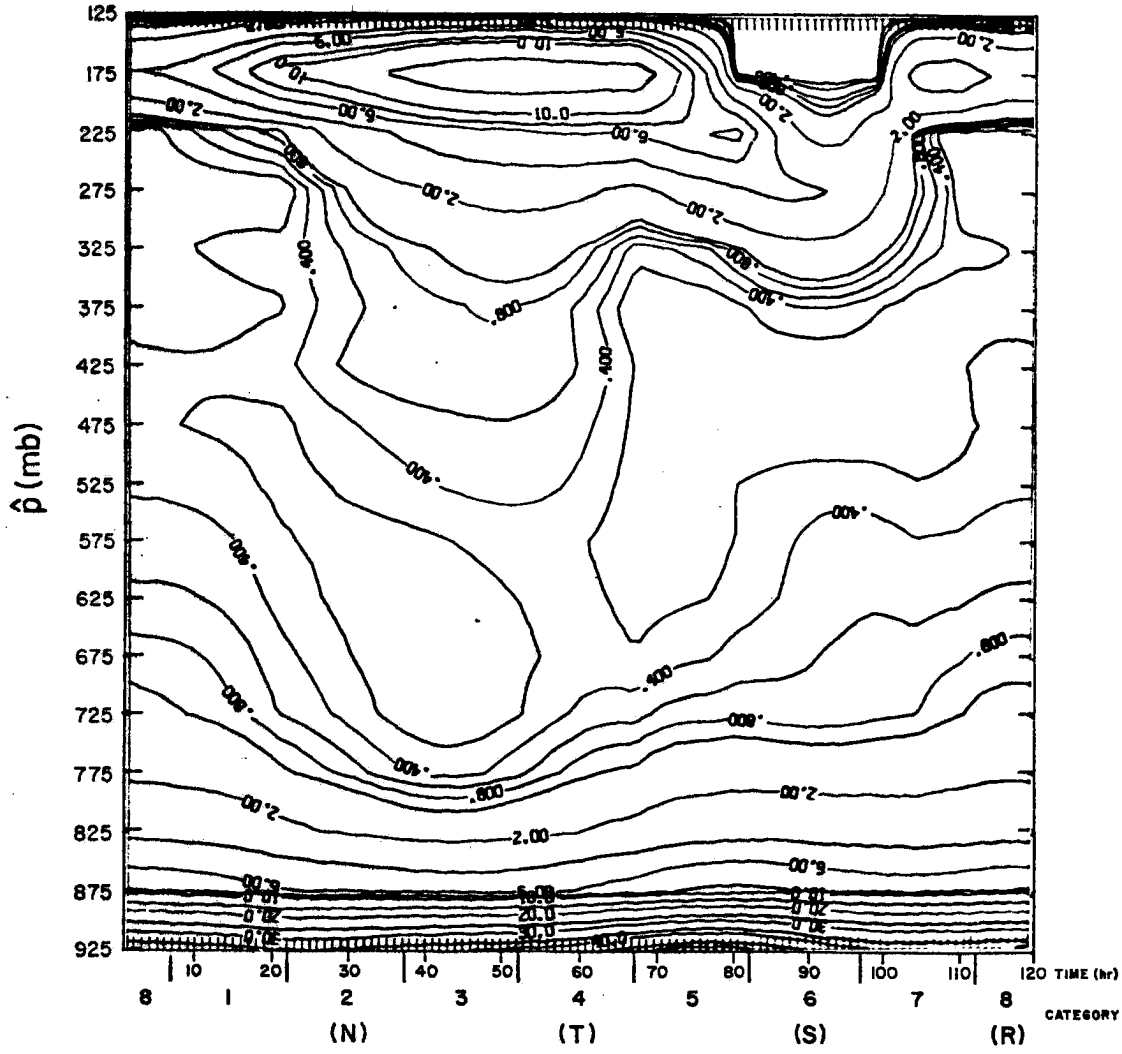

Fig. 4.14a This figure shows the results of experiment B3 in which $V_S = V_S(t)$, $\lambda^- = 0$, c_0 is cloud type dependent and the radiative cooling is a function of time. Cloud base mass flux in $kg\,m^{-2}\,hr^{-1}$.

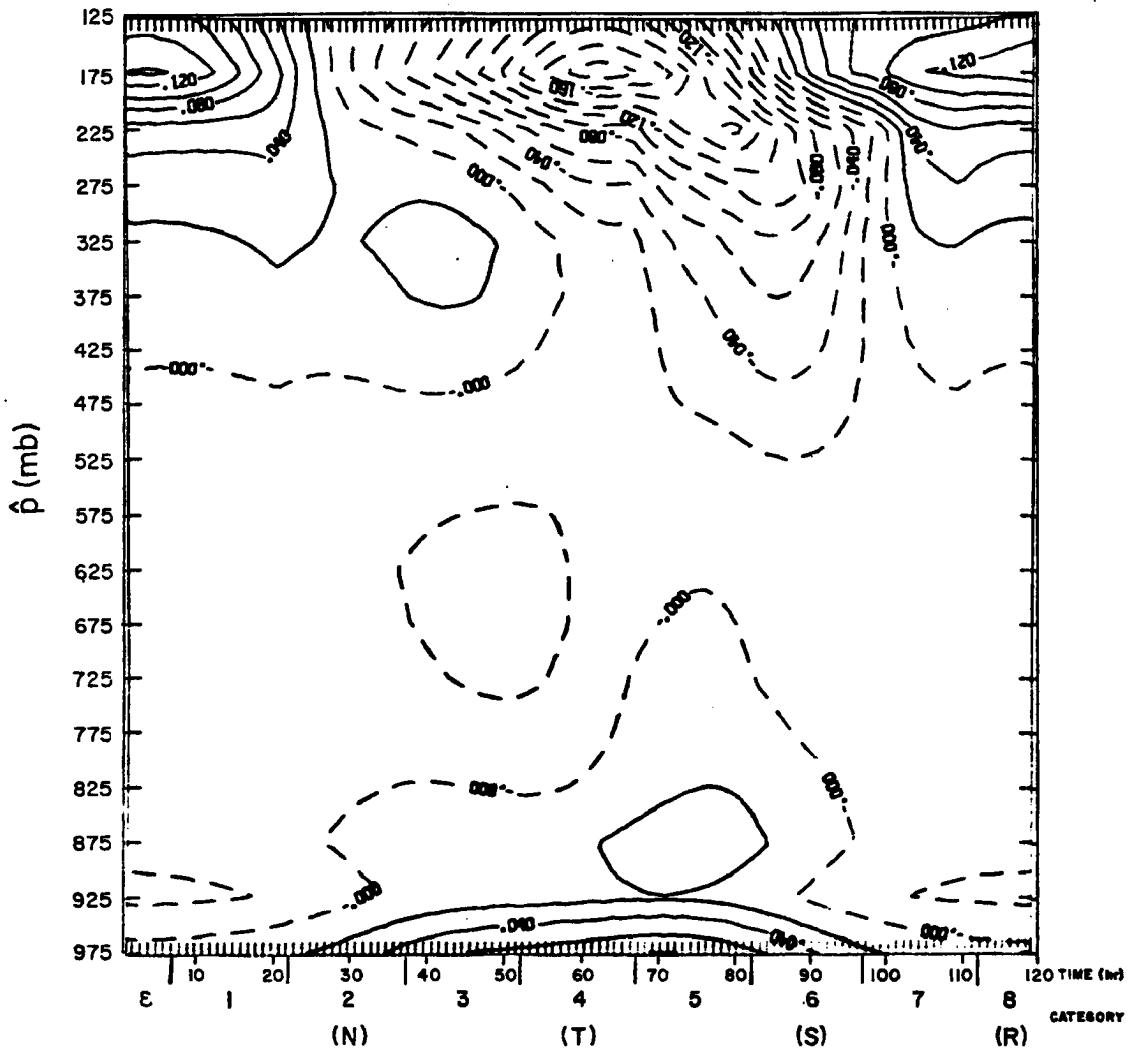

Fig. 4.14b Temperature tendency (°C hr^{-1}) in experiment B3.

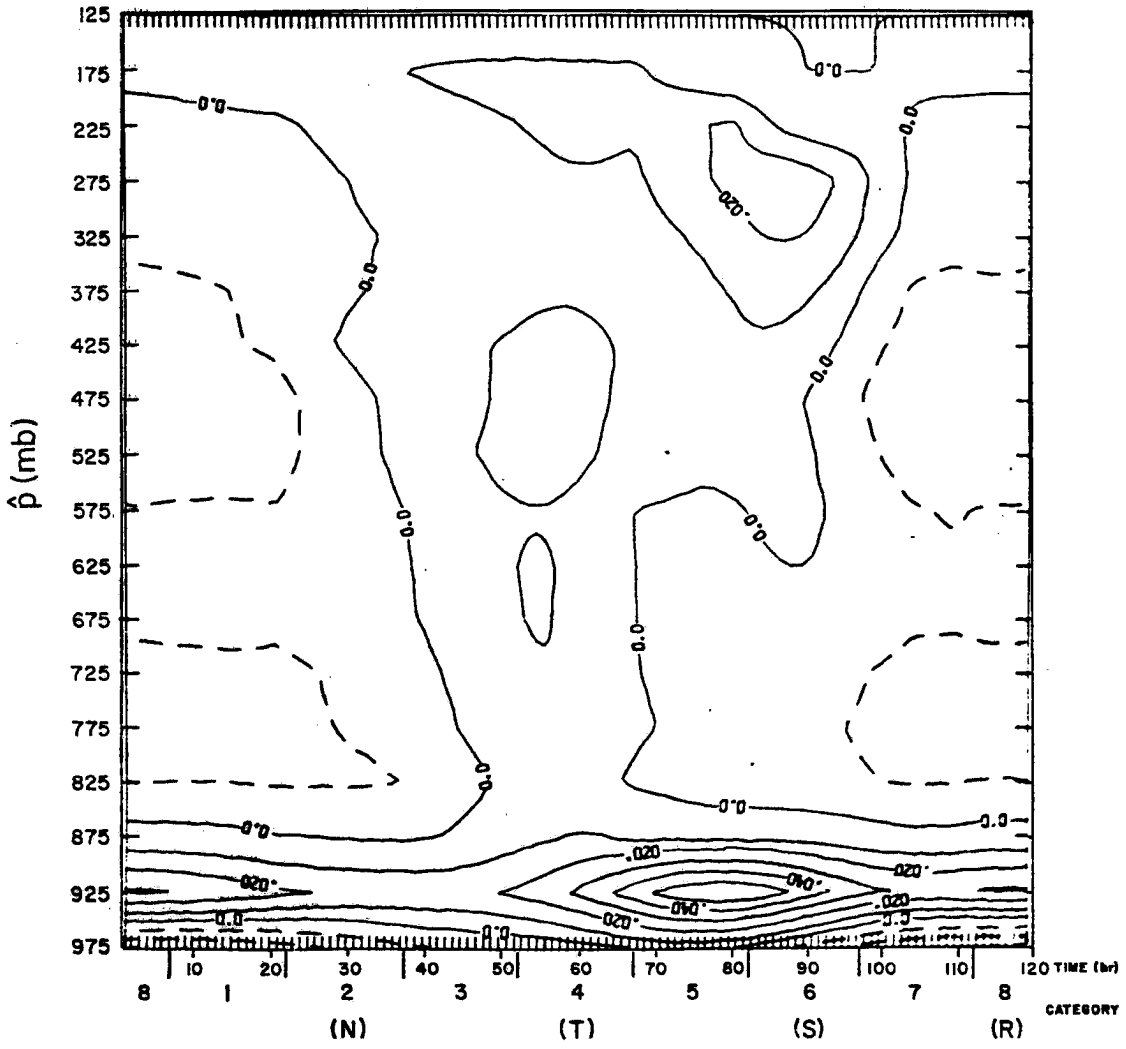

Fig. 4.14c Moisture tendency (g kg^{-1} hr^{-1}) in experiment B3.

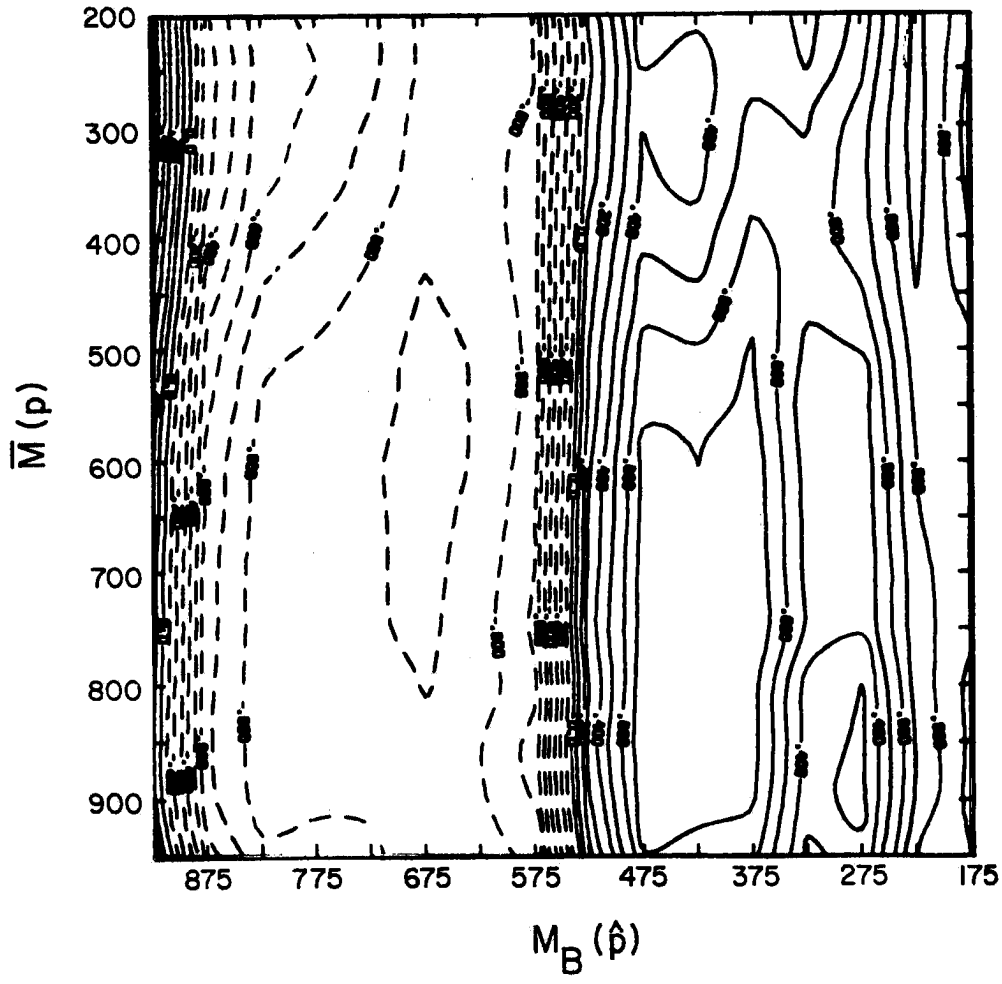

Fig. 4.14d Correlation coefficient between $\bar{M}(p)$ and $M_B(\hat{p})$ in experiment B3.

compensating subsidence but also by the continuous detrainment of cloud properties s_c, q_c and ℓ all the way up to its detrainment level. The efficiency of both deep and shallow clouds in reducing A of any cloud, as measured by the kernel, was observed to be smaller with $\bar{\lambda}$ different than zero and following a complicated pattern. In Fig. 4.15a the cloud base mass flux of case C3 is shown.

The modulation of M_B when subjected to the same forcing as in case B3, as well as the same values of $c_o(j)$, is the same, except for the shallowest cloud type (j = 17) and the deepest one (j = 2) where a significant deviation from the previous patterns is observed. Cloud type 2 shows two maxima: the first is centered between categories 1 and 2 and the second in the trough category, being the strongest and of about the same magnitude of the one observed in case B3. Cloud type 17 instead of having its cloud base mass flux increased in categories 5 and 6, as observed in the preceding cases, is inhibited in this region while all other cloud types, deeper than it, tend to follow the general pattern.

The relationship between $\bar{M}$ at all levels and M_B of all cloud types is shown in Fig. 4.15d through the correlation coefficient matrix as previously defined. The general pattern is again similar to the one obtained in case B3: cloud type 2 ($\hat{p}$ = 175 mb) is better correlated with $\bar{M}$ at level p = 900 mb, cloud type 3 ($\hat{p}$ = 225 mb) with $\bar{M}$ at p = 200 mb (right above its detrainment level); cloud types 4 and 5 ($\hat{p}$ = 275 mb and $\hat{p}$ = 325 mb respectively) have the highest correlation with $\bar{M}$ at the half level just below the detrainment level (p = 300 mb and p = 350 mb respectively); cloud types 6 to 9 ($\hat{p}$ between 375 mb and

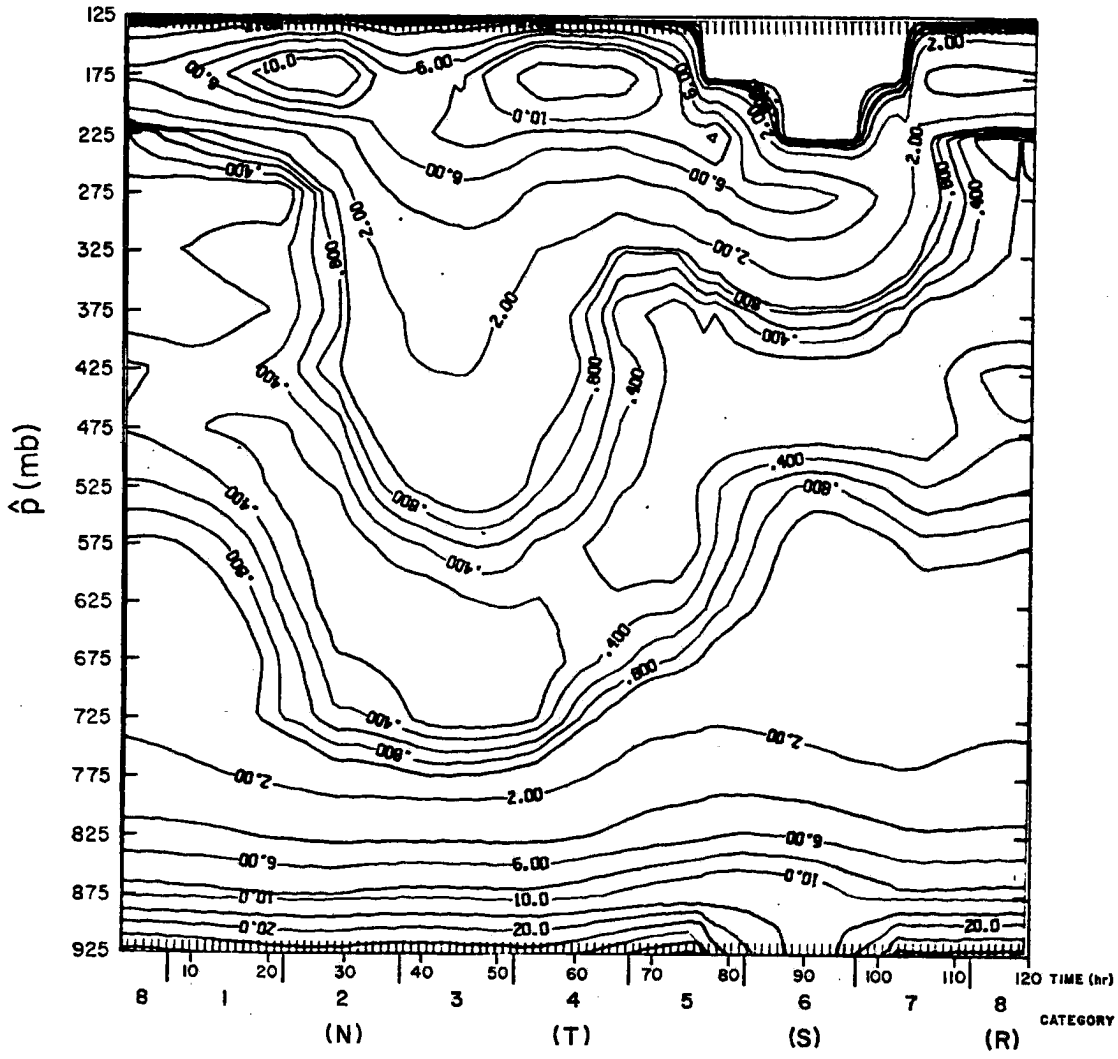

Fig. 4.15a This figure shows the results of experiment C3 in which $V_S = V_S(t)$, λ^- and c_0 are cloud type dependent and the radiative cooling profile is a function of time. Cloud base mass flux is kg m^{-2} hr^{-1}.

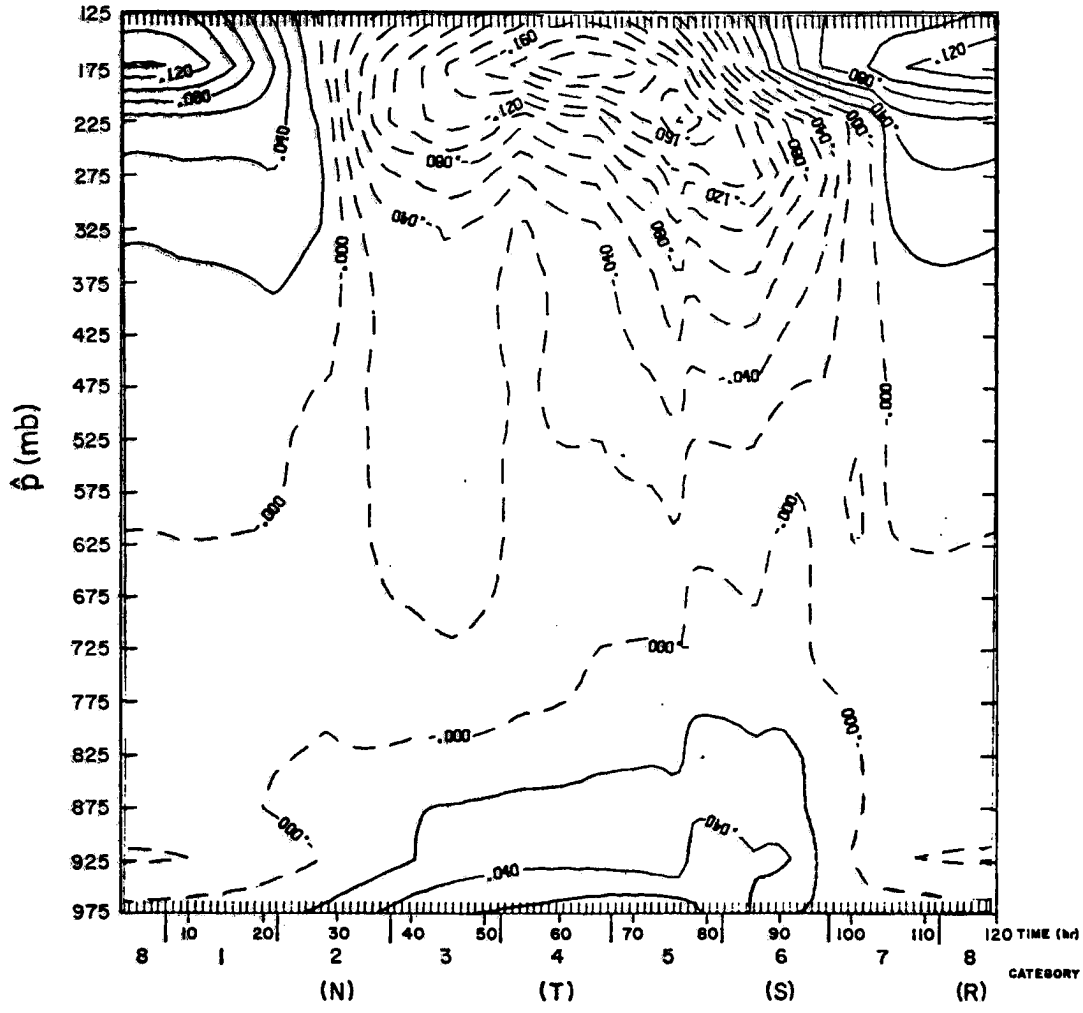

Fig. 4.15b Temperature tendency (°C hr^{-1}) in experiment C3.

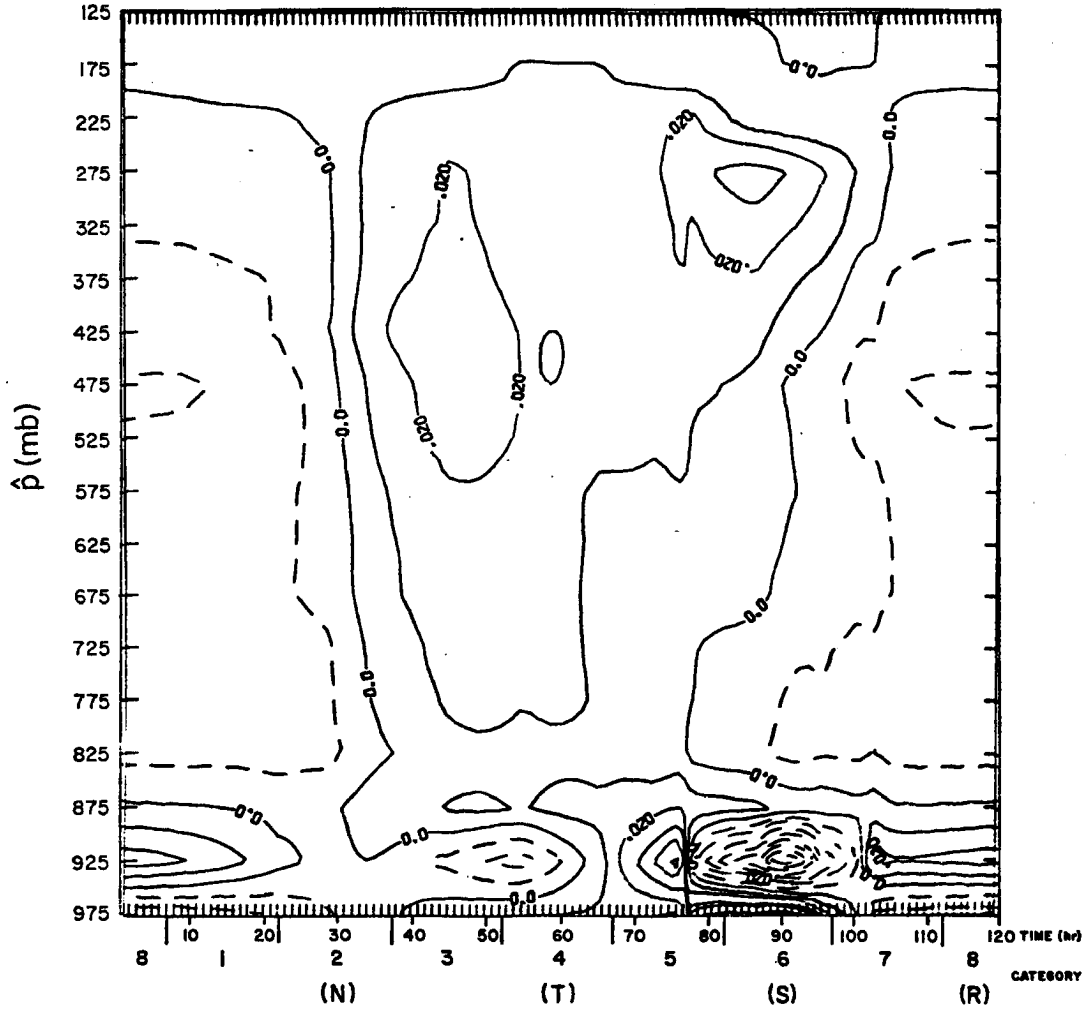

Fig. 4.15c Moisture tendency (g kg^{-1} hr^{-1}) in experiment C3.

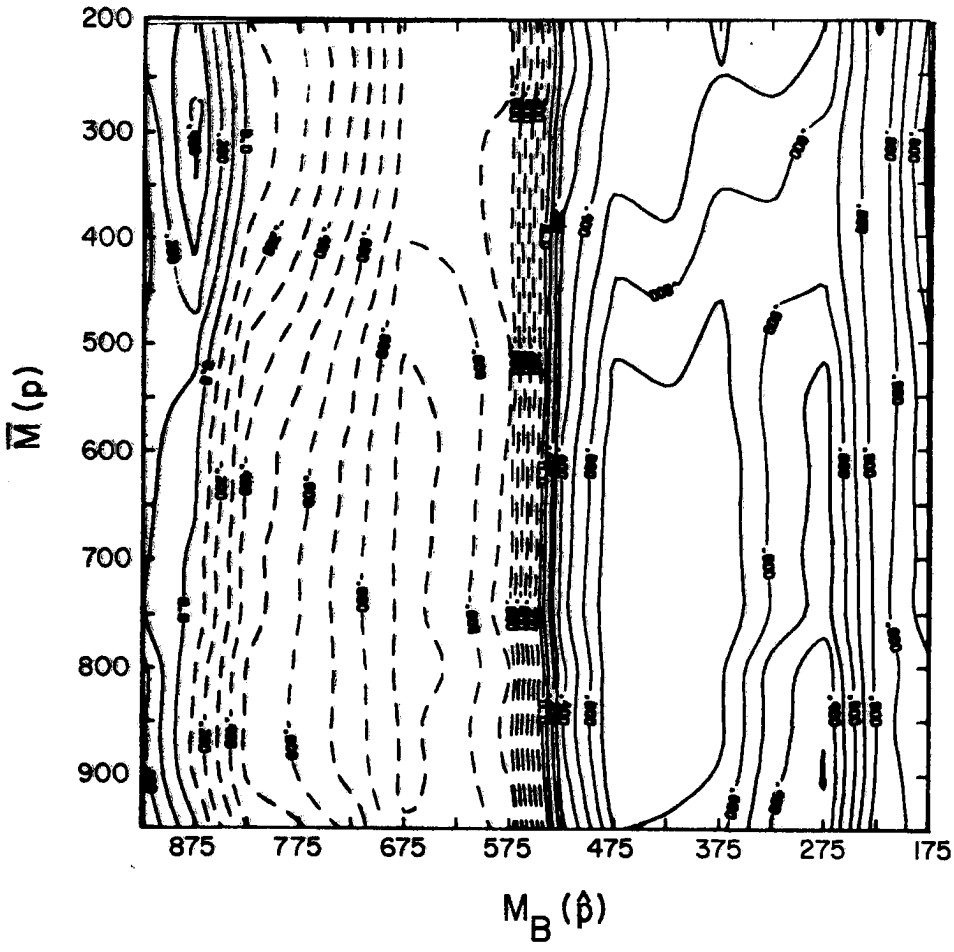

Fig. 4.15d Correlation coefficient between $\bar{M}(p)$ and $M_B(\hat{p})$ in experiment C3.

525 mb) are better correlated with $\bar{M}$ at about 300 mb below the detrainment level; shallower clouds, down to cloud type 15 ($\hat{p}$ = 825 mb), are negatively correlated to $\bar{M}$ with maximum magnitude at approximately the detrainment; cloud type 16 is negatively correlated with $\bar{M}$ at lower levels but positively correlated at upper levels (small values in magnitude) and cloud type 17 is positively but poorly correlated with $\bar{M}$ at all levels. The major differences between case B3 and C3, in terms of the correlation coefficient matrix (Fig. 4.14d and 4.15d respectively), are in cloud types 2 and 17 as discussed before; the coefficients are smaller, showing less significative correlations in case C3. This different behavior of cloud types 2 and 17 was found in experiment C1 (not shown here) suggesting that it is related to the introduction of the lateral detrainment rather than to changes in surface fluxes or radiative cooling profile.[1]

Concerning temperature and moisture tendencies (Fig. 4.15b and 4.15c respectively), both the B3 and C3 cases present the same general pattern in terms of positive and negative regions but the magnitudes tend to be larger in C3. An interesting difference between B3 and C3 is related to the moisture tendency at the boundary layer: large positive tendencies are observed in category 6 (0.06 $g\,kg^{-1}\,hr^{-1}$) while while right above cloud base (p = 925 mb) large negative tendencies are present (-0.06 $g\,kg^{-1}\,hr^{-1}$). This is related to the anomalous distribution of $M_B(17)$ and $M_B(2)$ in category 6 thus producing an unreasonable result.

---

[1]Experiments with different forms of $\lambda^{-}(\hat{p})$ have shown similar results.

A certain unsmoothness in the distribution of $M_B(2)$ and $M_B(17)$ has been observed in the previous cases in category 6. Fig. 4.16 shows the time series of $B(j) = A(j)_{LS} - A_c(j)$ for all possible cloud types j, i.e. the adjustment to be made by cumulus convection, for experiment A1. The region of maximum upward large-scale vertical motion is associated with the largest values of B(j). No sharp changes in the forcing are found at category 6. Thus, how can we explain the peculiar behavior of $M_B(2)$ in this category? The author is currently studying the effect of possible instabilities in the solution of the cloud base mass flux as given by the linear programming approach.

4.5 Comparison with Observations

Let us compare now the heating and moistening patterns observed in section 4.4 with Reed and Recker's temperature and relative humidity field shown in Figs. 4.17 and 4.18, respectively. Since we are interested in comparing gross features we may associate regions of high relative humidity in Fig. 4.18 with regions of high moisture content in the atmosphere because the temperature deviations are small. It must be observed at this point that in this study we have computed the temperature and moisture tendencies while Reed and Recker's data refer to temperature deviations and the actual moisture field. Thus, we will be looking at regions of largest tendencies and accumulated moisture and temperature changes.

In the trough region the strong cooling at upper levels observed by Reed and Recker (Fig. 4.17) is predicted by the model. However the warming region centered at about 300 mb is shown as a blob of warm air

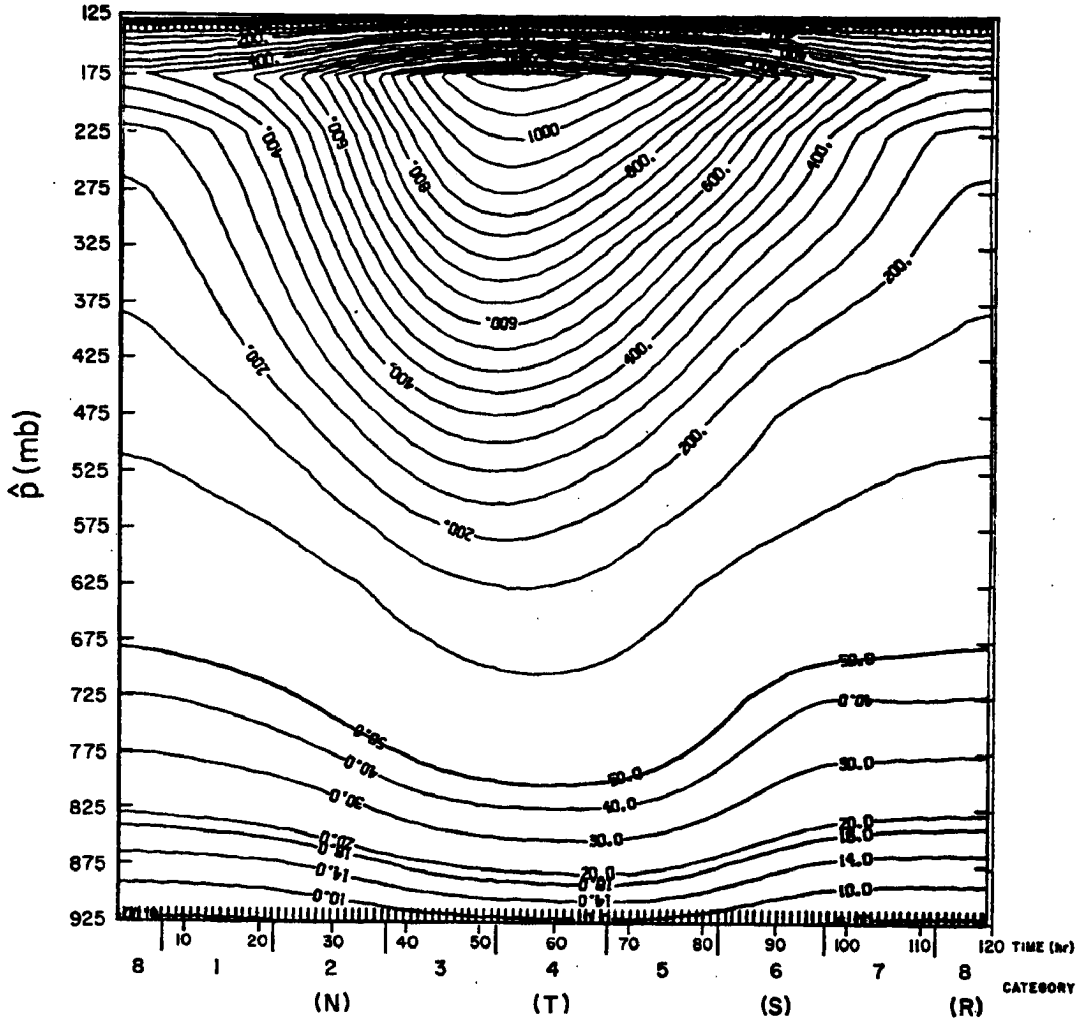

Fig. 4.16 The necessary adjustment to be made by cumulus convection in terms of $A(\hat{p})_{LS} - A_c(\hat{p})$ as a function of cloud type $\hat{p}$ (ordinate) and time or wave category (abscissa). The critical value of the cloud work function is given by the average profile of $\bar{s}$ and $\bar{h}$ shown in Figure 4.1 (units in $J\,kg^{-1}$).

in the lower troposphere by the model, including the boundary layer where a large cooling should be observed. The later problem may be related to the neglect of the effect of rain falling through the lower part of the atmosphere. The warm region in the ridge between p = 100 mb and p = 200 mb is shown in the model mainly by cases A3, B3 and C3, although the depth of the warming region increases in this same order. The cooling region in the middle troposphere is picked up by the model when the time dependent radiative cooling profile is considered, i.e. when the largest loss of energy by radiation occurs in the ridge category, corresponding to the clear region profile of radiation. The warm region between the surface and 625 mb is not observed in the model.

The moist region ahead of the trough in Fig. 4.18 is shown by the model in all cases. In addition, the largest negative moisture tendencies tend to occur in the ridge category which may conceivably produce the driest spots just to the east of the ridge as observed by Reed and Recker (Fig. 4.18). The moisture tendencies, as observed by the model, present the largest discrepancies with observations in the lower troposphere, e.g. in categories 5 and 6 where the most intense surface evaporation is observed. The intense evaporation enhances the activity of shallow clouds, producing a larger moistening of the lower troposphere (compare cases A1 and A2).

The above results and the frequently observed discontinuity in the moisture and temperature tendencies between the boundary layer level (p = 975 mb) and the integer level right above cloud base (p = 925 mb) suggest that the parameterization of the boundary layer in terms of cloud base fluxes of heat and moisture should be improved. The author

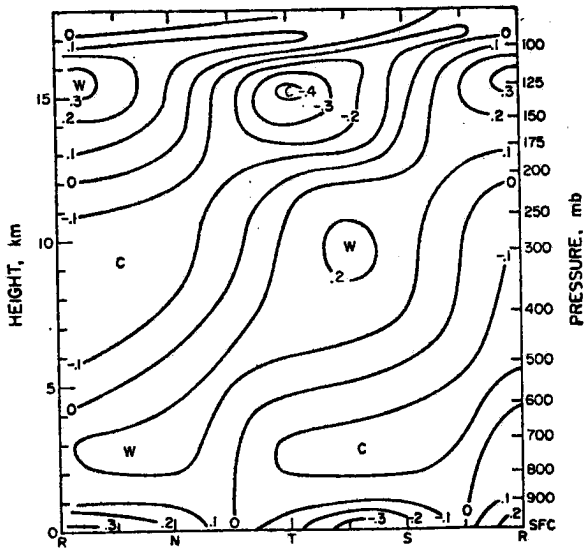

Fig. 4.17 Temperature deviation field as a function of height and wave category (after Reed and Recker, 1971).

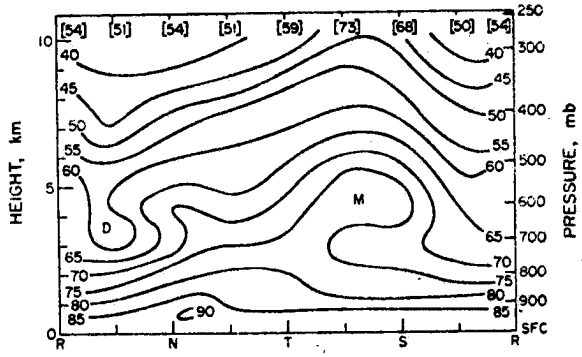

Fig. 4.18 Relative humidity field as a function of height and wave category (after Reed Recker, 1971).

is currently working on a model which allows a variable depth mixed layer. Another important mechanism which affects the lower troposphere is related to the cumulus downdrafts which were neglected in this study (Betts, 1976). Johnson (1976), using a similar diagnostic cloud spectral model, showed that the neglect of cumulus downdrafts and their associated rainfall evaporation leads to the diagnosis of an excessively large population of shallow cumulus clouds in highly convective situations. Important effects on the sub-cloud layer moisture budget by the downdraft water vapor transport in this region were also observed. Since the cloud population, as determined by M_B, is linked to the moisture and temperature changes in all layers through the kernel, we may expect significant changes in the results shown in section 4.4 with a more realistic model.

It has to be emphasized at this point that, although the large-scale advection of heat and moisture into each wave category (as shown by Reed and Recker, 1971) has a small effect compared to the temperature and moisture changes made by the large-scale vertical advection, the tendencies predicted by this model are comparable to the horizontal advection effect in the middle troposphere. Larger deviations are found in the lower troposphere, which were already discussed, and in the upper troposphere around the trough category where most of the deep convection occurs. The later deviation may be caused by the assumption that clouds do not overshoot their level of vanishing buoyancy (Frank, 1976). Thus, we see that in order to obtain a more quantitative comparison with observational studies it is necessary to make a study, similar to this

one, in which horizontal transports are also taken into account. This might best be done using GATE data.

It is interesting to compare the observed and the computed rainfall from moisture budget considerations (Reed and Recker, 1971), shown in Fig. 4.19a and 4.19b respectively, with the rainfall predicted by the model in cases B3 and C3 (Figs. 4.20a and 4.20b respectively). Fig. 4.19a includes the precipitation observed at the basic triangle of stations (Kwajalen, Eniwetok and Ponape) as a solid line and the average precipitation over all 10 stations of the network used in Reed and Recker's composite analysis as a dashed line.

The rainfall predicted by the model is within 20% of the computed rainfall from the moisture budget in categories 2 through 7. The largest deviations occur in categories 1 and 8; however the predicted values, using the average radiative cooling profile shown in Fig. 4.4 (which is smaller in the trough than the clear region type used in experiments B3 and C3) are only about 20% larger than the values in Fig. 4.19b in categories 1 and 8. Comparing Fig. 4.19a with Fig. 4.20 we see that the agreement between the observed precipitation and the predicted values is good when the values for the 10 station average precipitation are considered.

Yanai et al. (1976) studied the correlation of deep and shallow cumuli with large-scale processes using the data taken in the Marshall Islands area for a 100-day period. A correlation coefficient between $M_B(\hat{p})$ and $\bar{M}(p)$ for all pairs of discrete values of $\hat{p}$ and p were also computed and their result is shown in Fig. 4.21. The correlation is not as high as in the experiments shown in section 4.4 because a

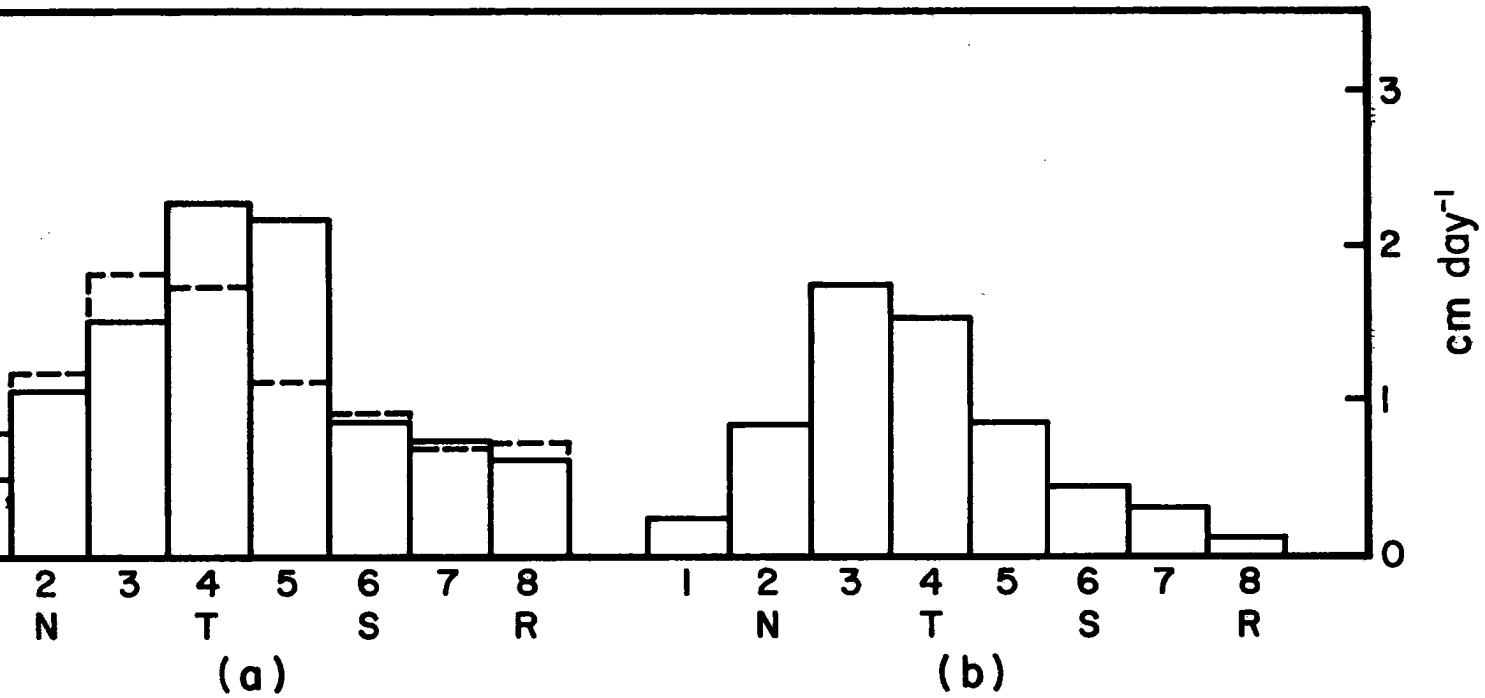

4.19 Observed (a) and computed (b) average precipitation in various wave categories (after Reed and Recker, 1971). In (a) the continuous line represents the average precipitation in the triangle of stations (KEP) and the dashed line is the precipitation for all 10 stations in the network used by Reed and Recker.

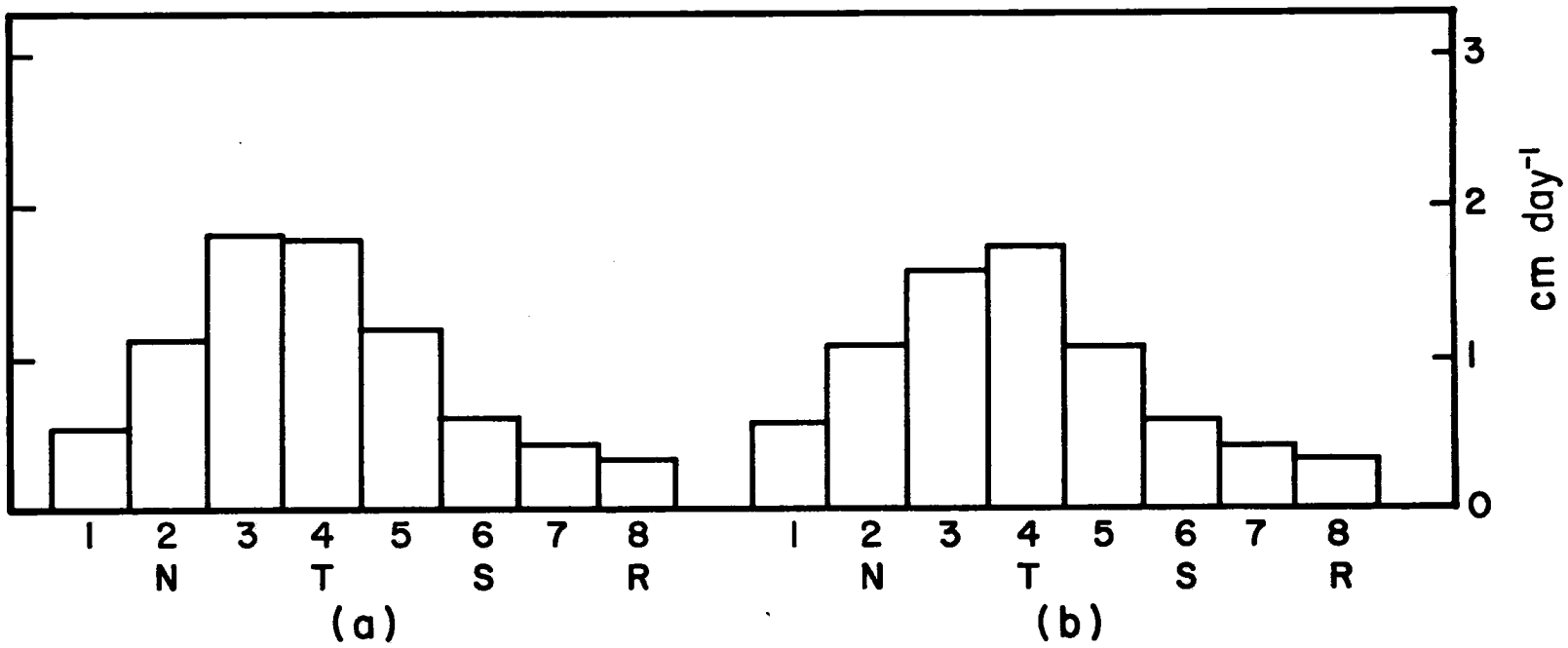

Fig. 4.20 Predicted precipitation for each wave category in experiment B3 (a) and C3 (b).

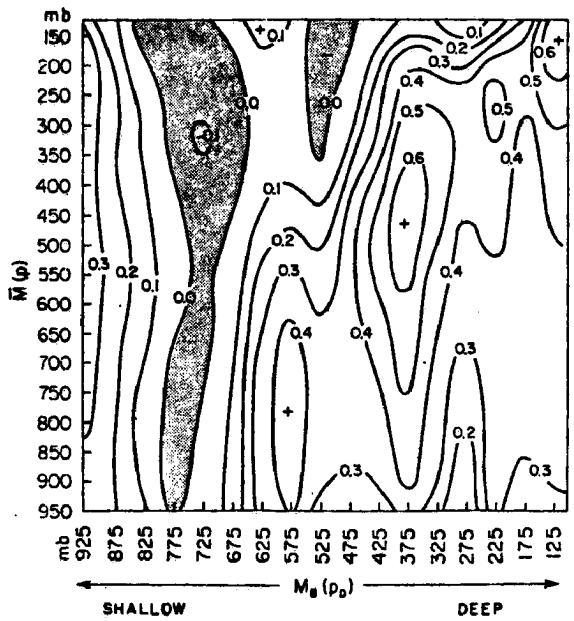

Fig. 4.21 Correlation coefficients between the time series of the large-scale mass flux M(p) of all discrete levels and the cloud base mass flux $\bar{M}_B$ of various cloud types $\hat{p}$ (after Yanai et al., 1976).

sinusoidal wave in which the vertical motion at each level is highly correlated with the vertical motion at other levels was used in this study. However, some similarities are found with cases A2, A3, B3 and C3, such as the strong correlation between the mass fluxes associated with deeper clouds (smaller $\hat{p}$) and the large-scale vertical motion at or near the detrainment level except for cloud type 2 ($\hat{p}$ = 175 mb). Another similarity is the negative region near $\hat{p}$ = 775 mb and positive correlations again toward shallower clouds. This effect was shown to be related to the boundary layer forcing in terms of surface fluxes. The negative region seems to be related to the suppression of the shallow type of convection when deep convection is present although they coexist.

However one has to be careful in interpreting the correlation coefficient matrix, defined in terms of $M_B(\hat{p})$ and $\bar{M}(p)$, as a cause and effect relationship in terms of pure dynamical forcing as we have shown when comparing experiments A1 and A2.

5. SUMMARY AND CONCLUSIONS

The objective of this research was to study the Arakawa-Schubert cumulus parameterization theory with the quasi-equilibrium assumption formulated as an optimization problem. A simple experiment was devised in which the forcing is imposed through a large-scale vertical motion (dynamical forcing), large-scale radiative cooling profile and surface wind speed (which controls surface fluxes of heat and moisture through the bulk aerodynamic formula). Assuming a time dependent functional expression for the above three types of forcing, their effects on the mass flux distribution function and the temperature and moisture tendencies were studied. The basic atmosphere upon which cumulus convection is supposed to act is given by Yanai's Marshall Islands observations which are located in the ITCZ and the dynamical forcing is given by Reed and Recker's (1971) $\bar{\omega}$-field (Fig. 4.3). The time dependent functional relation for the surface wind speed was obtained by fitting the evaporation predicted by the model to Reed and Recker's evaporation curve and the cloud/cloud-free radiative cooling profile was obtained from Frank (1976). Changes in some internal parameters like the auto-conversion coefficient c_0 in the rain parameterization, lateral detrainment λ^- and different weights in the objective function of the minimization problem associated with the quasi-equilibrium assumption were also considered (section 4.2).

In order to test the effect of the various forcing mechanisms and the internal parameters discussed above, three basic types of experiments were devised: the first experiment maintains a constant radiative cooling profile and surface wind speed while the dynamical

forcing is given by Reed and Recker's $\bar{\omega}$-field; the second experiment introduces the time dependent surface wind speed and the time dependent radiative cooling profile is considered in the third experiment. Each of the above three experiments was performed assuming different sets of the model parameters c_0 and $\bar{\lambda}$.

The use of constant weights for the slack variables associated with each cloud type (c(i), i = 1, 2, ...17) has produced a spectrum of clouds not displaced toward the shallow type of convection such as in the case of a generalized subsidence field (Nitta, 1975; Yanai et al., 1976). Best results were obtained when considering c(i) inversely proportional to the maximum adjustment to be made by each cloud type i (i.e., $c(i) = b(i)^{-1}$). The author is currently performing a rigorous sensitivity analysis on the linear programming approach to check the possibility of the existence of an optimum choice of the matrix α.

A suppressive effect of deep convection on the shallow type of convection was observed in experiment A1; the controlling effect of the boundary layer forcing, in terms of surface fluxes, on the shallow cloud population was the main conclusion of experiment A2 and the role of the radiative cooling in determining the population of clouds was studied through experiment A3. Concerning the later experiment, the main results were the production of a bi-modal distribution of M_B in the ridge and a slight decrease in the mass flux associated with clouds in the trough region where the radiative forcing is smaller than in case A2.

The inclusion of a cloud type dependent auto-conversion coefficient which made deep clouds more efficient and shallow clouds less

efficient in producing rain is shown in experiment B3. The results show that the population of clouds is little affected by such modification but the magnitude of the temperature and moisture tendencies are decreased (because the detrainment of cloud liquid water to the environment is sensitive to c_0).

A non-zero lateral detrainment coefficient $\lambda^-(\hat{p})$ is introduced in experiment C3. The magnitude of the cloud base mass flux is altered but the main modifications are observed in cloud type 2 ($\hat{p}$ = 175 mb) and cloud type 17 ($\hat{p}$ = 925 mb) which produced some unreasonable results in the temperature and moisture tendencies. The results seem to question the usefulness of introducing the lateral detrainment coefficient which also requires an empirical relationship between λ^+ and λ^- (4.1).

According to the Arakawa-Schubert cumulus parameterization theory, the temperature and moisture changes are not independent of each other; the link is accomplished by the quasi-equilibrium assumption in terms of the cloud work function which is a measure of the sub-ensemble conditional instability. The quasi-equilibrium assumption, as originally formulated, is not a well posed mathematical problem and a new interpretation was given leading to the so-called optimal adjustment method (section 3.4.4). The idea is to minimize the change of the cloud work function, induced by the larger scale and surface forcing, through the stabilizing effect of cumulus convection. The discrete form of this problem is solved by linear programming and the unknowns are considered to be $\frac{\partial A(\hat{p})}{\partial t}$ and $M_B(\hat{p})$; the objective is to minimize some gross measure of $\frac{\partial A(\hat{p})}{\partial t}$ subjected to $M_B(\hat{p}) \geq 0$.

The optimal adjustment method was shown to yield reasonable cloud base mass flux distributions and rainfall rates but temperature and

moisture tendencies seem to be too large at the lower and upper boundaries of the model.

The stabilizing effect of cumulus convection in a very active region (e.g., in the trough category) was attained by warming the lower levels and cooling above. This apparent paradox is a consequence of the constraint imposed on the cloud work function which is an integral measure of the buoyancy, i.e. a warming below and cooling above may reduce A of a deep cloud since all clouds share the same cloud base conditions. Reed and Recker's observations in the trough indicate a cooling at lower levels, warming in the middle troposphere and cooling above. A reduction in the cloud work function could be obtained by such a heating pattern. The discrepancies observed in this model at the upper and lower boundaries suggest that it may be important to include the effect of evaporation of rain, downdrafts and overshooting clouds. Such cloud models could, conceivably, have a different mode of reducing the cloud work function.

The temperature and moisture tendencies observed in the middle troposphere tend to be of the order of magnitude of the neglected terms in the large-scale processes (horizontal advection) except at the upper and lower boundaries. Therefore, it would be useful to test this new approach to the Arakawa-Schubert theory in a consistent data set such as those provided by GATE. Concerning the use of experimental data, another point of the theory that deserves more research is the quasi-equilibrium assumption. Time series of the cloud work function should be computed and a comparision between the time changes of $A(\hat{p})$ and $A(\lambda^{+})$ should be made.

High resolution cloud models, such as those revised by Cotton (1975), may be useful in specifying the model parameters $\bar{\lambda}$ and c_o as well as suggesting more realistic parameterization schemes in the cloud model (downdrafts, evaporation of rain and overshooting).

REFERENCES

Albrecht, B. and S. K. Cox, 1975: The large-scale response of the tropical atmosphere to cloud-modulated infrared heating. J. Atmos. Sci., 32, 16-24.

Arakawa, A., 1969: Parameterization of cumulus convection. Proc. WMO/IUGG Symp. N.W.P. in Tokyo, November 26-December 4, Tokyo, Japan Meteorological Agency, IV, 1-6.

_____,1972: Design of the UCLA general circulation model. Numerical Simulation of Weather and Climate, Technical Report 7, Dept. of Meteorology, University of California, Los Angeles.

_____, Y. Mintz and collaborators, 1974: The UCLA atmospheric general circulation model. Dept. of Meteorology, UCLA, Los Angeles, California.

_____, and W. H. Schubert, 1974: Interaction of a cumulus cloud ensemble with the large-scale environment, Part I. J. Atmos. Sci., 31, 674-701.

Augstein, E., H. Riehl, F. Ostapoff and V. Wagner, 1973: Mass and energy transports in an undisturbed Atlantic trade wind flow. Mon. Wea. Rev., 101, 101-111.

Betts, A., 1975: Parametric interpretation of trade-wind cumulus budget studies. J. Atmos. Sci., 32, 1934-1945.

_____, 1976: The thermodynamic trasformation of the tropical subcloud layer by precipitation and downdrafts. J. Atmos. Sci., 33, 1008-1020.

Charney, J. G. and A. Eliassen, 1964: On the growth of the hurricane depression. J. Atmos. Sci., 21, 68-75.

Cho, H. R. and Y. Ogura, 1974: A relationship between cloud activity and the low-level convergence as observed in Reed-Recker's composite easterly wave. J. Atmos. Sci., 31, 2058-2065.

_____, 1977: Contributions of cumulus cloud life-cycle effects to the large-scale heat and moisture budget equations. J. Atmos. Sci., 34, 87-97.

Cotton, W. R., 1975: Theoretical cumulus dynamics. Rev. of Geo. Spa. Phy., 13, 419-447.

Fraedrich, K., 1973: On the parameterization of cumulus convection by lateral mixing and compensating subsidence, Part I. J. Atmos. Sci., 30, 408-413.

Fraedrich, K., 1974: Dynamic and thermodynamic aspects of the parameterization of cumulus convection, Part II. J. Atmos. Sci., 31, 1838-1849.

_____, 1976: A mass budget of an ensemble of transient cumulus clouds determined from direct cloud measurements. J. Atmos. Sci., 33, 262-268.

Frank, W. M., 1976: The structure and energetics of tropical cyclones. Colorado State University, Atmospheric Science Paper No. 258, Fort Collins, Colorado.

Gray, W. M., 1973: Cumulus convection and large-scale circulations. I Broadscale and mesoscale circulations. Mon. Wea. Rev., 101, 839-855.

_____, E. Ruprecht and R. Phelps, 1975: Relative humidity in tropical weather systems. Mon. Wea. Rev., 103, 685-690.

Hack, J. J. and W. H. Schubert, 1976: Design of an axisymmetric primitive equation tropical cyclone model. Colorado State University, Atmospheric Science Paper No. 263, Fort Collins, Colorado.

Hack, J. J., 1977: Numerical experiments with an axisymmetric tropical cyclone model. Thesis, Department of Atmospheric Science, Colorado State University, Fort Collins, Colorado.

Holland, J. Z. and E. M. Rasmusson, 1973: Measurements of the atmospheric mass, energy and momentum budgets over a 500-kilometer square of tropical ocean. Mon. Wea. Rev., 101, 44-55.

Jacobson, R. W. and W. M. Gray, 1976: Diurnal variation of oceanic deep cumulus convection. Colorado State University, Atmospheric Science Paper No. 243, Fort Collins, Colorado.

Johnson, R. H., 1977: The effects of cloud detrainment on the diagnosed properties of cumulus populations. J. Atmos. Sci., 34, 359-366.

Jordan, C.L., 1958: Mean soundings for the West Indies area. J. Meteor., 15, 91-92.

Kuo, H. L., 1965: On the formation and intensification of tropical cyclones through latent heat release by cumulus convection. J. Atmos. Sci., 22, 40-63.

Lopez, R. E., 1973: A parametric model of cumulus convection. J. Atmos. Sci., 30, 1354-1373.

Luenberger, D. G., 1973: Introduction to linear and nonlinear programming. Addison Wesley Publishers, 365 pp.

Manabe, S., J. Smagorinsky and R. Strickler, 1965: Simulated climatology of a general circulation model with hydrological cycle. Mon. Wea. Rev., 93, 769-798.

Nitta, T., 1975: Observational determination of cloud mass flux distribution. J. Atmos. Sci., 32, 73-91.

_____, 1977: Response of cumulus updraft and downdraft to GATE A/B-Scale motion system. Tropical Meteorology Paper No. 18, Dept. of Atmospheric Sciences, University of California, Los Angeles, California.

Ogura, Y., 1964: Frictionally controlled thermally driven circulations in a vortex with applications to tropical cyclones. J. Atmos. Sci., 21, 610-621.

_____, and H. R. Cho, 1973: Diagnostic determination of cumulus cloud population from observed large-scale variables. J. Atmos. Sci., 30, 1276-1286.

Ooyama, K., 1964: Numerical simulation of the life-cycle of tropical cyclones. J. Atmos. Sci., 26, 3-40.

_____, 1971: A theory on parameterization of cumulus convection. J. Meteor. Soc. Japan, 46, 178-201.

_____, 1973: A preliminary test of the CONTRIBE parameterization of cumulus convection. Paper presented at Study Conference on the Modeling Aspects of GATE, Joint Organizating Commitee for GARP, Talahasse, Florida.

Reed, R. J. and R. E. Recker, 1971: Structure and properties of synoptic scale wave disturbances in the Equatorial Western Pacific. J. Atmos. Sci., 28, 1117-1133.

Rosenthal, S. L., 1973: Hurricane modeling experiments with a new parameterization for cumulus convection. NOAA Technical Memorandum, ERL WMPO-4, U. S. Department of Commerce, National Hurricane Research Laboratory, Miami, Florida.

Schubert, W. H., 1974: Cumulus parameterization theory in terms of feedback and control. Colorado State University, Atmospheric Science Paper No. 226, Fort Collins, Colorado.

Williams, K. T. and W. M. Gray, 1973: Statistical analysis of satellite-observed trade-wind cloud clusters in the Western North Pacific. Tellus, 25, 313-336.

Yanai, M., S. Esbensen and J. H. Chu, 1973: Determinations of bulk properties of tropical cloud clusters from large-scale heat and moisture budgets. J. Atmos. Sci., 30, 611-627.

Yanai, M., J. H. Chu, T. E. Stark and Tsuyoshi Nitta, 1976: Response of deep and shallow tropical cumuli to large-scale processes. J. Atmos. Sci., 33, 976-991.

APPENDIX A

It was emphasized in section 2.3.2 that clouds are classified according to their detrainment level ($\hat{p}$) rather than their fractional rate of entrainment as in Arakawa and Schubert (1974). However, since the cloud properties defined in the static control are dependent on $\lambda^+(\hat{p})$ this parameter has to be determined. It is assumed that clouds detrain where they lose buoyancy or, equivalently, where the cloud and the environment share the same virtual temperature. As shown by Arakawa and Schubert (1974), this condition is given by

$$h_c(p,\hat{p}) = \hat{h}^*(\hat{p}) \ , \tag{A.1}$$

where

$$\hat{h}^*(\hat{p}) = \bar{h}^*(\hat{p}) - \frac{[1+\gamma(\hat{p})]L\,\varepsilon(\hat{p})\,\delta}{[1+\gamma(\hat{p})\varepsilon(\hat{p})\delta]}\,[\bar{q}^*(\hat{p}) - \bar{q}(\hat{p})] \ . \tag{A.2}$$

In (A.2) the effect of liquid water is ignored. As discussed in section 3.4.1, (A.1) with the definition of $h_c(p,\hat{p})$ (from (2.29)) is an implicit relation for $\lambda^+(\hat{p})$ and consequently has to be solved by an iterative process.

Let us consider now some of the properties of the solution of (A.1) in the continuous case. The solution of the moist static energy budget for the sub-ensemble $\hat{p}$ (see (2.29)) is

$$h_c(\hat{p},\hat{p}) = \frac{1}{n(\hat{p},\hat{p})}\left[h_M - \lambda^+(\hat{p})\int_{p_B}^{\hat{p}} \bar{h}(p')n(p',\hat{p})dp'\right] \ . \tag{A.3}$$

Substituting (A.3) into (A.1) we get

$$\eta(\hat{p},\hat{p})\hat{h}^*(\hat{p}) = h_M + \lambda^+(\hat{p})\int_{p_B}^{\hat{p}} \eta(p',\hat{p})\bar{h}(p')dp' \qquad (A.4)$$

and subtracting the identity

$$\eta(\hat{p},\hat{p})\hat{h}^*(\hat{p}) - \hat{h}^*(\hat{p}) = \int_{p_B}^{\hat{p}} \frac{\partial\eta(p',\hat{p})}{\partial p}\,\hat{h}^*(\hat{p})dp' \qquad (A.5)$$

into (A.4) we get

$$\hat{h}^*(\hat{p}) - h_M = -\lambda^+(\hat{p})\int_{p_B}^{\hat{p}} \eta(p',\hat{p})[\hat{h}^*(\hat{p}) - \bar{h}(p')]dp' \ . \qquad (A.6)$$

Therefore, the entrainment rate λ^+ of the cloud type which detrains at $\hat{p}$ has to satisfy (A.6). The integral on the RHS of (A.6) is a weighted measure of the difference between $\hat{h}^*$ at the detrainment level $\hat{p}$ and $\bar{h}$ between cloud base p_B and cloud top $\hat{p}$. From (A.6)

$$\lambda^+(\hat{p}) = \frac{h_M - \hat{h}^*(\hat{p})}{\int_{\hat{p}}^{p_B} \eta(p',\hat{p})[\hat{h}^*(\hat{p}) - \bar{h}(p')]dp'} \ . \qquad (A.7)$$

However, $\lambda^+(\hat{p})$ is a positive parameter by definition and since

$$h_M \geq \hat{h}^*(\hat{p}) \qquad (A.8)$$

is a necessary condition for cloud type $\hat{p}$ to exist, the integral in the denominator of (A.7) has to be positive. Fig. A.1 shows a typical profile of $\bar{h}$ and $\hat{h}^*$ based on Yanai's data. This figure shows that when computing $\lambda^+(\hat{p})$ the integrand in (A.7) gives a negative

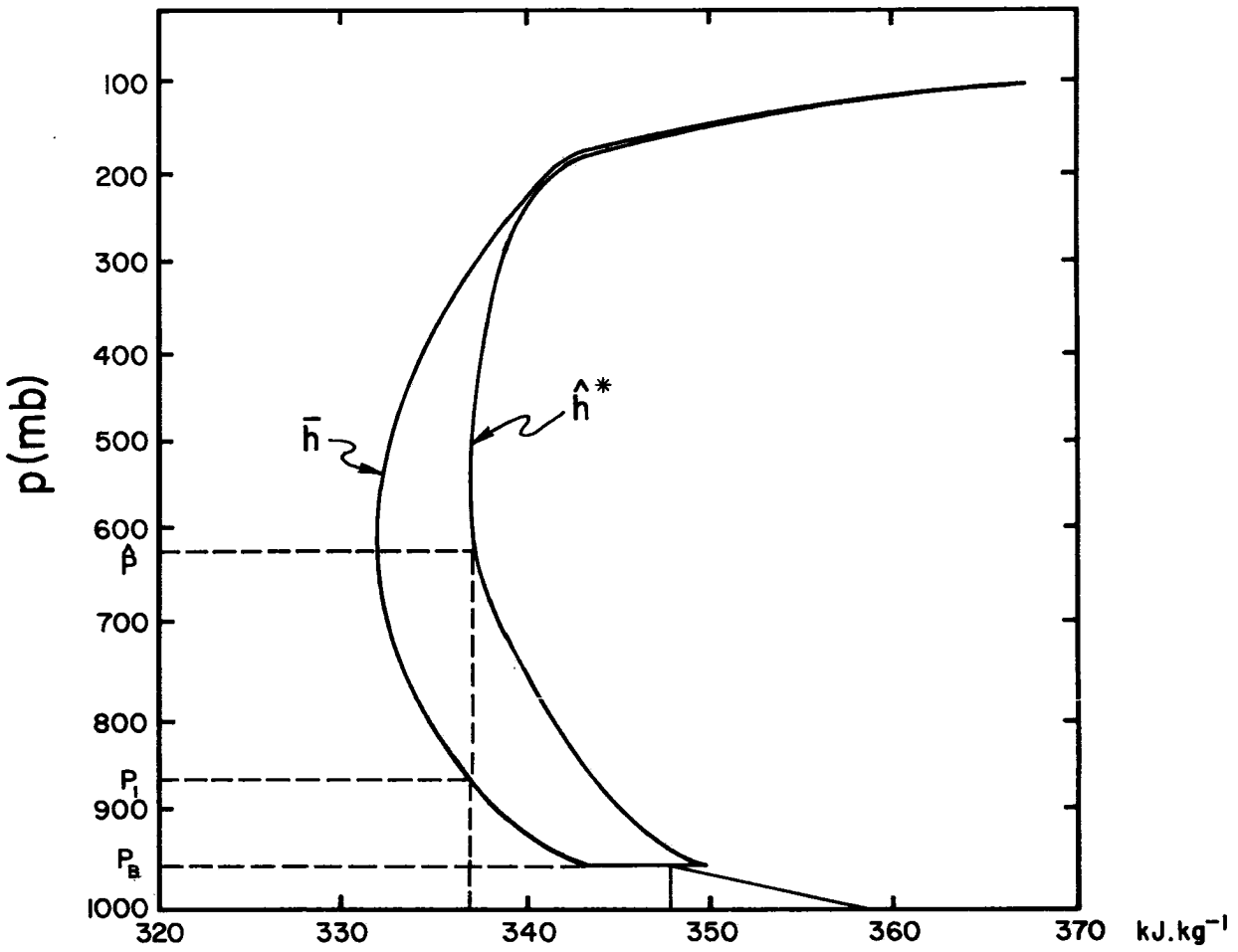

Fig. A1 Typical vertical profiles of $\bar{h}$ and $\hat{h}^*$ in the tropics. This figure shows that when computing $\lambda^+(\hat{p})$ the integrand in (A.7) gives a negative contribution between p_1 and p_B.

contribution between p_1 and p_B. However, in the region where the integrand is positive the difference

$$\hat{h}^*(\hat{p}) - \bar{h}(p') \ , \qquad \text{for} \quad \hat{p} \le p' \le p_1$$

is more heavily weighted because η increases as p' decreases and, as a result, (A.7) usually gives a realistic value of $\lambda^+(\hat{p})$. But there are situations in which, although (A.8) is satisfied, the iterative process fails to converge. It is our experience that the non-negativity of the integrand in (A.7) is not satisfied in these cases. Typically, a moist layer above cloud base yields this situation as can be easily observed in Fig. A.1.

The term $\frac{\partial \lambda^+(\hat{p})}{\partial t}$ which appears in the kernel (section 2.3.3) is obtained by taking the time derivative of (A.1). The result is

$$\frac{\hat{\partial \lambda^+(\hat{p})}}{\partial t} = \frac{\frac{\partial h_M}{\partial t} - \frac{\partial}{\partial t}\hat{h}^*(\hat{p}) - \lambda^+(\hat{p})\int_{\hat{p}}^{p_B} \eta(p',\hat{p})[\hat{h}^*(\hat{p}) - \bar{h}(p')]dp'}{[1+\lambda^+(\hat{p})]\int_{\hat{p}}^{p_B} \eta(p',\hat{p})[\hat{h}^*(\hat{p}) - \bar{h}(p')]dp'} \qquad \text{(A.9)}$$

which is valid provided that (A.7) is well defined.

BIBLIOGRAPHIC DATA SHEET	4. Report No. CSU-ATSP-275	

4. Title and Subtitle
Experiments with a Spectral Cumulus Parameterization Theory

5. Report Date
July 1977

6.

7. Author(s)
Pedro Leite Silva Dias and Wayne H. Schubert

8. Performing Organization Rept. No. 275

9. Performing Organization Name and Address
Department of Atmospheric Science
Colorado State University
Fort Collins, CO 80523

10. Project/Task/Work Unit No.

11. Contract/Grant No.
DES 74-11438
ATM 76-09370

12. Sponsoring Organization Name and Address
National Science Foundation

13. Type of Report & Period Covered

14.

15. Supplementary Notes

16. Abstracts

The thermodynamic equation and the water vapor equation, with the effects of cumulus convection parameterized according to the Arakawa-Schubert theory, are integrated during a short time interval and the resultant temperature and moisture tendencies are then studied. The quasi-equilibrium assumption is formulated as an optimization problem in which the objective is to minimize the changes in the cloud work function. The feedback loop consists of temperature and moisture changes due to large-scale vertical motion, radiative cooling and surface fluxes. The response of the model to different patterns of the above three types of forcing is compared to observations.

The model suggests a suppressive effect of deep convection on shallow convection, which is shown to be strongly coupled to boundary layer forcing through surface fluxes of heat and moisture. The distribution of clouds is shown to be sensitive to the choice of the radiative cooling profile when the dynamical forcing is small.

17. Key Words and Document Analysis. 17a. Descriptors

Convective Clouds
Cumulus Clouds
Cumulus Parameterization

17b. Identifiers/Open-Ended Terms

17c. COSATI Field/Group

18. Availability Statement	19. Security Class (This Report) UNCLASSIFIED	21. No. of Pages 132
	20. Security Class (This Page UNCLASSIFIED	22. Price